Fluid Flow and Heat Transfer in Transonic Turbine Cascades

by

S V Janakiraman

Thesis submitted to the Faculty of the

Virginia Polytechnic Institute and State University

in partial fulfillment of the requirements for the degree of

Master of Science

in

Mechanical Engineering

APPROVED:

John Moore

J. Moore, Chairman

H.L. Moses

S. Jayaram

May, 1993

Blacksburg, Virginia

C.2

Fluid Flow and Heat Transfer in Transonic Turbine Cascades

by

S V Janakiraman

J. Moore, Chairman

Mechanical Engineering

(ABSTRACT)

The aerodynamic and thermodynamic performance of an aircraft gas turbine directly affects the fuel consumption of the engine and the life of the turbine components. Hence, it is important to be able to understand and predict the fluid flow and heat transfer in turbine blades to enable the modifications and improvements in the design process. The use of numerical experiments for the above purposes is becoming increasingly common. The present thesis is involved with the development of a flow solver for turbine flow and heat transfer computations.

A 3-D Navier-Stokes code, the Moore Elliptic Flow Program (MEFP) is used to calculate steady flow and heat transfer in turbine rotor cascades. Successful calculations were performed on two different rotor profiles using a one-equation q-L transitional turbulence model. A series of programs was developed for the post-processing of the output from the flow solver. The calculations revealed details of the flow including boundary layer development, trailing edge shocks, flow transition and stagnation and peak heat transfer rates.

The calculated pressure distributions, losses, transition ranges, boundary layer parameters and peak heat transfer rates to the blade are compared with the available experimental data. The comparisons indicate that the q-L transitional turbulence model is successful in predicting flows in transonic turbine blade rows. The results also indicate that the calculated loss levels are independent of the gridding used while the heat transfer rate predictions improve with finer grids.

Acknowledgements

I would like to extend my sincere appreciation to Dr. John Moore and Mrs. Joan Moore for their insight, help, guidance and constant support for this work. Once again, I thank Dr. Moore for the interest he showed in this work during his supervision of this thesis.

I wish to thank Dr. S. Jayaram for being a friend and guide from my first day at Blacksburg. He has been a source of continuous support, valuable counsel and encouragement.

The support of this project, from Rolls Royce plc., under a cooperative agreement with Virginia Tech, is gratefully acknowledged.

I would also like to thank my friends - Mahesh, Ramesh, Satish and Ashraf for their help in the past year and a half.

Last but not least, I thank my parents for their steadfast support and encouragement at all stages of my life.

Table of Contents

List of Illustrations

List of Tables

Nomenclature

C_p	Specific Heat Capacity
C_{ax}	Blade Axial Chord
C_t	Blade Tangent Chord
d_{te}	Diameter of the trailing edge
D	Dissipation Term
e	Energy defect thickness
F_{vd}	Van Driest Correction Factor
F_{tu}	Intermittency Function
H	Boundary Layer Shape Factor
k	Ratio of Specific Heat Capacities
L	Prandtl Mixing Length
M	Isentropic Mach Number
MA_2	Exit Mach Number based on tank pressure
P	Production Term
p	Pressure
q	Square root of the turbulence kinetic energy
Q	Gas to wall heat transfer

R	Gas Constant
Re	Reynolds Number
$\frac{1}{R}$	Curvature
R_{tu}	Reynolds number of turbulence
S	Distance along the blade surface
S_0	Blade surface length
y^+	Transverse coordinate for the law of the wall
u	Velocity
δ_1, δ^*	Boundary layer displacement thickness
δ_{99}, δ	Boundary layer thickness
$\delta_{0.8}$	Normal distance from wall at $\frac{u}{u_e} = 0.8$
ε	Total loss based on pressure
η	Primary Efficiency
θ	Boundary layer momentum thickness
μ_{eff}	Effective Viscosity
μ_l	Laminar Viscosity
μ_t	Turbulent Viscosity
ξ	Mixed-out losses based on kinetic energy
ρ	Density
τ	Wall shear stress

Subscripts

$_d$	Downstream mixed-out value
$_e$	Edge of the boundary layer
$_{fre}$	Freestream

g	Gas
is	Isentropic
nw	Near-Wall
n	Normal to the wall
q	Square root of the turbulence kinetic energy
s	Isentropic
u	Upstream value for the mixing analysis
w	Wall
x	Cartesian coordinate in the axial direction
y	Cartesian coordinate in the pitchwise direction
0	Stagnation conditions
$2, ex$	Exit Conditions

1.0 Introduction

Rapid increases in fuel costs and depleting natural resources dictate that aircraft gas turbines operate at the highest possible efficiency. The optimization of the aerodynamic and thermal performance of turbomachinery blading hence assumes importance. This requires a detailed knowledge of the mechanisms that induce loss production and promote heat transfer to the blade, including blade boundary layer growth, transition from laminar to turbulent flow, trailing edge shocks and mixing losses downstream of the blade trailing edge.

The boundary layers on the surface of a modern gas turbine blade affect both the aerodynamic and thermal performance of the blade, through such mechanisms as throat area blockage, profile loss and gas to wall heat transfer. Understanding and controlling the boundary layer development is important in the design of efficient blading. A laminar boundary layer is associated with low heat transfer levels and profile losses while a turbulent boundary layer is less susceptible to separation due to shock boundary layer interactions but has higher levels of heat transfer associated with it. The high rate of gas to wall heat transfer due to transition is a significant factor in determining blade life, through the mechanism of thermal loading. The location of the start of this transition and the length of the transition zone depend strongly on a number of the flow parameters including the Reynolds number, free stream turbulence and the pressure gradient.

The optimized design of a blade profile, taking into account the synergistic effects of the above, often conflicting, factors has traditionally been associated with wind tunnel experiments. Of late however, due to the huge investments required in terms of time, space and money for such experiments, as also due to the availability of relatively inexpensive computing facilities and a growing number of dedicated flow solvers, the turbomachine designer is looking increasingly towards CFD to provide his solutions. Hence there is a need for developing computer codes to predict turbine blade performance and for well documented test cases on scale models of real blade sections at engine representative operating conditions.

In the present thesis, a 3-D flow solver for turbomachinery applications, the Moore Elliptic Flow Program is being developed to predict turbine blade performance. Calculations are performed for two turbine rotor blade sections for which extensive test data is available. These are the Rolls Royce RT27A/B22 and the ACE/RD turbine blades, tested at the University of Oxford and Cambridge University, respectively. These two test cases provide data on blade pressure distributions, boundary layer growth, transition, heat transfer, total pressure losses and flow turning angles.

The calculation results are compared with the available experimental data and this allows an assessment of current modeling capabilities. Areas where an improvement of the modeling is possible and suggestions for further work are also discussed.

2.0 Literature Review

2.1 Transonic Flow Computations with the MEFP

The code used for the present computational study, the Moore Elliptic Flow Program, MEFP, solves the steady form of the continuity, momentum and energy equations, using a pressure correction method. The MEFP can be described as a program to calculate fully three-dimensional inviscid, laminar or turbulent, compressible or incompressible flow which is steady in stationary or rotating coordinates. This code was applied for subsonic viscous flows in linear turbine rotor cascades (Moore, J., and Moore, J.G., 1985), and provided good agreement with the overall flow field and losses.

Moore, J., and Moore, J.G., 1987, discuss the extensions necessary to allow the pressure correction method to handle supersonic flows with shock capturing and also present a computation of the flowfield in a transonic turbine rotor blade. Moore, J., and Moore, J.G., 1990, detail the development of a one-equation q-L transitional turbulence model for the MEFP.

The present study involves the computation of the flowfield for two different transonic turbine rotor profiles at various conditions. The results are being used to evaluate the 3-D

viscous flow code with its transition model for predicting the overall flowfields, losses and heat transfer for flows in transonic turbine rotor passages.

2.2 Turbine Rotor Profiles

The two turbine rotor profiles considered in this thesis, the RT27A/B22 (hereafter referred to as the RT27) and the ACE/RD (hereafter referred to as the ACE) are shown in Figure 1 along with the key parameters of their geometries. The blades are designed for operation in a single stage, high temperature, high pressure gas turbine rotor. They possess thick coolable trailing edges, straight backed suction surfaces and turn the flow over large angles.

The RT27 is designed for operation at an isentropic exit Mach number of 0.92 and an exit Reynolds number based on true chord of 1E6, turning the flow through 111°. The profile geometry is available as a 1005 point coordinate file from Nicholson, J.H., 1981. The profile has been designed for a high aerodynamic efficiency. The ACE is designed for operation at a supersonic exit Mach number of 1.15 and a Reynolds number of 0.9E6, turning the flow through 123°. The profile geometry is tabulated in Haller, B.R., 1980, and is typical of blade sections intended for high work capacity transonic operation.

2.3 Cascade Studies

The RT27 and ACE rotor blade profiles have been tested extensively at the University of Oxford and Cambridge University, respectively. The different research groups, the characteristic di-

mensions of their cascades and the nature of the relevant test data available from their publications are summarized in Table 1. The present study focuses on modeling, for the RT27 profile, the conditions of Mee et al., 1992a, who provide extensive data on the boundary layers and their development around the blade, Mee et al., 1992b, who studied the RT27 profile with reference to losses and Nicholson, J.H., 1981, who studied the blade profile with reference to the gas to wall heat transfer.

Figure 2 shows a typical cascade arrangement for adiabatic testing at the transonic blowdown wind tunnel at the University of Oxford. This is a short duration facility capable of three or more seconds of steady flow, designed for aerodynamic studies of gas turbine blades. A row of parallel rods is used to generate turbulence in the free stream. The cascade flow exits as a free jet and the flow is adjusted by moving the shutters to vary the bleed of air past the end blades.

2.4 Blade Loading

The blade loading for the two profiles at their design conditions are shown in comparison in Figure 3. In the RT27 cascade, the design flow accelerates uniformly to a Mach number of around unity at 42 % of axial chord. The Mach number is maintained at that value until the trailing edge. The design flow in the ACE shows that the blade is more uniformly loaded. The Mach number in the leading edge region of the suction surface is around 0.7 and rises to a peak value of 1.25 at 60 % of axial chord before experiencing an oblique shock. The flow remains supersonic over the rest of the passage. The RT27 seems to have been designed with an aft-loading philosophy. The flow is accelerated quickly to a high value and is maintained at that state over the rest of the suction surface. The ACE seems to be more uniformly and highly loaded.

2.5 *Overall Losses and Loss Coefficients*

2.5.1 Introduction

The overall losses in a 2-D turbine cascade can be considered in terms of 3 individual components (Mee et al., 1992b)

1. The Boundary Layer Profile Loss
2. The Shock Losses
3. The Mixing Loss

The normalized total losses and the individual components for a turbine rotor cascade are shown in Figure 4, from Mee et al., 1992b. The boundary layer loss is quantified in terms of the loss in kinetic energy due to the formation of the boundary layer on the blade profile. These losses are mostly produced in the suction surface boundary as the pressure surface boundary layer is an order of magnitude thinner. As the exit Mach Number rises, the boundary layer thickness decreases (Mee et al., 1992b) and hence the boundary losses too should decrease.

The total pressure of a flow decreases when it passes through a shock wave. Hence, the kinetic energy that is obtained if this flow is expanded to a given static pressure is also decreased. The loss due to the shock waves can be estimated from the total pressure decrement in the wake free regions downstream of the trailing edge.

The losses that occur downstream of the trailing edge when the flows from either side of the blade merge together to form a uniform mixed flow are called mixing losses. These are determined by application of the conservation laws between two planes of a control volume. The overall losses of the cascade are evaluated by calculating the flow properties at this mixed-out state.

2.5.2 Mixed - Out Loss Coefficients

The mixed-out or overall loss coefficient, quantified in terms of the total pressure is given by

$$\varepsilon_{mixed} = \frac{P_{01} - P_{0d}}{P_{0d} - P_d}$$

An alternative approach is to express the overall losses in terms of a primary efficiency. Amecke, 1970, defines a primary efficiency η as the ratio of the actual kinetic energy of the flow at the mixed out plane to that which would be present if the flow expanded isentropically from the inlet conditions to the mixed-out static pressure. In terms of the enthalpies,

$$\eta = \frac{h_{0d} - h_d}{h_{01} - h_{2s}}$$

while the mixed loss is defined as,

$$\xi_{mixed} = 1 - \eta$$

2.5.3 Trailing Edge Thickness

Figure 1 allows a comparison of the trailing edge radius and the ratio of trailing edge radius over axial chord for the two turbine rotor profiles. The trailing edges have been designed with sufficient thicknesses ($\frac{d_{te}}{C_{ax}}$ = 2.65 % for the RT27 and 2.82 for the ACE, respectively) to enable film cooling of the trailing edge region. Xu and Denton, 1987 studied the losses associated with the trailing edges of cooled transonic turbine blades. The trailing edge loss is a significant component of the profile loss and is proportional to the trailing edge thickness.

Table 1. Studies on the Blade Profiles

RT27A / B22 Turbine Blade

Reference	Facility	Details of Cascade	Relevant Data
Nicholson ,J.T., 1981	ILPT Univ of Oxford	Ct = 43.291 Span = 50 Pitch=36.294	Heat Transfer Mex = 0.959 Tg/Tw = 1.5
Mee et al., 1990a	ILPT Univ of Oxford	Ct = 300 Span = 300 Pitch = 252.1	Adibatic Tests Mex = 0.92 Boundary Layer data. Transition locs
Mee et al., 1990b	Transonic Blowdown Wind Tunnel	Ct = 100 Span = 300 Pitch = 84	Adiabatic Tests Mex = 0.7 - 1.1 Boundary layer parameters, Schlieren pics Losses

ACE / RD Turbine Rotor Blade

Haller, B.R. 1983	Variable Density Transonic Test Facility	Ct = 41.7 Span = 101.6	Adiabatic Tests Mex = 0.8 - 1.2 Losses, Exit Flow Angles
Camus et al., 1983	Variable Density Transonic Test Facility	Ct = 41.7 Span = 101.6	Adiabatic Tests Mex = 0.7 - 1.2

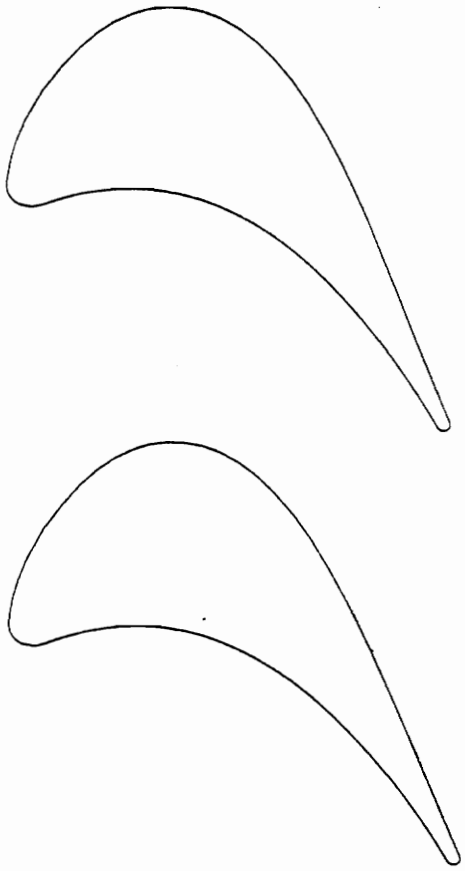

ACE

Haller Cascade

Cax = 34.86 mm
Pitch = 35.15 mm
Span = 101.6 mm
Ct = 41.70 mm

Radii

T.E. = 0.492 mm

Inlet Angle = 56.7 deg
Exit Angle = 66.0 deg

Design Re = 0.9E6
Design Mex = 1.15

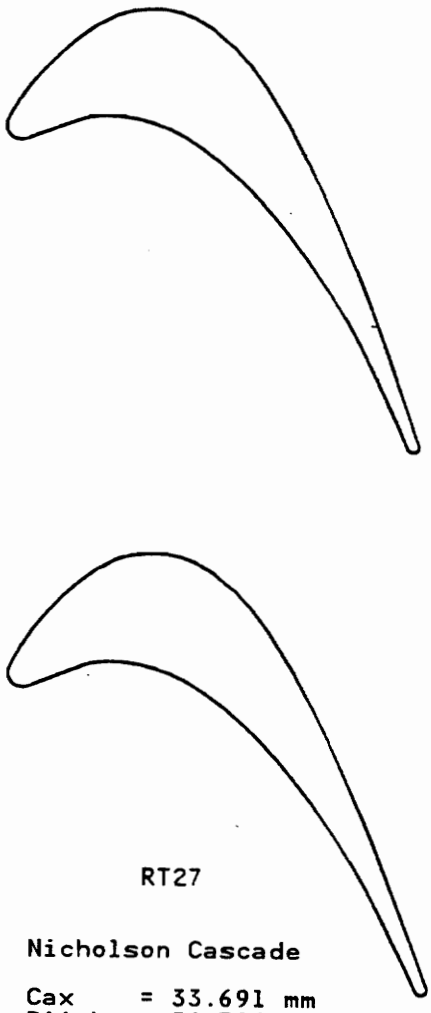

RT27

Nicholson Cascade

Cax = 33.691 mm
Pitch = 36.794 mm
Span = 50.000 mm
Ct = 43.791 mm

Radii
L.E. = 1.183 mm
T.E. = 0.448 mm

Inlet Angle = 42.75 deg
Exit Angle = 68.7 deg

Design Re = 1E6
Design Mex = 0.92

Figure 1. Typical Turbine Rotor Profile Sections

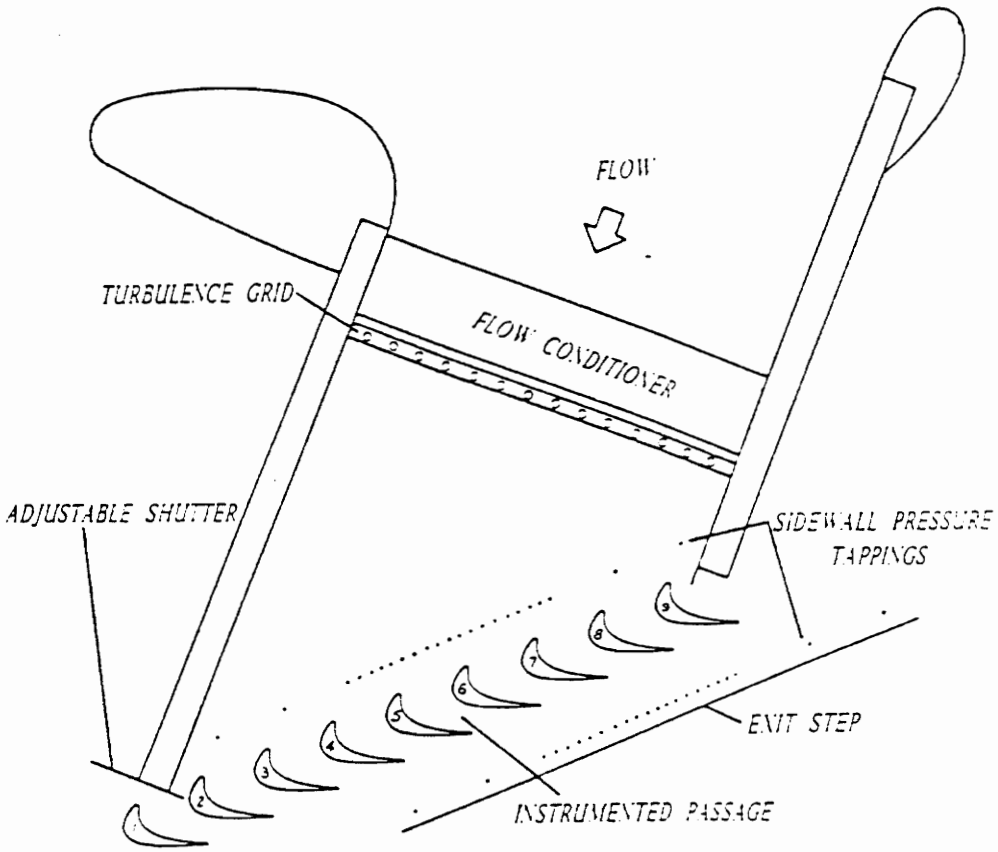

Figure 2. Cascade Arrangement for Adiabatic Tests

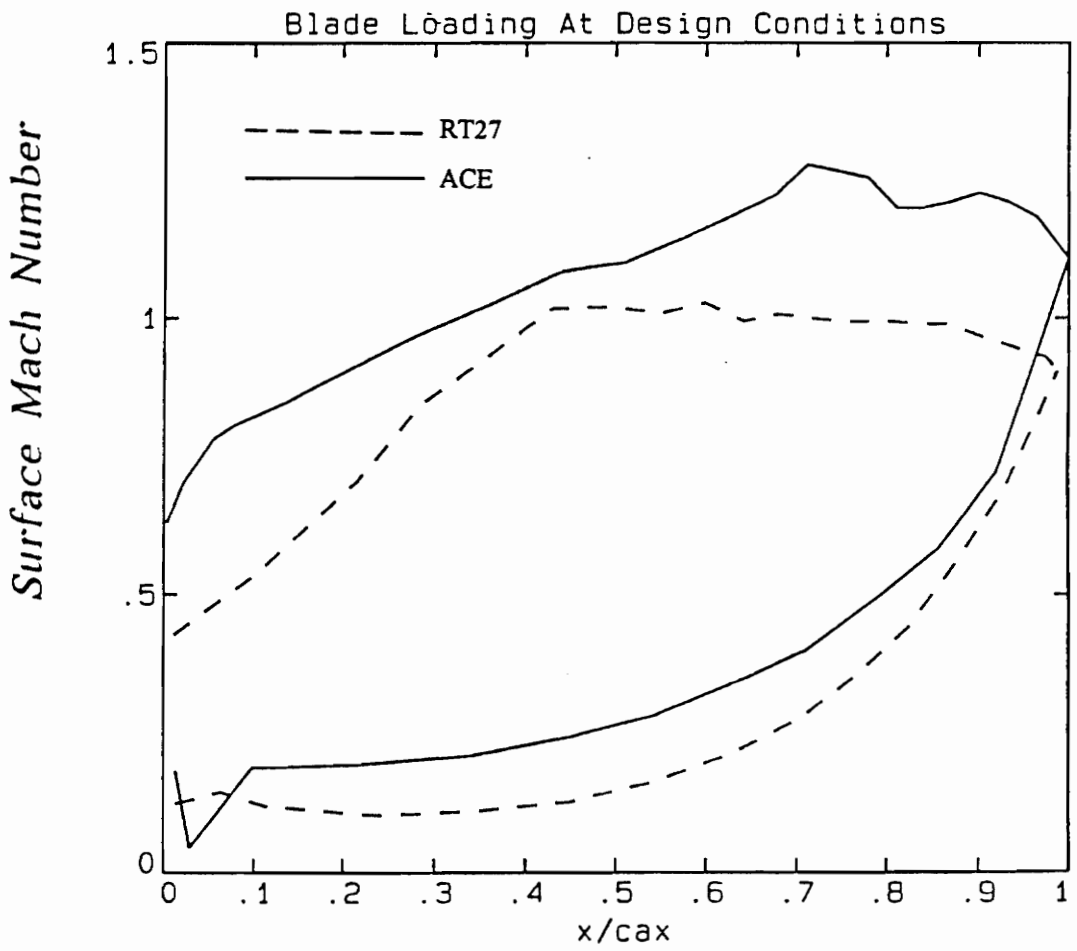

Figure 3. Design Blade Loading for the Profiles

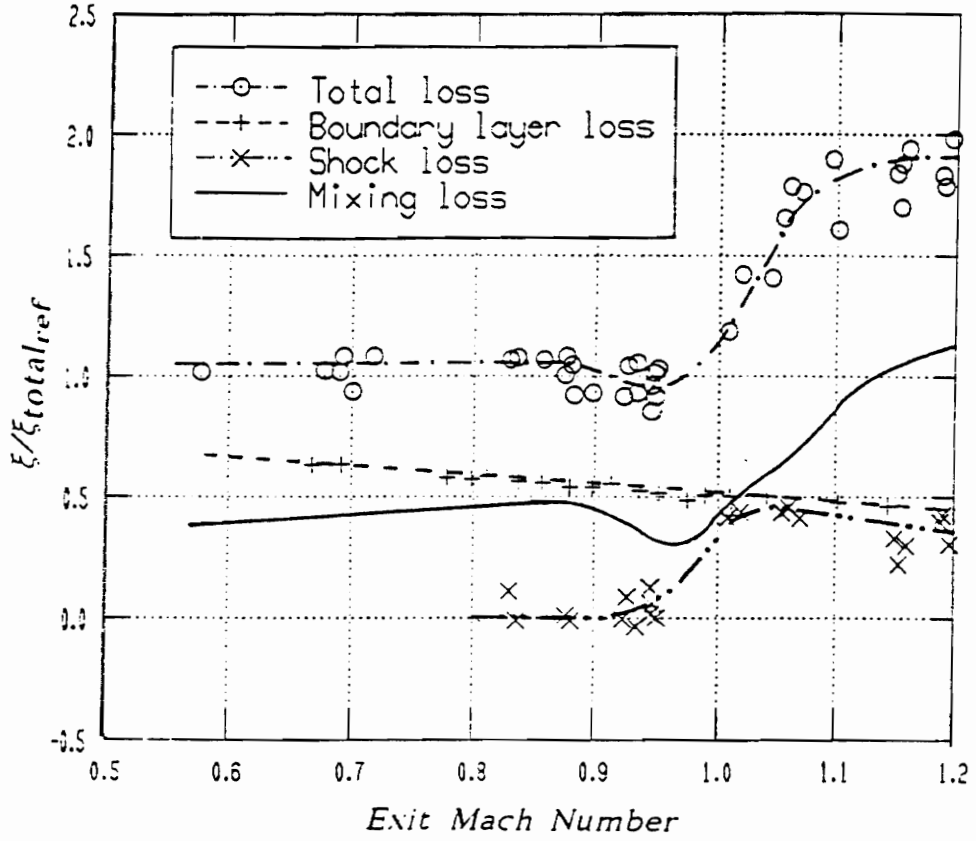

Figure 4. **Individual Components of the Loss For the RT27 Cascade at Re_{ex} = 1E6 (Mee et al., 1992b)**

2.6 *Factors Influencing Blade Performance in Steady Flow*

2.6.1 Mach Number

The trend in modern gas turbine design is toward high pressure ratios with operating speeds in the transonic range. The flow is accelerated quickly over the suction surface to a high Mach number, held constant at that high Mach number for as long as possible without boundary layer separation and then expanded to the trailing edge velocity. Generally the exit Mach number and Reynolds number for a turbine rotor are fixed by the choice of the design point.

2.6.1.1 Isentropic Exit Mach Number

The isentropic exit Mach number quoted by Haller, B.R., 1980, is based on a downstream tank static pressure and the inlet total pressure. This is equivalent to the Mach number based on the mixed-out static pressure. From the calculation results, this can be evaluated as follows:

$$M_{2d} = \left[\frac{2}{k-1} \left(\frac{p_0}{p_d}^{\frac{k-1}{k}} - 1 \right) \right]^{1/2}$$

The isentropic exit Mach number quoted for the studies on the RT27 is based on the inlet total pressure and the downstream static pressure as determined by the arithmetic average of six

equally spaced static pressure tappings placed 65 % of the axial chord downstream of the trailing edge and across the instrumented passage.

2.6.2 Reynolds Number

The performance of axial turbines generally deteriorates as Reynolds number is decreased. In low Reynolds number flows encountered in small engine components, the boundary layer tends to remain laminar. Such a laminar flow may separate before the boundary layer becomes turbulent, resulting in large losses. A higher Reynolds number promotes the boundary layer transition and leads to an increased momentum transfer between the freestream and the boundary layer. The choice of the Reynolds number for a gas turbine is dependent on the design point.

2.6.3 Transition

In a high pressure turbine, the primary role of transition is in affecting the gas to wall heat transfer. The boundary layer can be visualized as an insulating blanket around the blade, and for a given profile the heat transfer to the blade will reduce as the boundary layer thickens. In addition, the heat transfer to a blade through a turbulent boundary layer is higher than that through a laminar boundary layer. Turbulent heat transfer levels can be three to five times the laminar values. Since turbine blades fail locally, there is a need to predict the start of transition to turbulence and hence the rise in heat transfer levels. Figure 5 shows the effect of transition on heat transfer. It is seen that the gas to wall heat transfer is doubled from the laminar value, after the transition to turbulence is complete.

2.6.4 Free Stream Turbulence

In turbomachinery flows, the free stream turbulence influences the transition of the boundary layer from laminar to turbulent. A lower value of the free stream turbulence tends to result in a laminar boundary layer, while a higher value of the free stream turbulence tends to promote transition.

2.6.5 Trailing Edge Shock Structure

The flow pattern at a supersonic trailing edge is quite well understood and documented (Hah, C., 1990). The general features of the flow are illustrated in Figure 6. Figure 7 shows the trailing edge shock structure for the ACE turbine cascade. The flow immediately upstream of the trailing edge will usually be supersonic on the suction surface and close to sonic on the pressure surface. At exit Mach numbers above unity, a supersonic expansion of the flow occurs around the trailing edge followed by recompression in the wake. The pressure side shock propagates toward the suction surface of the adjacent blade and interacts with the blade boundary layer in the phenomenon referred to as shock boundary layer interaction. The other shock, which is usually much stronger, runs downstream away from the blades and interacts with the blade rows that follow.

2.6.6 Heat Transfer

The quest for higher thermal efficiencies has led to increasing turbine entry temperatures and pressure ratios. The maximum allowable inlet temperature is limited by material and coolant considerations. Without cooling, the blade metal temperature would be beyond the material

capability, and with inadequate cooling the blade life would be unacceptably short. In film cooled turbine blades, the addition of a layer of cooling air over the surface of the blade results in a reduction in the turbine efficiency. To minimize the loss of efficiency due to cooling, it is necessary to predict the external heat transfer to the blade accurately to enable the design of an optimal cooling configuration. Also, turbine blades have the tendency to fail locally due to thermal loading. Hence it is important to predict local peaks in the gas to wall heat transfer, which is a complex process affected by such factors as the Reynolds number, boundary layer development, free stream turbulence, curvature and transition.

In the present thesis, the plan of investigation and presentation of the results is as follows:-

1. Description of the Moore Elliptic Flow Program

2. Computational study of the RT27 blade profile

    a. Adiabatic flow calculations detailing boundary layer development and transition.

    b. Calculation of the heat transfer to the blade.

3. Computational study of the ACE blade profile

    a. Adiabatic flow calculations detailing passage shocks and loss development.

4. Conclusions arising from the study.

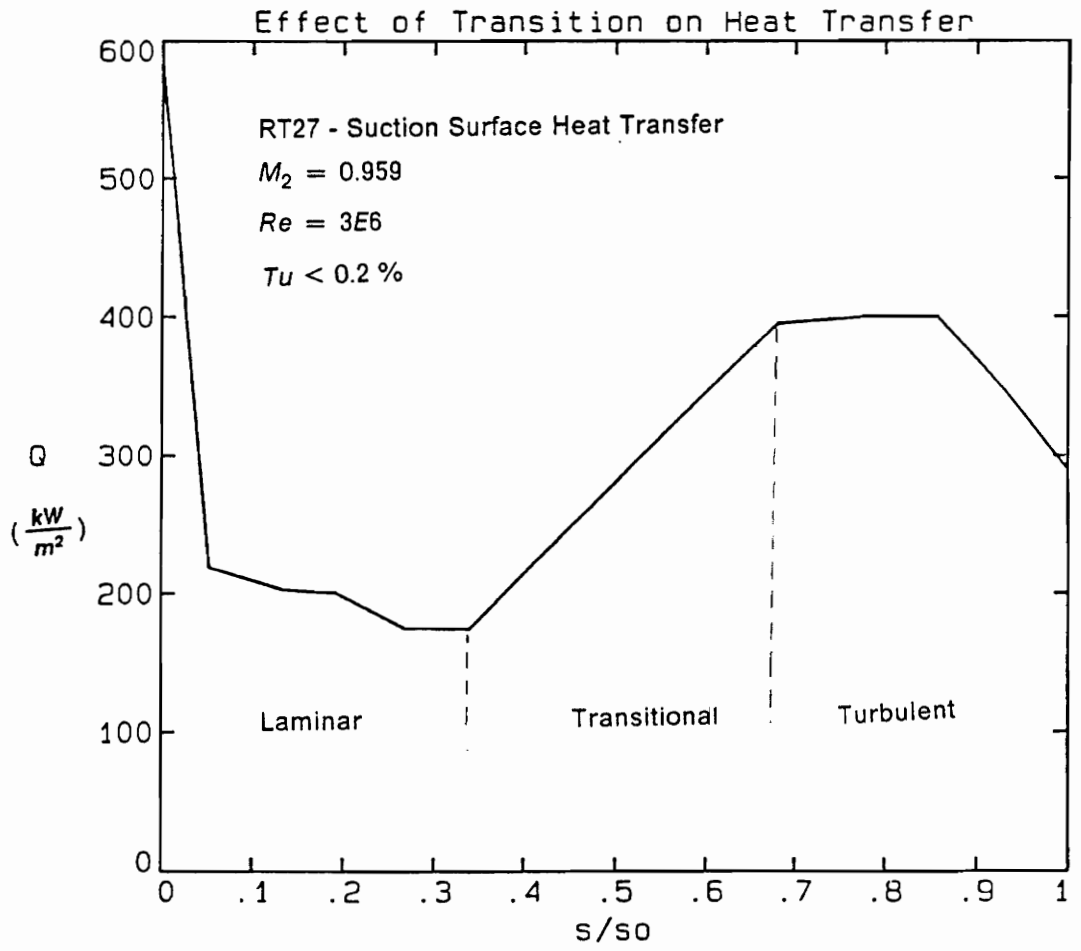

Figure 5. Effect of Transition on Gas-To-Blade Heat Transfer (Nicholson, J.H., 1981)

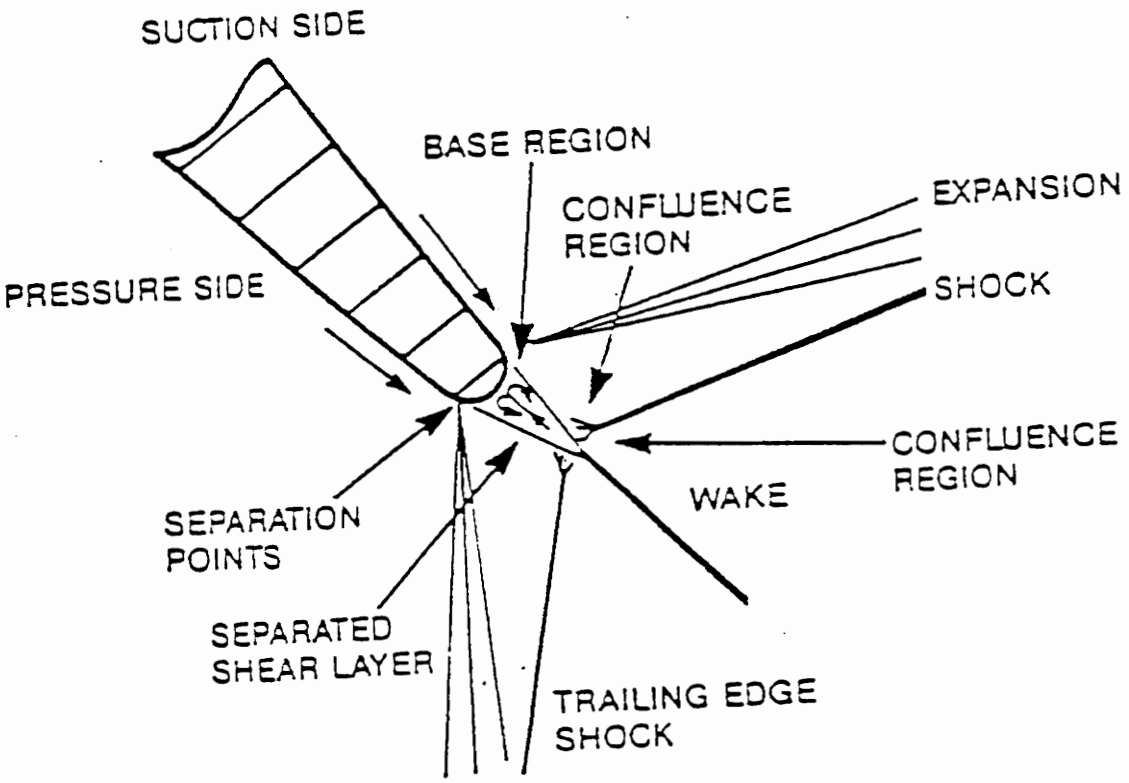

Figure 6. Structure of the Supersonic Trailing Edge Flow (Hah., C., 1990)

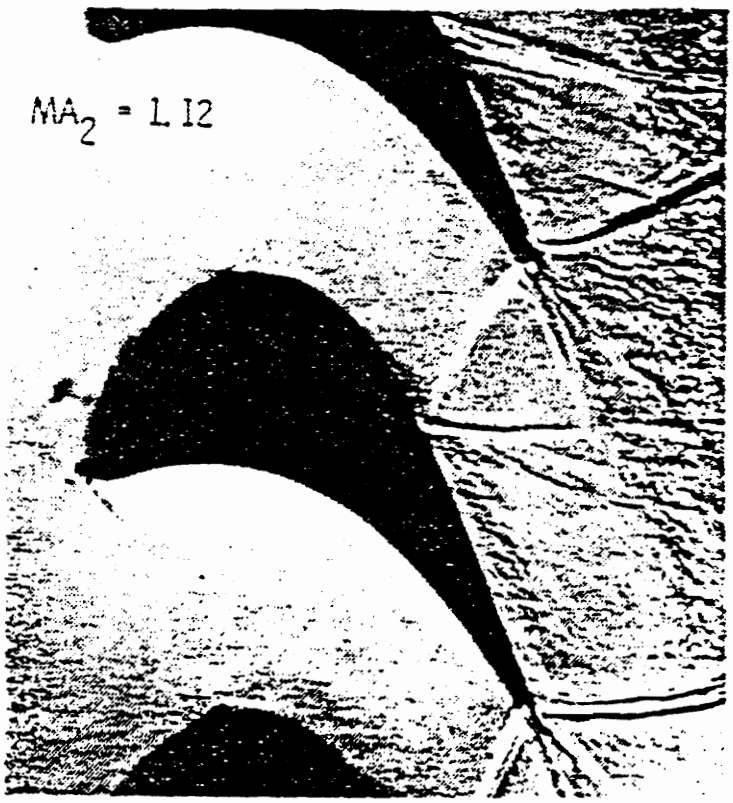

Figure 7. Trailing Edge Shock Structure for the ACE Turbine Blade (Haller, B.R., and Camus, J-J., 1977)

3.0 The Moore Elliptic Flow Program

3.1 Governing Equations

The MEFP (Moore, J.G., and Moore, J., 1987) solves for steady flows in turbomachinery blade rows in steady or rotating coordinates. The governing equations are the basic conservation laws and the equation of state for a perfect gas:-

1. Conservation of mass

$$\nabla \cdot \rho \underline{u} = 0$$

2. Conservation of Momentum

$$\rho \underline{u} \cdot \nabla \underline{u} - \nabla \cdot \mu \nabla \underline{u} = \nabla . \mu \overline{\nabla \underline{u}}^T - \nabla p - 2\rho \Omega \times \underline{u} - \rho \Omega \times (\Omega \times \underline{r})$$

3. Conservation of Energy

$$\rho \underline{u} . \nabla H - \nabla . \mu \nabla H = 0$$

4. Equation of State

$$p = \rho RT$$

$$H = C_p T + 0.5(\underline{u}.\underline{u}) - 0.5(\Omega \times \underline{r} \,.\, \Omega \times \underline{r})$$

3.2 q-L Turbulence Model

Turbulent and transitional flows are modelled using a q-L turbulence model (Moore, J.G., and Moore, J., 1990), where L is the mixing length and q is the square root of the turbulence kinetic energy.

$$q = \sqrt{k} = \frac{(\overline{u'_1{}^2} + \overline{u'_2{}^2} + \overline{u'_3{}^2})^{1/2}}{2}$$

q is predicted by solving the following partial differential equation,

$$\rho \underline{u}.\nabla q - \nabla.\mu_{eff}\nabla q = P_q - D_q$$

Physically, the four terms of the one equation transition turbulence model represent the particle rate of increase of q, the diffusion rate for q, the production rate for q and the dissipation rate for q, respectively. The production and dissipation of the kinetic energy of turbulence are modelled as,

$$P_q = 0.5\, C_\mu\, \rho\, L\, F_{vd}\, F_{tu,p}\, "(dU/dy)"^2$$

$$D_q = 0.5\, C_\mu^3\, \rho\, F_{vd}^{0.5}\, F_{tu,d}\, q^2/L$$

while the viscosity is given by,

$$\mu_{eff} = \mu_l + \mu_t$$

$$\mu_t = C_\mu \rho q L F_{vd} F_{tu,\mu}$$

3.3 Mixing Length

In boundary and shear layers, the mixing length, L is determined as the smaller value of Ky and $A_d\delta$. A van Driest near-wall correction is applied using

$$F_{vd} = 1 - e^{(-A_\mu K y \rho q/\mu_l)}$$

Outside of boundary layers the mixing length is taken as constant.

$$L = L_{fre}$$

So that the mixing length does not have a jump but is continuous at the edge of boundary layers, the mixing length is modified outside the layer so that the slope is less than K

$$\left|\frac{\partial L}{\partial y}\right| \leq K$$

The values of the constants are $K = 0.41$, $A_d = 0.08$, $A_\mu = 0.0295$ $C_\mu = 0.548$.

The reduction factors for transition, $F_{tu,n}$ are determined in terms of linear relations of the turbulence Reynolds number, R_{tu},

$$R_{tu} = A_d C_\mu \int_0^\delta \rho \frac{q}{\mu_l} dy$$

In the transition model 2F (Moore, J.G., and Moore, J., 1990) used here,

$$F_{tu,p} = F_{tu,d} = F_{tu,\mu}$$

and the relationship between the reduction factors and the turbulence Reynolds number is shown in Figure 8.

Figure 9 shows a typical F_{tu} plot used for transition evaluation. On the suction surface, the F_{tu} values are low until the onset of transition determined by a sharp rise to a high value near unity before dropping and gradually increasing to a value of one denoting the end of transition.

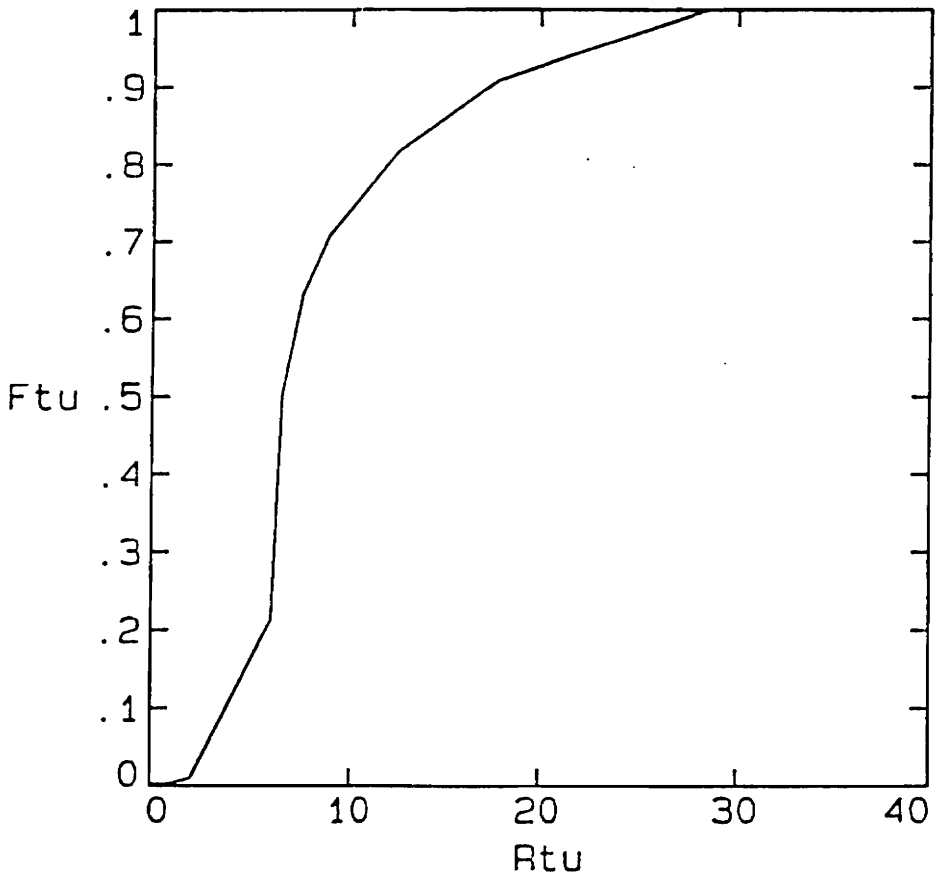

Figure 8. $F_{tu} - R_{tu}$ Relationship in Model 2F.

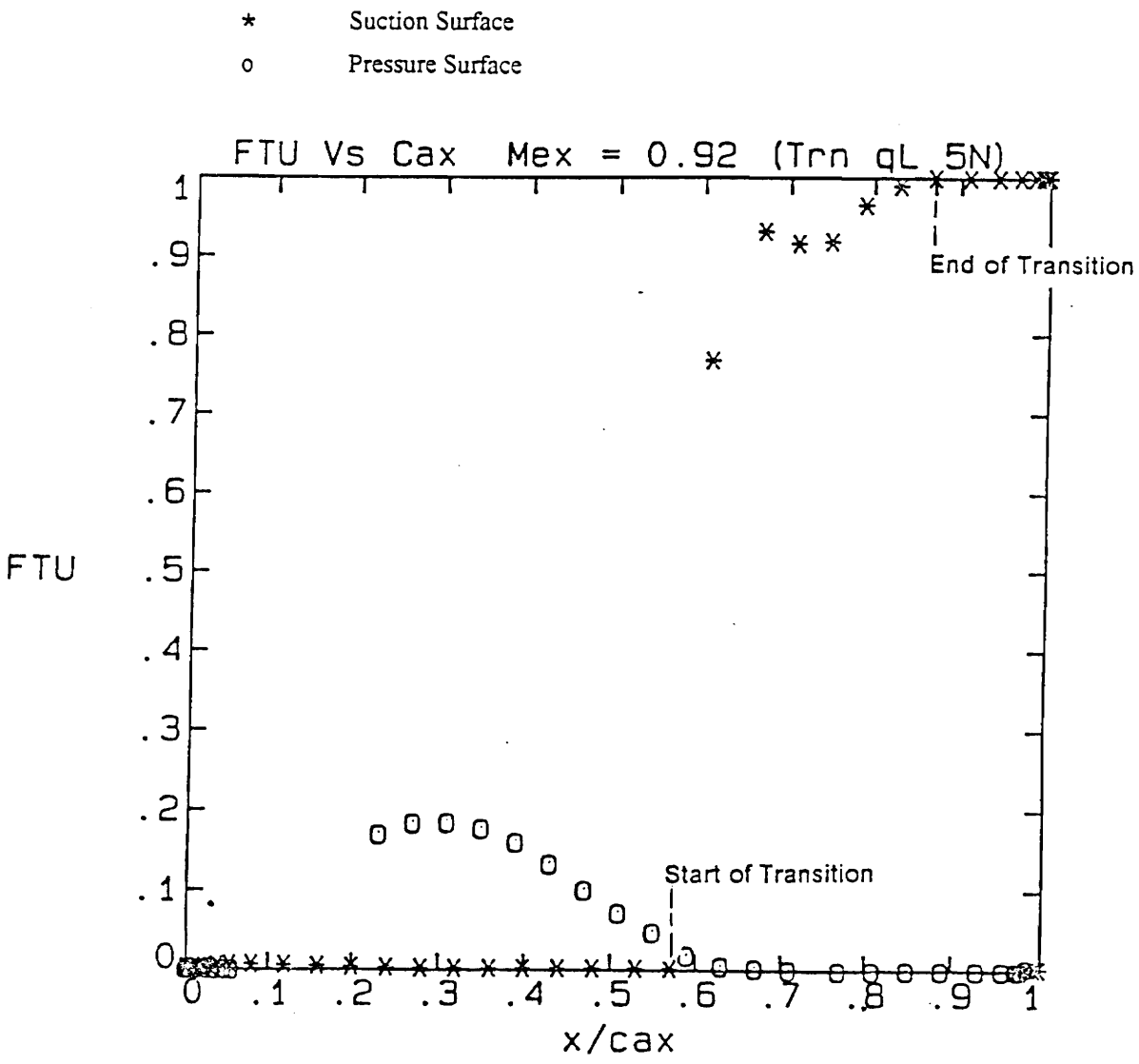

Figure 9. Typical F_{tu} Plot for Transition Evaluation

3.4 Grid Generation

The calculation grid is constructed after the validity of the blade profile is established with a comparison of the curvature variations. The important steps in constructing the calculation grid are : -

1. Definition of the blade profile, including the leading and trailing edge shapes.

2. Curvature analysis of the profile.

3. Choice of the four corner points of the blade profile.

4. Creation of a master geometry grid.

5. Estimation of an appropriate near-wall grid spacing around the blade.

6. Addition of grid lines for the calculation grid.

7. Optimization of the grid.

The compatibility conditions for the construction of the master geometry grid are :-

1. Same number of grid points on the plane of the leading and trailing edges.

2. Equal number of points on the suction and pressure surfaces of the blade profile.

3. Grid geometry to be appropriate for the boundary conditions used.

4. Line types to be specified properly for each grid point.

5. The individual control volumes should not have angles too acute or large aspect ratios.

The calculation grid extends a full axial chord downstream of the trailing edge approximately at the blade exit angle. The grid extends from repeating boundary to repeating boundary in the pitchwise direction.

3.4.1 Near-Wall Distance

Physically the near-wall distance is the spacing between the walls of the blade and the nearest grid line wholly in the flow field. It is evaluated in terms of the boundary layer thickness normalized by the blade pitch or leading edge radius. The importance of the near-wall distance stems from the fact that the calculated parameters of the flowfield are linearly interpolated from the near-wall value to the wall value. Therefore, for predicting the boundary layer, it is important that the near-wall grid line lie within the linear region near the wall. Similarly, for heat transfer calculations, the assumption of linear variation in the calculated temperature profile is valid only if the near-wall distance used is appropriate.

The method for estimating the near-wall distance is described in the 1987 MEFP User's Guide.

1. Modelling the leading edge flow as a laminar boundary layer growing on a circular cylinder.

2. Estimating the boundary layer displacement thickness δ_1, at $\phi = 90^0$ using

$$\frac{\delta_1}{R}(\rho U \frac{R}{\mu})^{1/2} = 0.9$$

3. With the near-wall point at this spacing from the blade, evaluating the ratio of near-wall spacing to blade pitch, $\frac{\delta_1}{p}$, to see relative spacing in the blade-to-blade direction.

3.4.2 Grid Optimization

The grid is optimized considering parameters such as the regularity of the control volume shapes, spacing between grid surfaces, uniformity of near-wall spacing, smoothness of the grid lines and the control volume aspect ratio (Moore, J.G., 1991).

4.0 RT27 Turbine Rotor Cascade

4.1 Geometry

4.1.1 Introduction

The RT27 - B22 is a single stage high pressure turbine rotor profile designed on the basis of aerodynamic criteria for high efficiency. It is meant for use in high bypass ratio civil engines. The objective of the present study is to model and understand the flow in RT27 cascades. Adiabatic and heat transfer calculations were performed for the profile at existing test data conditions.

Experimental data for RT27 cascades is available from the works of Nicholson, J.H., 1981, who studied the aerodynamics of the profile, Mee, Baines and Oldfield (Mee et al., 1992a), who studied the boundary layer development on the profile, Mee, Baines, Oldfield and Dickens (Mee et al., 1992b) who studied the profile with reference to the losses produced. These experimental studies are summarized in Table 2. The above studies have been conducted on various scaled versions of the RT27 profile as summarized in Table 3. The size of the

cascades used and the test facility have differed depending on the nature and scope of the tests conducted. All the calculations in the present study have been performed on the cascade of Nicholson, J.H., 1981. The calculated data has been suitably scaled wherever comparisons are made with measurements.

4.1.2 Profile

The RT27 is a highly loaded, unshrouded, single stage, high pressure turbine rotor blade. The RT27 profile is shown with the key parameters of its geometry in Figure 10. It has been designed for operation with a high aerodynamic efficiency in large fan engine applications.

4.1.3 Calculation Grid

The details of the cascade profile used are available as a 1005 point coordinate data file from Nicholson, J.H., 1981. The calculation grid constructed from this coordinate file is shown in Figure 11.

The calculation grid for the RT27 blade profile was generated and optimized by the principles detailed in the earlier chapter. The optimized calculation grid for the RT27 cascade consists of 6560 points (82, 40 and 2 planes in the x, y and z directions, respectively), with a total of 74 points to envelope the profile.

4.1.4 Curvature

The geometric curvature of the flow domain exerts an influence on the computed flowfields. The smoothness of the computed static pressure distributions is dependent on the smoothness of the curvature variations of the calculation profile used. The boundary layer development around the blade is also affected by the curvature, as detailed in Adams, E.W., and Johnston, J.P., 1984. Hence it is important to construct a blade profile for the numerical calculations with curvature variations similar to the one the flow finds in an actual experiment. The curvature variations of the large chord blade (used by Mee et al., 1992a) are available (from King, P.I., 1986), calculated using finite difference programs according to the formula,

$$\frac{1}{R} = \frac{y''}{(1 + y'^2)^{3/2}}$$

In the MEFP, the curvature at a point is determined in terms of the radius of a circle passing through the point and its two neighbors. The two approaches may be shown to be the same. The curvature distribution computed for the calculation profile is scaled to the large chord value and is compared with the curvature distribution given by King, P.I., 1986 , in Figure 12. The pressure side has an almost constant radius of curvature just aft of the leading edge before rising to a peak value at $\frac{X}{C_{ax}} = 0.23$. It then falls in steps to a low value by $\frac{X}{C_{ax}} = 0.88$. On the suction surface the rise and fall in curvature are steeper with the maximum curvature at $\frac{X}{C_{ax}} = 0.32$

4.2 Design Condition and Similarity Considerations

The design values of isentropic exit Mach number and exit Reynolds number for the RT27 blade are 0.92 and 1E6, respectively. The exit Mach number is based on the inlet total pressure and measurements of sidewall exit static pressure, and the exit Reynolds number (calculated assuming isentropic flow) is based on the same total and static pressures, the inlet total temperature and the true chord of the blade.

The calculation results have been compared with measurements where available. Since all the calculations were performed on a cascade corresponding to the one used by Nicholson, J.H., 1981, suitable scaling has been applied to the calculated data when compared with measurements obtained from a cascade of a different size. For example, all length measurements are scaled by $X = \frac{C_{ax,\,measurementcascade}}{C_{ax,\,calculationcascade}}$.

4.3 Summary of Data Available

4.3.1 Adiabatic Test Data

Adiabatic test data on the RT27 blade profile is available from the publications of Mee et al., 1992a and Mee et al., 1992b. The nature and extent of the data in these sources is described below and summarized in Table 4.

1. Mee et al., 1992a

Adiabatic testing of the RT27 blade profile has been conducted by Mee, Baines and Oldfield (Mee et al., 1992a) with special reference to the development of the boundary layer

around the blade at an isentropic exit Mach number of 0.92, for exit Reynolds numbers of 1E6 and 2E6.

The boundary layer profile has been measured at ten stations on the suction side and three on the pressure side using a flattened pitot tube. The data is presented as non-dimensionalized boundary layer profiles. The length scale is non-dimensionalized with the boundary layer thickness on the suction surface at $\frac{X}{C_{ax}} = 0.99, Re = 1E6, M_2 = 0.92$ (the reference location) and the velocity scale with the local freestream value. The value of the boundary layer thickness at the reference location is not provided. However, it can be determined from data provided by Dickens,T.E., 1990, as described in Appendix A. The value of $\frac{\delta^*_{ref}}{C_{ax}}$ is found to be 4.36E-3.

Variations of the boundary layer parameters, such as δ^*, θ, e and H around the blade are also provided at the two test conditions. The thicknesses are non-dimensionalized by the displacement thickness δ^* at the reference location.

The beginning and end of transition at the test conditions are determined by the sharp rise in the dynamic pressure as measured by the pitot probes.

2. Mee et al., 1992b

Mee, Baines, Oldfield and Dickens (Mee et al., 1992b) conducted adiabatic tests on the RT27 profile for a range of exit Mach numbers at a single exit Reynolds number of 1E6. Their measurements involved using a flattened pitot probe for boundary layer measurements, a trident probe to determine overall loss and a hot-wire probe to detect transition.

The variation of boundary layer, shock and mixing losses and the overall loss as a function of Mach number is provided. All the loss values are non-dimensionalized by the total loss at $M_2 = 0.92$, $Re = 1E6$, but the absolute magnitude of this loss is not given.

Variations in the boundary layer parameters such as displacement, momentum and energy thicknesses and shape factor are graphed against Mach number. The thicknesses are scaled by the δ^* value at the reference location. Again, the reference value is not made

available in the paper. Schlieren pictures of the flowfield in the cascade at the different test conditions are also shown.

4.3.2 Heat Transfer Data

Experiments with heat transfer were conducted on the RT27 profile by Nicholson, J.H., 1981, in the Isentropic Light Piston Tunnel at the University of Oxford. The ILPT is a transient flow facility suited for measurements of heat transfer to the blade.

The heat transfer to the blade is determined around the profile by means of thin film gauge surface resistance thermometers painted on to the blade surface. A total of 27 thin film gauges are used on the suction and pressure surfaces and on the leading edge.

Surface pressure distributions for the cascade are measured at the test conditions from static pressure tappings arranged around the blade. Data on the onset and end of transition are also available from this study, as determined from the fluctuations of the heat transfer rate signals.

4.4 Calculation Results

4.4.1 Summary of calculations

A series of adiabatic flow calculations was performed on the RT27 blade profile and is summarized in Table 5. These calculations were planned to span the range of test data available from the adiabatic experiments of Mee et al., 1992a, and Mee et al., 1992b. The calculations were performed for transonic exit Mach numbers at an exit Reynolds number of one million.

A few other calculations were performed at other Reynolds numbers. Calculations with heat transfer were performed with the MEFP at two exit Reynolds numbers on the RT27 cascade. The key parameters involved are summarized in Table 6.

All the calculations have been performed on a smooth blade profile corresponding to the Nicholson cascade. Each calculation run lasted for 300 passes. Boundary conditions of uniform velocity distribution and fixed total pressure at inlet and a fixed uniform static pressure at exit were enforced.

4.4.2 Results of the Adiabatic Calculations

This chapter outlines the nature and extent of the adiabatic test data available for the RT27 profile and discusses the results of the adiabatic calculations.

4.4.2.1 Pressure Distribution

Adiabatic Data

The measured surface Mach number distributions for the RT27-B22 rotor are shown in Figure 13. These measurements are the results of the adiabatic experiments of Mee et al., 1992b. The difference in the pressure distribution at the low exit Mach number of 0.7 and the higher exit Mach numbers is that the passage is almost choked at the design Mach number of 0.92 but unchoked at the lower value.

At the low exit Mach number, the flow is accelerated to a peak surface Mach number of 0.88 and then slowly diffused to give the correct exit Mach number. At the design condition, the suction surface Mach number is approximately constant at a value of unity from 42 % to 82 % of the blade axial chord. A subsonic diffusion follows to give the correct blade exit ve-

locity. At an exit Mach number of unity, the suction surface Mach number is constant at a value just above unity between 42 % and 74 % of the blade axial chord. It then undergoes supersonic acceleration until 93 % of the blade axial chord where there is a normal shock. At a supersonic exit Mach number of 1.1, the flow undergoes a supersonic acceleration after the throat before experiencing an oblique shock wave across the passage. The flow remains supersonic over the rest of the profile. The acceleration after the throat and the subsequent deceleration due to the recompression shock are quite rapid and occur over 15 % of the blade axial chord.

Comparison of the pressure distributions with data

A comparison of the predictions from the MEFP and the adiabatic test measurements of Mee et al., 1992b are shown in Figures 14 through 17. Figure 14 compares the calculated distributions for the low exit Mach number of 0.7 with the measurements. The calculations predict the overall distribution well. At the leading edge, the calculated pressure distribution shows the stagnation point, where the Mach number goes to zero, and also two suction peaks. The suction peak on the pressure surface has been discussed by Nicholson, J.H., 1981. The calculations also show two suction peaks at the trailing edge, due to the turning of the flow around the trailing edge to mix in the wake.

At the design condition, Figure 15, and at an exit Mach number of 1.0, Figure 16, the overall pressure distribution is very well predicted over both the surfaces. At the supersonic exit Mach number of 1.1, the flow at the throat is well modelled. The supersonic acceleration on the suction surface just beyond the throat seems reduced and the peak Mach number is lower. Correspondingly, the predicted passage shock is also weaker. The acceleration on the suction surface initiates earlier in the predictions than in the measurements. The shock may also be smeared out due to an absence of sufficient number of grid points. The flowfield corresponding to this exit Mach number and the possible courses to model it better are discussed section 4.44.

4.4.2.2 *Transition*

The accurate prediction of transition to turbulence of a laminar boundary layer is an important feature of turbine flow computations. The location and extent of transition is of interest to the designer. A laminar boundary layer is associated with a greater aerodynamic efficiency than a turbulent boundary layer but is more prone to separation and hence, higher losses, due to shock boundary layer interactions than is a turbulent boundary layer.

The present calculations use the one equation q-L model for turbulence (Moore, J.G., and Moore, J., 1990). This model and the relationship between the turbulence Reynolds number, R_{tu}, of the boundary layers and the intermittency function, F_w, are described earlier.

Experimental Data on Transition

Data on the onset and extent of transition on the suction surface of the RT27 - B22 rotor profile is available from the works of Mee et al., 1992a; Mee et al., 1992b; and Nicholson, J.H., 1981.

Mee et al., 1992a, used a Pitot traverse arrangement with corrections for wall interference effects and determine the ratio of the dynamic pressures near the surface and in the local freestream around the blade. This dynamic pressure ratio decreases in a region of a growing laminar or turbulent boundary layer but increases sharply in regions of transition.

Mee et al., 1992b, measured transition location on the suction surface at the design condition using a hot wire probe. The form of the signal from the probe is used to determine the start and end of transition.

Nicholson, J.H., 1981, used the fluctuations in surface heat transfer rates as detected by thin film gauges painted onto the blade surface to determine the onset and end of transition. For a laminar boundary layer, the mean heat transfer level is low, and the fluctuations in heat transfer are low too. As transition begins, the boundary layer has turbulent bursts that create sharp upward peaks at random intervals and increase the mean heat transfer rate. Towards

the end of transition, the boundary layer is largely turbulent with a higher heat transfer rate, with short spots of embedded laminar flow, which cause sharp downward peaks on the traces.

Calculated Transition Ranges

The calculations use the Model 2F of the one equation q-L model for turbulence. The start and end of transition in the calculations is determined from the plots of the intermittency function, F_{tu}. The calculated transition range is determined from the F_{tu} plot as the fraction of the axial chord between which the F_{tu} value grows from 0 (corresponding to a laminar boundary layer) to 1 (corresponding to a turbulent boundary layer). The F_{tu} values do not rise monotonically from zero to one. They usually rise steeply, drop a little and then increase gradually to one. Figure 9 is a typical F_{tu} plot showing the beginning and end of transition.

Comparison of the Calculations with Measurements

Table 8 lists the measured transition ranges along with the corresponding calculated values. Transition plots show the variation of the intermittency factor, F_{tu}, the wall shear stress, τ, and the turbulence Reynolds number, R_{tu}, around the blade.

The adiabatic measurements of transition are closely matched by the predictions of the q-L model. At the design condition, the beginning of transition is predicted at 56.8 percent of the axial chord. This agrees well with the measurements of Mee et al., 1992a (53.1 % of C_{ax}), and Mee et al., 1992b (60 % of C_{ax}). The end of transition is predicted to within 8 percent of blade axial chord for the two cascades. Figure 18 shows the calculated and measured transition ranges at the design condition. A higher Reynolds number promotes earlier transition on the suction surface, as indicated by the measurements of Mee et al., 1992a. This trend is well predicted by the q-L model at a Reynolds number of 2E6 as seen in Table 8.

Table 9 seeks to extract the dependence of transition on various factors. It is seen that at a Reynolds number of one million, the flow tends to stay laminar at higher exit Mach num-

bers. While a laminar boundary layer reduces the boundary layer profile losses, it is more prone to separation under shock boundary layer interactions. Figure 19 shows the wall shear stresses for increasing exit Mach numbers. The method used to obtain these wall shear stress plots is detailed in Appendix B. The τ plots indicate that the suction surface flow is not near separation at the Mach numbers considered, suggesting the absence of a strong passage shock in the calculations.

An increase in the Reynolds number at an exit Mach number of 0.92 quickens the onset of transition while cooling the blade seems to delay the onset of transition in the calculations as is evident from the data in group 3 of Table 9.

4.4.2.3 Losses

The mixed out total losses for the different calculated cases were determined by the method due to Amecke. The procedure of determining the mixed out total loss is described in Appendix C, and the loss coefficients are defined in section 2.5.2.

The losses are tabulated for the different cases in Table 10. The computed loss coefficients are plotted in Figure 20 as a function of the exit Mach number. Primary loss coefficients are presented in Mee et al., 1992b, the data being scaled by the loss coefficient at an exit Mach number of 0.92 and a Reynolds number of one million. Since this measured reference value is not known, the calculated losses are non-dimensionalized by the calculated value at the same conditions and the variations are compared in Figure 21.

The measured relative loss variation stays almost constant up to an exit Mach number of 0.9. The losses then dip to the value at the design point before rising to supersonic levels by $M_2 = 1.1$. At the higher Mach numbers the magnitude of the predicted loss ratio is lower than the measurements. It is evident that there is no sharp rise in the losses between the exit Mach numbers of 1.0 and 1.1 as in the data.

Why are the calculated losses lower? The factors influencing the prediction of losses are the predicted onset and extent of transition, predicted size and shape of the boundary layer profiles on the blade surface and the prediction of the trailing edge shock structure. From the previous section, it seems that transition has been predicted quite well for the conditions for which measured data is available. But how well are the boundary layers and trailing edge shocks predicted?

4.4.3 Boundary Layer Analysis

4.4.3.1 Evaluation of Boundary Layer Parameters

A wealth of data is available from Mee et al., 1992a and Mee et al., 1992b, in terms of the boundary layer profile details, their development, and the variation of the boundary layer parameters with Mach number. The calculated boundary layer velocity and density profiles and the boundary layer parameters such as the boundary layer displacement thickness, δ^*, the boundary layer momentum thickness, θ, the boundary layer energy thickness, e and the boundary layer shape factor, H were evaluated from the calculated flowfield data.

$$\delta^* = \int_0^{\delta} \left(1 - \frac{\rho u}{\rho_e U_e}\right) dy$$

$$\theta = \int_0^{\delta} \frac{\rho u}{\rho_e U_e} \left[1 - \left(\frac{u}{U_e}\right)\right] dy$$

$$e = \int_0^{\delta} \frac{\rho u}{\rho_e U_e} \left[1 - \left(\frac{u}{U_e} \right)^2 \right] dy$$

$$H = \frac{\delta^*}{\theta}$$

where the subscript e refers to the edge of the boundary layer.

4.4.3.2 Comparison of Calculated Boundary Layer Parameters With Data

The measured velocity and density profiles normal to the wall at a location corresponding to $\frac{s}{s_0} = 0.755$, at $Re = 1E6$, $M_2 = 0.92$, for the large chord blade are available from Mee et al., 1992a. The calculated boundary layer velocity and density profiles are superposed on the measurements in Figure 22. There is a good correlation between the predictions and the data.

Figure 23 is a comparison of the measured boundary layer thickness, δ_{99}, around the suction side of the blade at the design condition with the calculated values. The measurements are for the large chord blade of Mee et al., 1992a. The calculations have been scaled to the large chord value for the comparison.

Figure 24 is a comparison of the measured and calculated displacement and momentum thicknesses around the blade at the design condition. It is seen that both the displacement and momentum thicknesses are well predicted up to 90 percent of the axial chord on both the pressure and suction surfaces. The calculated momentum thickness on the suction side is slightly higher than the measured value at the trailing edge. Since the measured loss at an operating point is a function of the trailing edge momentum thickness, this indicates that the magnitude of the predicted losses at the design condition could be higher than the measured value.

The calculated and measured shape factors around the blade are compared in Figure 25. According to Xu and Denton, 1987, the trailing edge loss is a function of θ and H at the trailing edge. The calculations predict the shape factor very well around the blade profile.

Some measured data is available on the variation of the boundary layer parameters with Mach number for Mee et al., 1992b. Figure 26 and Figure 27 show a comparison of the measured and calculated boundary layer thicknesses and shape factors.

The momentum thickness is well predicted up to a Mach number of one. But it can be seen that the momentum thickness at the higher Mach numbers is underpredicted indicating a lower loss than is measured. The shape factor is over-predicted at the high Mach numbers. It is worth noting from Table 9 that the calculated boundary layer stays laminar throughout the suction surface for the exit Mach numbers of 1.1 and 1.2. All these factors together indicate that the calculations may have underpredicted the boundary layer loss for Mach numbers greater than one.

4.4.4 Trailing Edge Shock Structure

The structure of a supersonic trailing edge flow is shown in Figure 6 while Figure 28 shows a Schlieren plot of the trailing edge shock structure for the RT27 flowfield at $M_2 = 1.1$. It appears that the RT27 possesses the classical trailing edge flow structure. Figure 29 shows the calculated local Mach number distribution for the same flowfield. It is seen that the trailing edge shock system is not as strong as the Schlieren indicates. The flowfield shows a shock originating in the trailing edge region but it does not grow into a strong passage shock as the Schlieren indicates it should.

The absence of a strong passage shock could affect the validity of the wall shear stress plots obtained at the higher Mach numbers for which the q-L model predicted a laminar

boundary layer on the suction surface. It may also explain why the calculated losses are lower.

A possible reason for the absence of a strong passage shock in the predictions could be the resolution of the grid used. In order to isolate the effect of gridding on the adiabatic solution, a separate calculation was performed at the same conditions, using a grid improved in terms of the near-wall spacing and grid point densities used. The results from this calculation indicate that the loss coefficients were unaffected by this change of grid resolution and that the absence of a strong passage shock may be due to the still insufficiently refined grid or the algorithm used for the shock capturing.

4.4.5 Calculation of Heat Transfer

The quest for improved efficiency has motivated the elevation of turbine inlet temperatures in modern gas turbines. As a result, the turbine blade material is exposed to very high temperatures. Any estimate of blade life and structural integrity requires a knowledge of the amount of heat transferred into the blade.

4.4.5.1 Transition

Transition measurements with heat transfer were performed on the RT27-B22 profile by Nicholson, J.H., 1981. The available transition data and the calculated transition ranges are summarized in Table 11. At the lower Reynolds number, transition initiates at around mid-chord, much like the adiabatic tests and calculations discussed earlier. The q-L model predicts the start and end of transition to within 3 percent of the blade axial chord. The transition plots for this condition are shown in Figure 30. At the higher Reynolds number, Nicholson's measurements indicate that transition begins very early on the suction surface and ends by

mid-chord. The transition plots for this condition are presented in Figure 31 and show transition starting after mid-chord. However inspection of the turbulence Reynolds number shows that it reached a level close to that associated with transition near the leading edge. This is seen more clearly in Figure 32 where the calculated turbulence Reynolds numbers are plotted on an expanded scale. In the transitional turbulence model 2F (see Figure 8), the intermittency function F_{tu} starts to rise rapidly at a value of R_{tu} equal to 2.0, which is nearly achieved at one percent of chord.

A second calculation was then performed at the higher Reynolds number with transition fixed near the leading edge. This was accomplished by forcing a large value of turbulence Reynolds number in the turbulence model. The transition plots for this case are shown in Figure 33.

4.4.5.2 Heat Transfer Predictions

The gas-to-wall heat transfer in turbine blades is a complex process dictated by a number of properties of the flow and the passage geometry (Graham, R.W., 1979). The gas flow through the blade rows is three dimensional with secondary viscous flow patterns that interact with the blade surfaces. In addition, upstream disturbances, stagnation flow, curvature effects and flow acceleration complicate the thermal transport mechanisms in the boundary layers. Some of the factors affecting the gas-to-wall heat transfer, their effects and relevance are listed in Table 12.

Figure 34 shows the computed and measured heat transfer rates at a Reynolds number of 1E6 and an exit Mach number of 0.959. The rise in heat transfer rate on the suction side due to transition is well predicted, as is the onset of transition and the general heat transfer level. The calculated length of transition is shorter than the measured value. Both the data and the predictions suggest that the heat transfer to the pressure surface is constant over the

blade. However, the pressure surface heat transfer rate is under-predicted by a factor of two to three.

The measured and calculated heat transfer variations at the higher Reynolds number are shown in Figure 35. In the calculation employing the q-L model, the magnitude of the heat transfer to the blade on the suction surface experiences a sharp rise where the transition to turbulence occurs. This increase is experienced earlier for the calculation with transition fixed. In both calculations the heat transfer levels are well below the measured values. The character of the measured heat transfer to the pressure surface is different from that at the lower Reynolds number. The data shows an increase in heat transfer by a factor of two after 50 percent of chord. In both calculations, the predicted heat transfer is lower than the measured values by a factor of two.

4.4.5.3 Discussion of the Heat Transfer Calculations

The prediction of the peak heat transfer rate is quite important due to blade life calculation considerations. There are a number of factors affecting the accuracy of the heat transfer predictions.

The heat transfer to the blade is evaluated in terms of the total temperature gradient at the wall. The linear truncation of the temperature profile from the near-wall value to the value at the wall may result in some loss of accuracy. (The present calculations are performed with a near-wall to pitch ratio of 0.0008.)

Calculations were performed with a finer grid (151, 67 and 2 planes in the x, y and z directions respectively). This represents a halving of the near-wall spacing, control volume lengths and widths. Figure 36 shows the calculated y^+ distribution for the two grids, where

$$y^+ \equiv \frac{\rho_w y \sqrt{\frac{\tau_w}{\rho_w}}}{\mu_w}$$

Figure 37 then shows the heat transfer to the suction surface of the blade as computed with the fine grid in comparison with the measurements and the calculations with the previous grid. The finer grid represents a halving of the y^+. It can be seen that the laminar heat transfer is insensitive to y_{nw}, but the turbulent heat transfer is predicted in a more realistic fashion. Stagnation point heat transfer and the turbulent heat transfer after transition are quite sensitive to y_{nw}, while the laminar boundary layer prior to transition is relatively insensitive.

Concave surface curvature produces instabilities in a boundary layer due to the formation of streamwise vortices within the layer. Characteristic disturbances, known as Taylor-Goertler vortices are known to be induced by the concavity of the pressure surface. These disturbances result in enhanced mixing and hence increased heat transfer to the blade. In regions of large convex curvature, the turbulent shear stress is rapidly reduced by an effect referred to as curvature stabilization. This stabilizing effect, once established, lasts for long distances downstream (Adams, E.W., and Johnston, J.P., 1984). Inclusion of these factors, presently neglected, should enhance the overall accuracy of gas-to-wall heat transfer predictions with the MEFP.

Table 2. Experimental Studies on the RT27 Profile

Studies on the RT27 Profile

Group	Cascade Cax (mm)	Nature of the Test	Test Rig
Nicholson	33.691	Heat Transfer	ILPT, Oxford University
Mee et al, 1992a	230.7	Adiabatic	ILPT, Oxford University
Mee et al, 1992b	76.9	Adiabatic	Transonic Blowdown Tunnel, Oxford University

Table 3. RT27 Profile - Details of the Different Cascades

Group	Cax mm	Pitch mm	Span mm	Tangent Chord mm
Nicholson	33.691	36.294	50.0	43.291
Mee et al, 1992a	230.7	252.1	300.0	300.0
Mee et al, 1992b	76.9	84.0	300.0	100.0

Table 4. Adiabatic Test Data Available

Mee et al., 1992a

Test Conditions		Data Published
Re	Mex	
1.E6	0.92	Non-dimensionalized boundary layer velocity profiles measured at 10 stations on the suction surface and 3 on the pressure surface. Values of the boundary layer parameters at the measurement stations. Onset and end of transition on the suction surface. Velocity and density profiles at 75.5% of the suction surface length.
2.E6	0.92	Non-dimensionalized boundary layer velocity profiles measured at 10 stations on the suction surface and 3 on the pressure surface. Values of the boundary layer parameters at the measurement stations. Onset and end of transition on the suction surface.

Mee et al., 1992b

Re	Mex	Data Published
1.E6	0.7 0.92 1.0 1.1	Blade surface Mach number distributions. Schlieren pictures of the flowfield. Variation of boundary layer parameters with Mach number. Total pressure and flow angle variations in the wake.
1.E6 2.E6	0.7 0.92 1.0 1.1	Non-dimensionalized total loss variations. Breakup of the above variations into profile, shock and mixing losses.
1.E6	0.69 0.9 1.04	Non-dimensionalized velocity profiles at 99% of the axial chord.

Table 5. Adiabatic Flow Calculations

Summary of Adiabatic Flow Calculations

RUN	Re	M2	Pzero (Pa)	Tzero (K)
9N	2.00E6	0.92	321926.7	285.0
6N	1.0E6	0.7	161057.9	285.0
5N	1.0E6	0.92	161057.9	285.0
7N	1.0E6	1.0	161057.9	285.0
8N	1.0E6	1.1	161057.9	285.0
11N	1.0E6	1.2	154442.7	285.0
10N	0.88E6	0.7	161057.9	285.0

Table 6. Calculations - Key Parameters

Calculations: Key Parameters

$$\mu_l = 4 \times 10^{-7} \times T^{0.68}$$

$$T_0 = 288.15\,K$$

$$q_{inlet} = 0.0749\,U_{inlet} = 1.72\,m/s$$

$$L_{fre} = 0.0015\,m$$

Table 7. Summary of Heat Transfer Calculations

Summary of Calculations with Heat Transfer

RUN	Re	M2	Tzero	Tg/Tw
4n	1.0E6	0.959	432.0	1.5
2n	2.0E6	0.959	432.0	1.5
3na (Transition Fixed)	2.0E6	0.959	432.0	1.5
31n	1.0E6	0.959	432.0	1.5

Table 8. Transition Location - Comparison with Measurements

Transition Location - Calculations and Measured Data

Source	Test case	Re	Mex	Cascade Cax mm	Transition Range Onset - End x/Cax Measured	Calculated
Mee et al., 1992a 90GT263	Adiabatic	1E6	0.92	230.7	.531-.869	.568-.87 (5N)
Mee et al., 1992b 90GT264	Adiabatic	1E6	0.92	76.9	.600-.95	.568-.87 (5N)
Mee et al., 1992a 90GT263	Adiabatic	2E6	0.92	230.7	.370-.64	.440-.75 (9N)
Nicholson	H.T. (Tg/Tw = 1.5)	1E6	0.959	33.691	.549-.905	.57 -.91 (4N)
Nicholson	H.T. (Tg/Tw = 1.5)	2E6	0.959	33.691	.110-.55	.527-.79 (2N)

Table 9. Transition Location - Calculated Range

Transition Location - Calculations

Re	Mex	Type	Calc Trn x/cax	Meas. Trn x/cax	Run
1.E6	0.7	Adiabatic	0.571 - 0.789		10n
1.E6	0.92	Adiabatic	0.568 - 0.823	.531 - .869	5n
1.E6	1.0	Adiabatic	0.748 - 1.000		7n
1.E6	1.1	Adiabatic	1.000 - -		8n
1.E6	1.2	Adiabatic	1.000 - -		11n
1.E6	0.92	Adiabatic	0.568 - 0.823	.531 - .869	5n
2.E6	0.92	Adiabatic	0.440 - 0.750	.370 - .640	9n
2.E6	0.959	Adiabatic	0.441 - 0.710		1n
2.E6	0.959	HT	0.527 - 0.793	.110 - .550	2n
2.E6	0.959	HT	0.527 - 0.793	.110 - .550	2n
2.E6	0.959	HT Fixed	0.003 - 0.100	.110 - .550	3na
2.E6	0.959	HT Fixed	0.003 - 0.100	.110 - .550	3na
1.E6	0.959	HT	0.568 - 0.912	.549 - .905	4n

Table 10. Calculated Loss Coefficients

Re	Mex	Amecke Loss	Loss coeff	Run
2.E6	0.92	0.046	0.067	9n
1.E6	0.7	0.042	0.054	10n
	0.92	0.048	0.072	5n
	1.0	0.052	0.081	7n
	1.1	0.063	0.107	8n
	1.2	0.062	0.114	11n
0.88E6	0.7	0.0434	0.0561	6n

Table 11. Transition Data for the Heat Transfer Tests

Re	Mex	Type	Calc Trn x/cax	Meas. Trn x/cax	Run
2.E6	0.959	Adiabatic	0.441 - 0.710		
2.E6	0.959	HT	0.527 - 0.793	.110 - .550	2n
2.E6	0.959	HT	0.527 - 0.793	.110 - .550	1n
2.E6	0.959	HT Fixed	0.003 - 0.100		3na
2.E6	0.959	HT Fixed	0.003 - 0.100	.110 - .550	3na
1.E6	0.959	HT	0.568 - 0.912	.549 - .905	4n

Table 12. Factors affecting gas-to-wall Heat Transfer (Graham, R.W., 1979)

Factor	Manifestation	Relevance to Present Analysis
Transitional Behavior	Transition from laminar diffusion transfer to turbulent shear transfer. Has a direct effect on the heat transfer to the blade.	Prediction of suction surface transition is good in the adiabatic calculations and the calculation with heat transfer at Re = 1E6.
Free-stream Turbulence	Influences the production and diffusion of boundary layer turbulence and stability through transitional behavior.	Free-stream turbulence intensity has been fixed at the measured value.
Profile Curvature	Influences boundary layer turbulence and dissipation. Affects the stability. May produce Taylor-Goertler vortices along concave surfaces with a consequent strong effect on the heat transfer.	Curvature modification to turbulence was not included in the present study.
Surface Roughness	Directly influences the stability and turbulence production of the boundary layer.	Tests and calculations performed on a smooth profile.
Free stream Velocity	Direct influence on the boundary layer thickness and profile shape. The boundary layer can be visualized as an insulating layer around the blade.	A comparison of the measured and predicted layer thickness and shape factor is shown in Figures 24 and 25. They indicate a good agreement of the calculations with measurements.
Flow separation and reattachment	Produces sharp local changes in the heat transfer.	Calculated flow comes very near separation on the pressure side just past the leading edge. It stays attached throughout on the suction side.

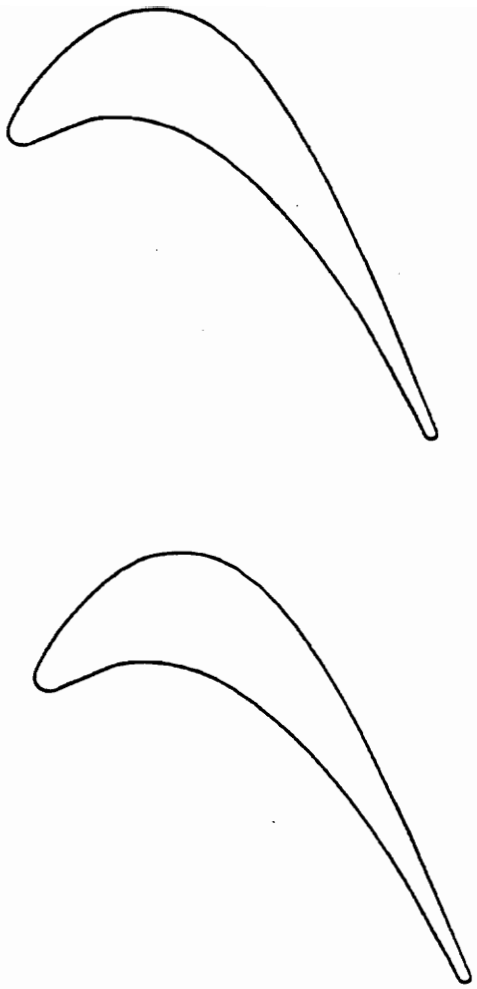

RT27

Nicholson Cascade

Cax = 33.691 mm
Pitch = 36.794 mm
Span = 50.000 mm
Ct = 43.791 mm

Radii
L.E. = 1.183 mm
T.E. = 0.448 mm

Inlet Angle = 42.75 deg
Exit Angle = 68.7 deg

Design Re = 1E6
Design Mex = 0.92

Figure 10. RT27 - B22 Blade Profile

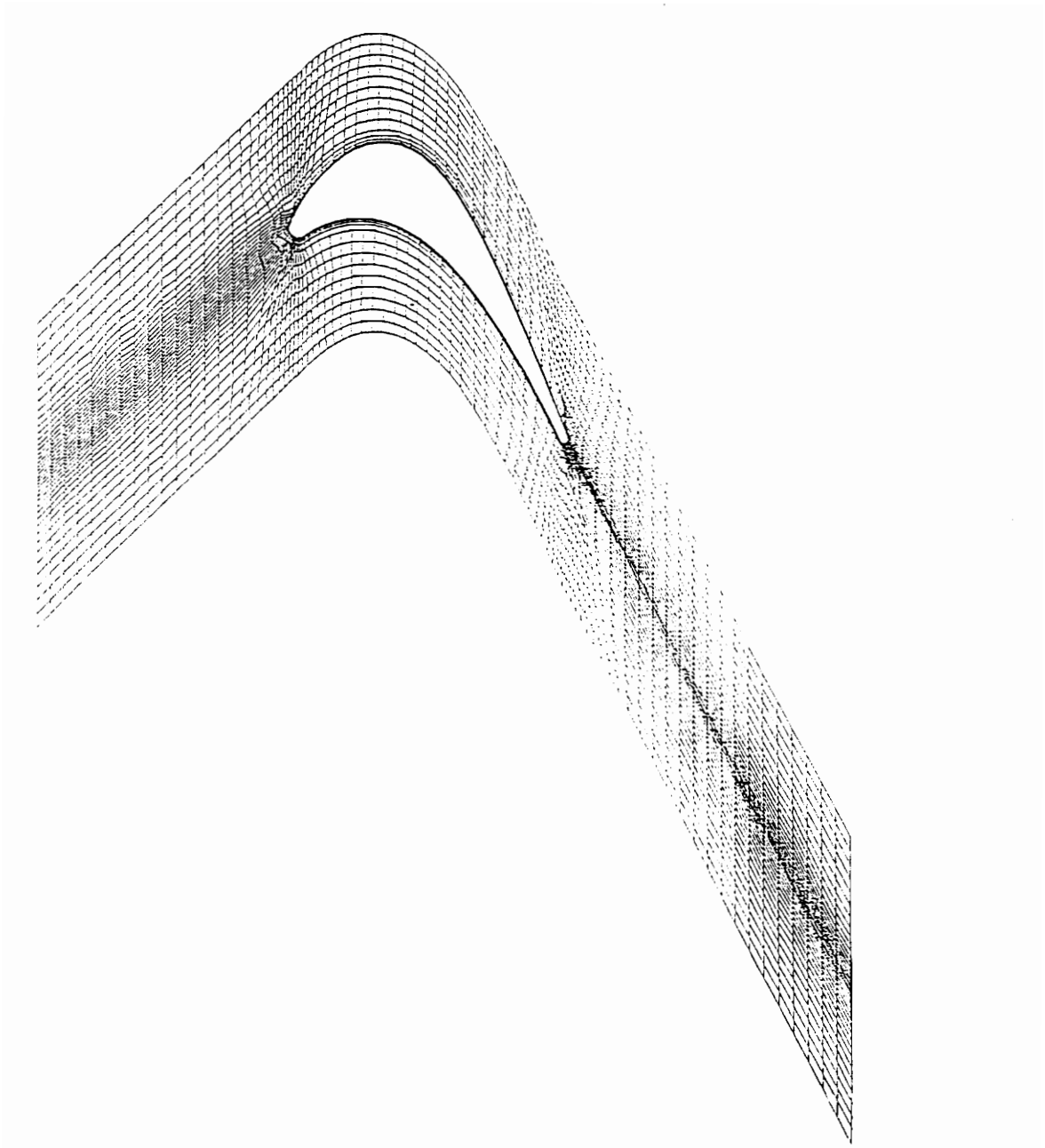

Figure 11. RT27 - Optimized Calculation Grid

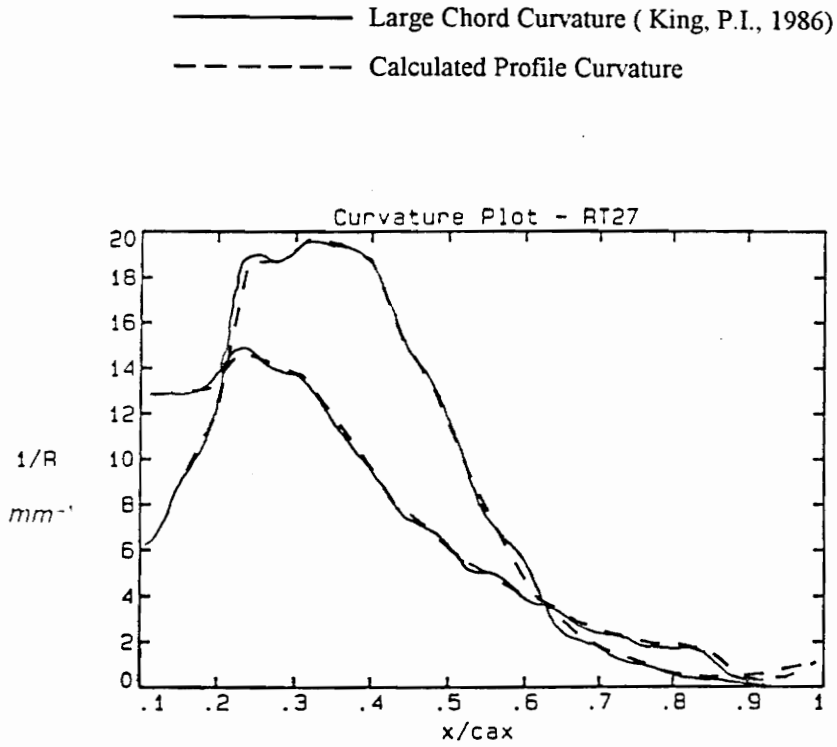

Figure 12. RT27 Comparison of Curvature Variations

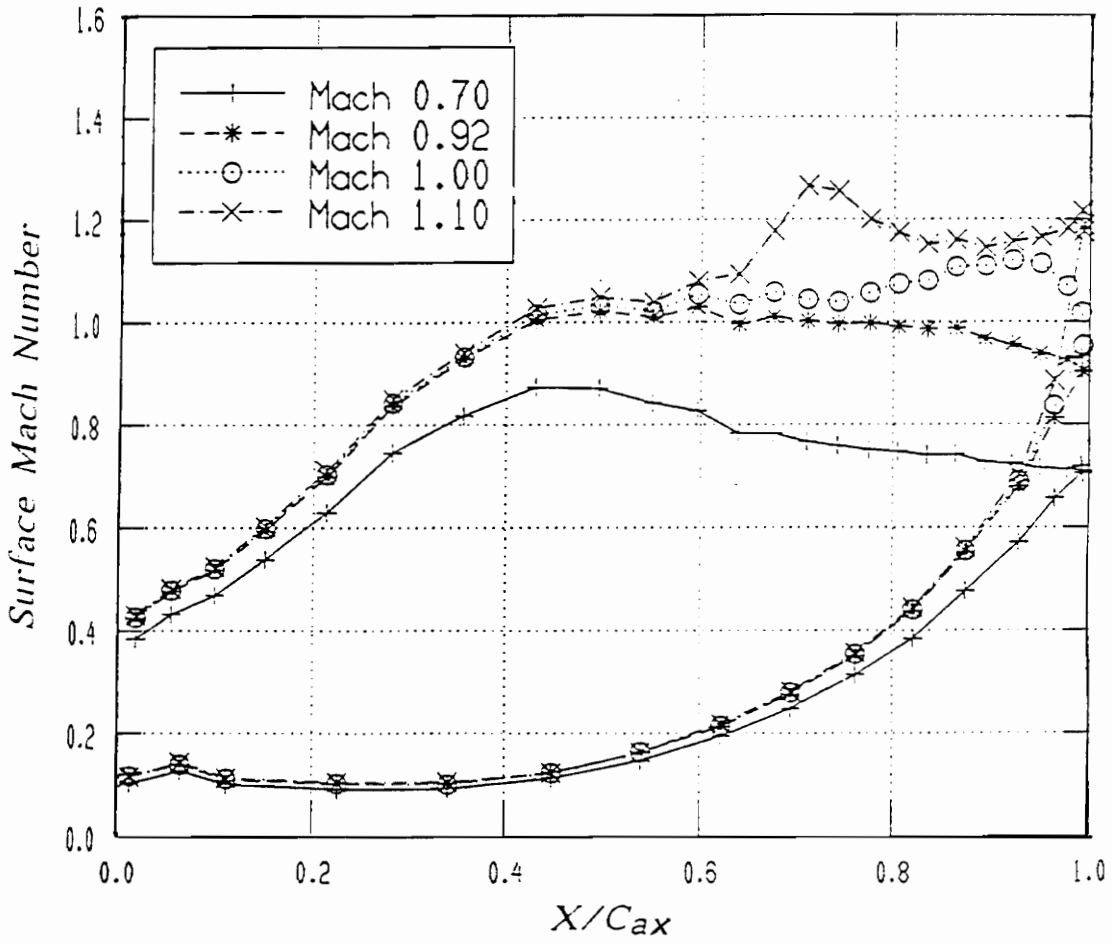

Figure 13. Measured Surface Mach Number Distributions, Mee et al., 1992b

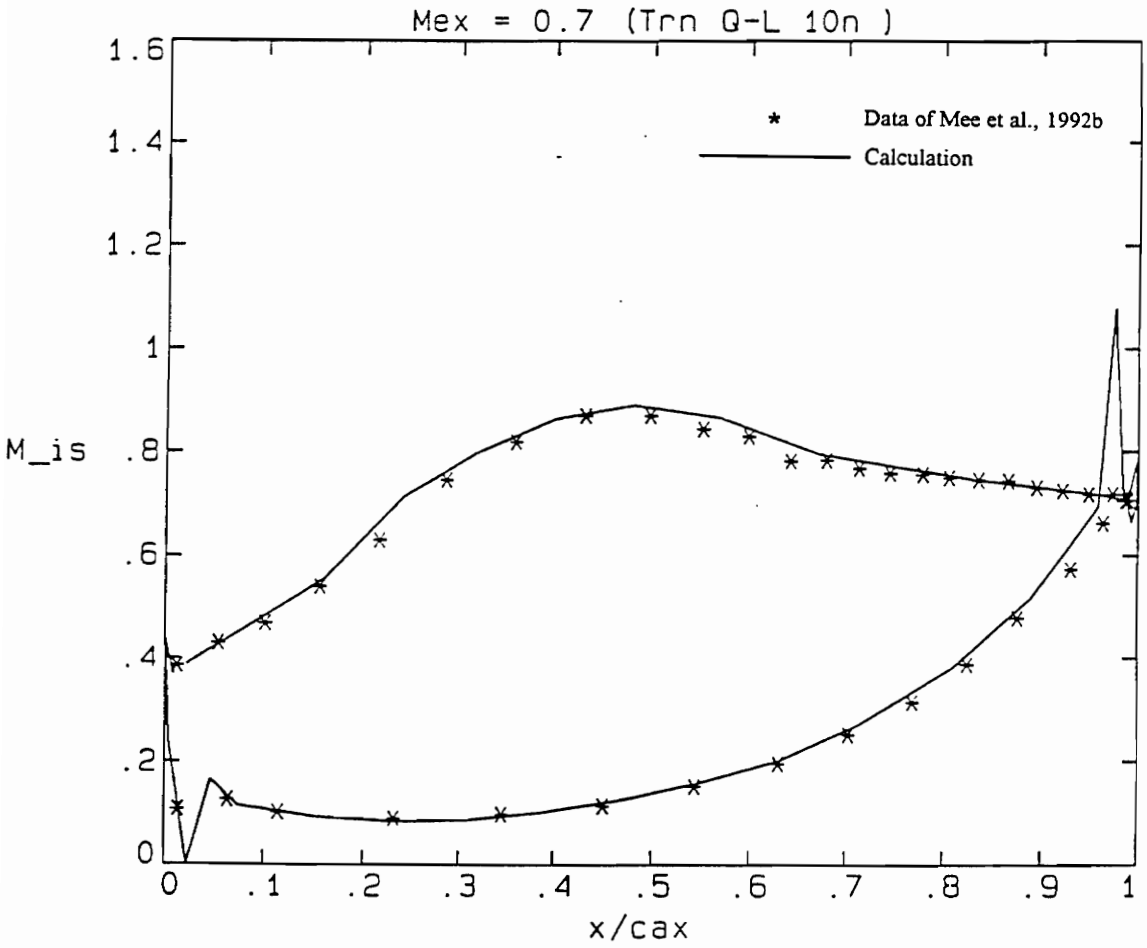

Figure 14. RT27 Surface Mach Number Distribution, $M_2 = 0.7$

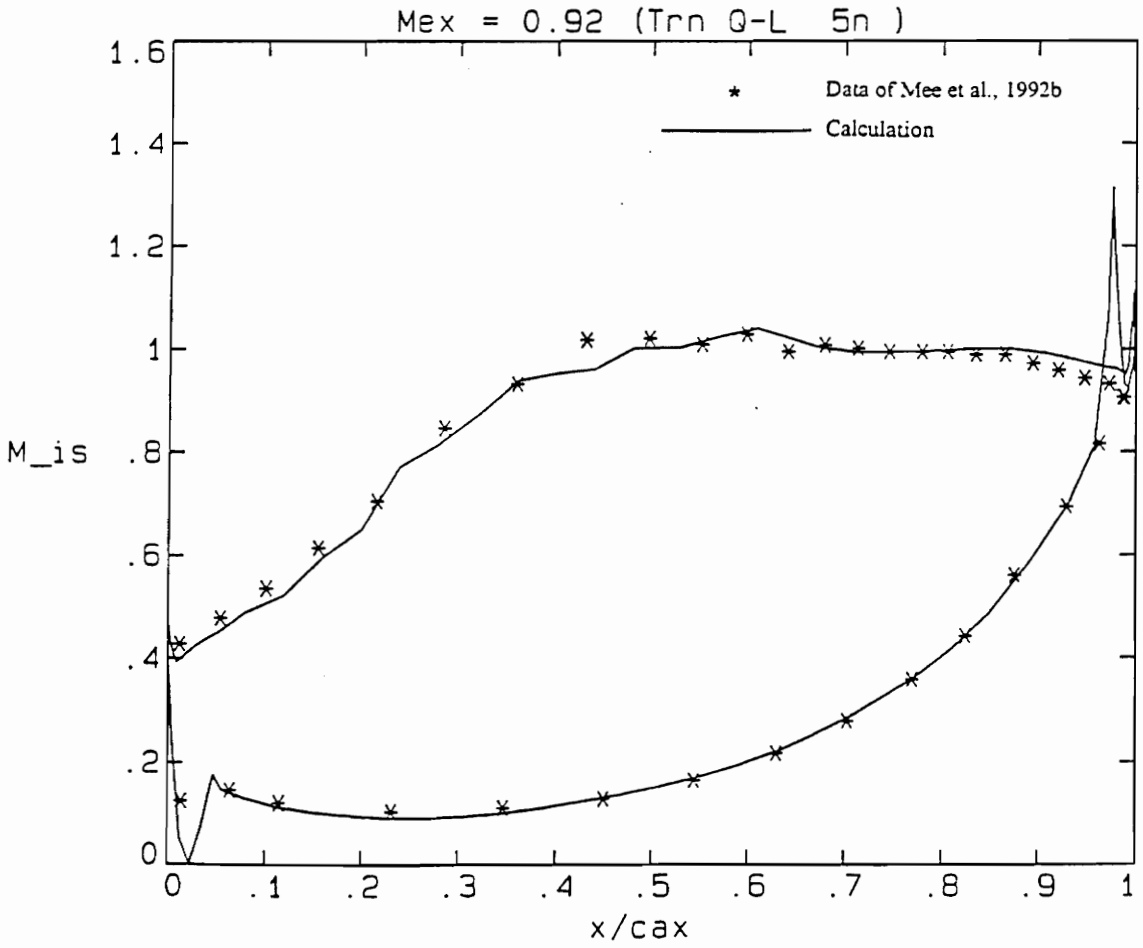

Figure 15. RT27 Surface Mach Number Distribution, $M_2 = 0.92$

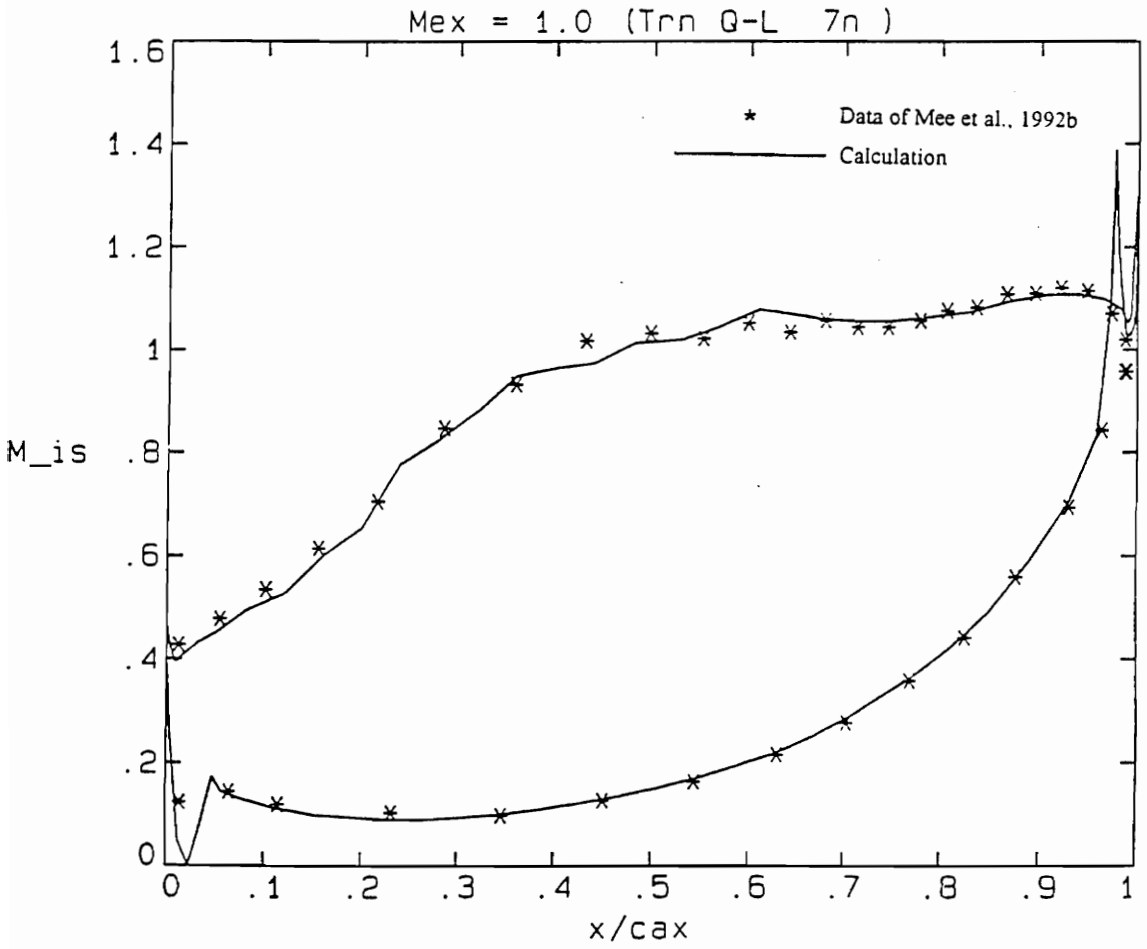

Figure 16. RT27 Surface Mach Number Distribution, $M_2 = 1.0$

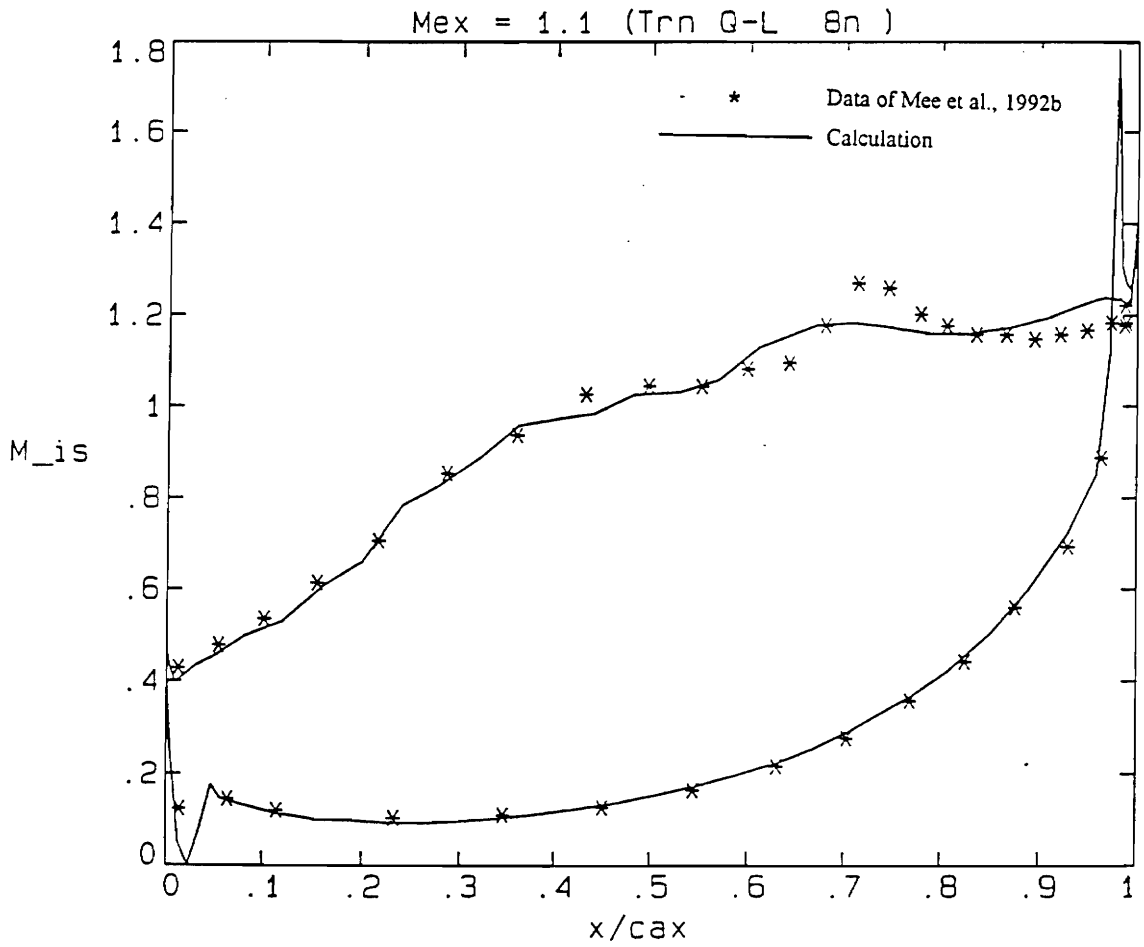

Figure 17. RT27 Surface Mach Number Distribution, $M_2 = 1.1$

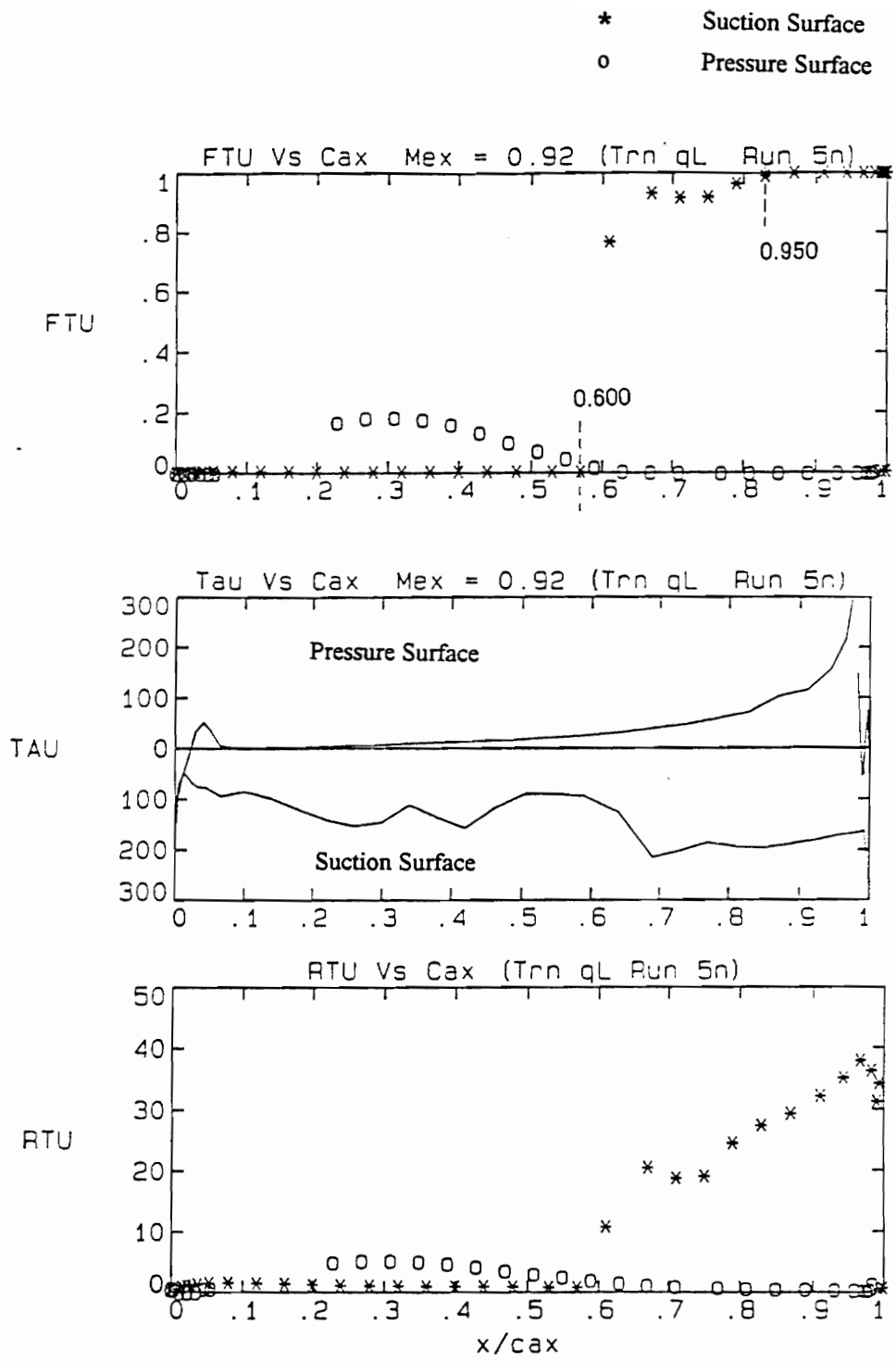

Figure 18. RT27 - Transition Plots, $M_2 = 0.92$, $Re = 1E6$

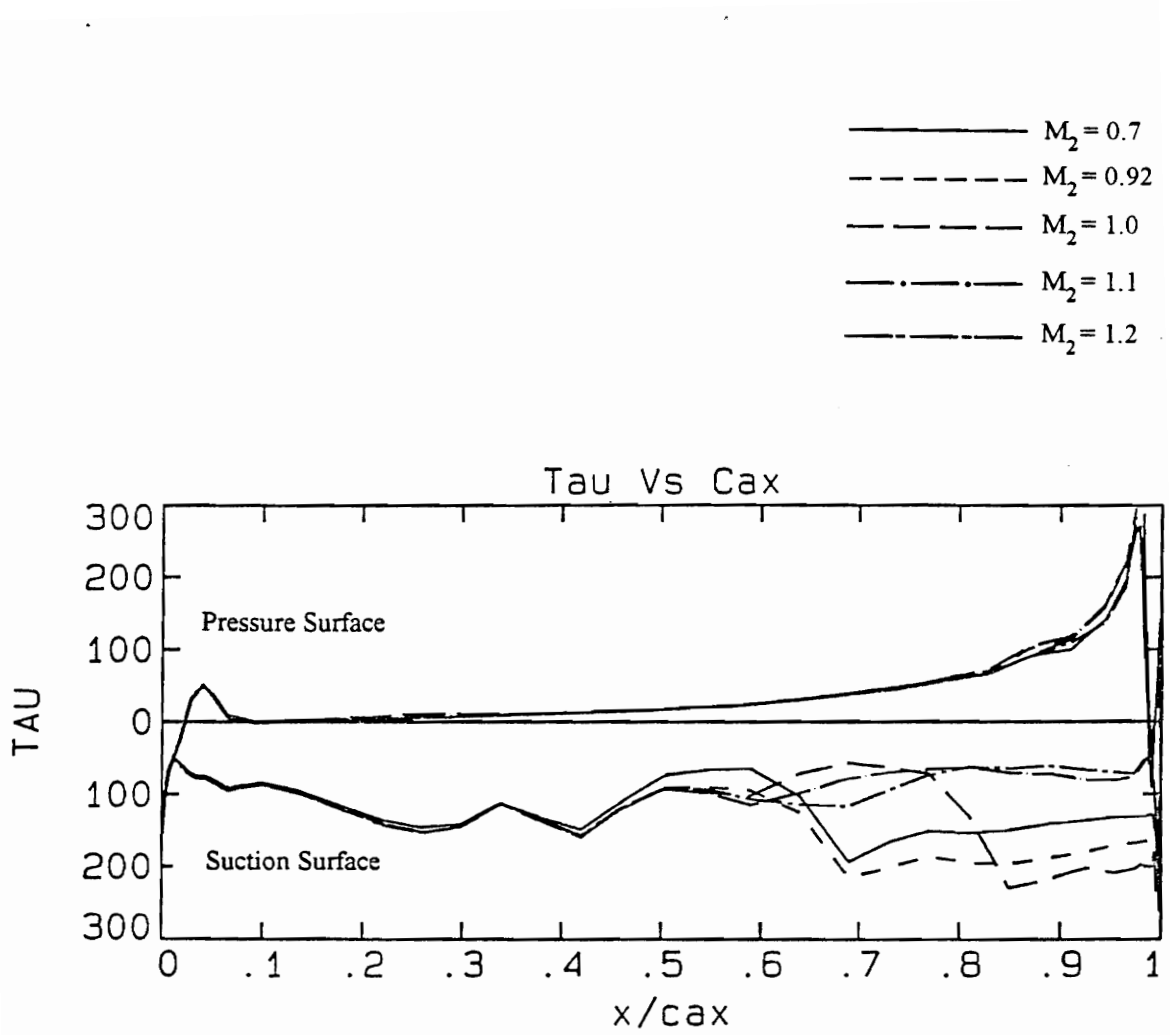

Figure 19. Shear Stress variations with Mach number

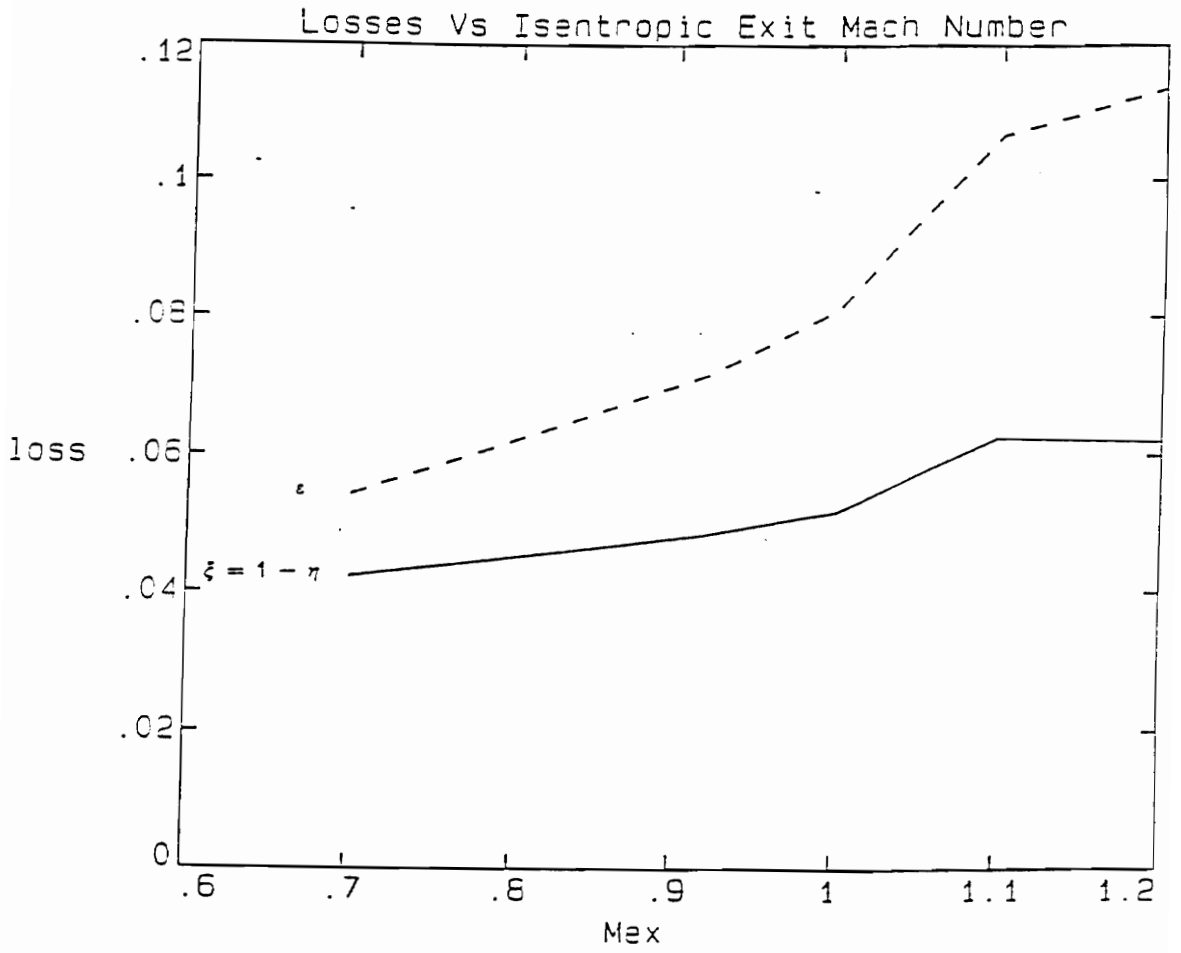

Figure 20. Calculated Loss Coefficients for Re = 1E6.

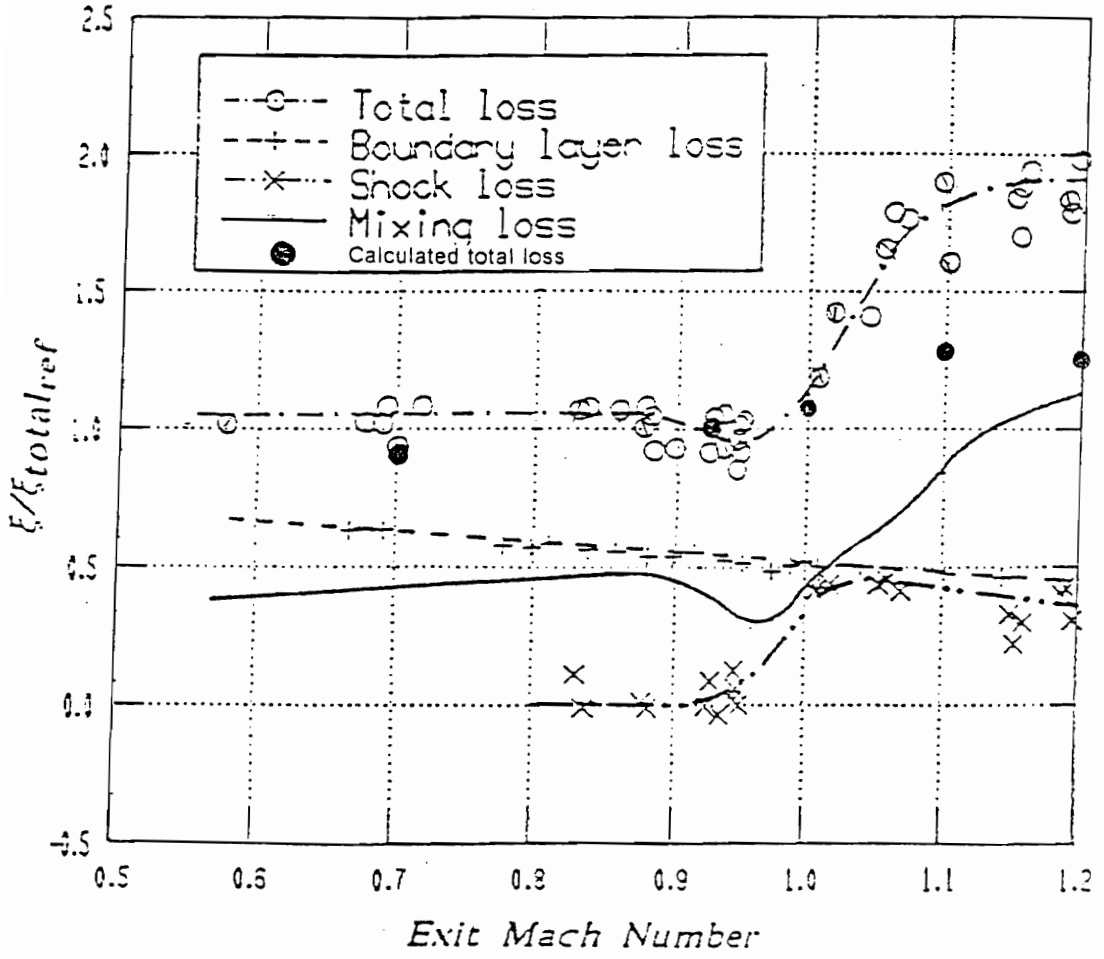

Figure 21. Comparison of the Non-Dimensionalized Primary Loss Coefficients

Data of Mee et al., 1992a	MEFP Calculation	
*	———	Boundary Layer Velocity Profile
o	– – – – –	Boundary Layer Density Profile

$$\frac{S}{S_0} = 0.755, \quad \text{Re} = 1\text{E}6, \quad M_2 = 0.92$$

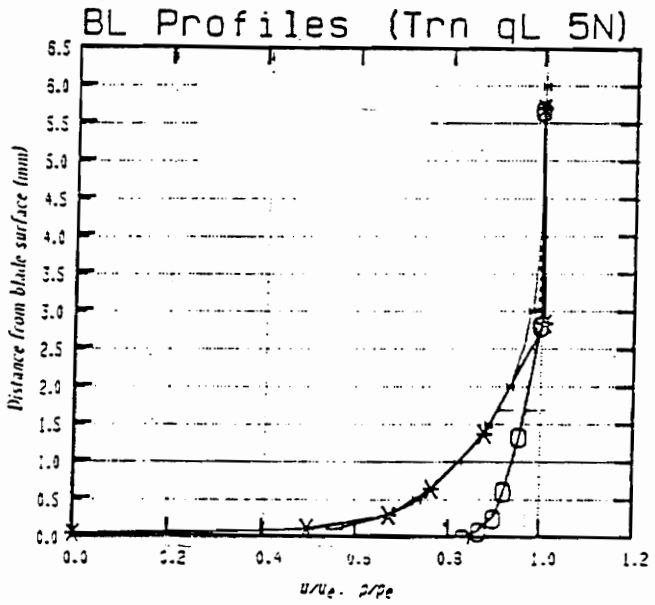

Figure 22. Comparison of Boundary Layer Velocity and Density Profiles

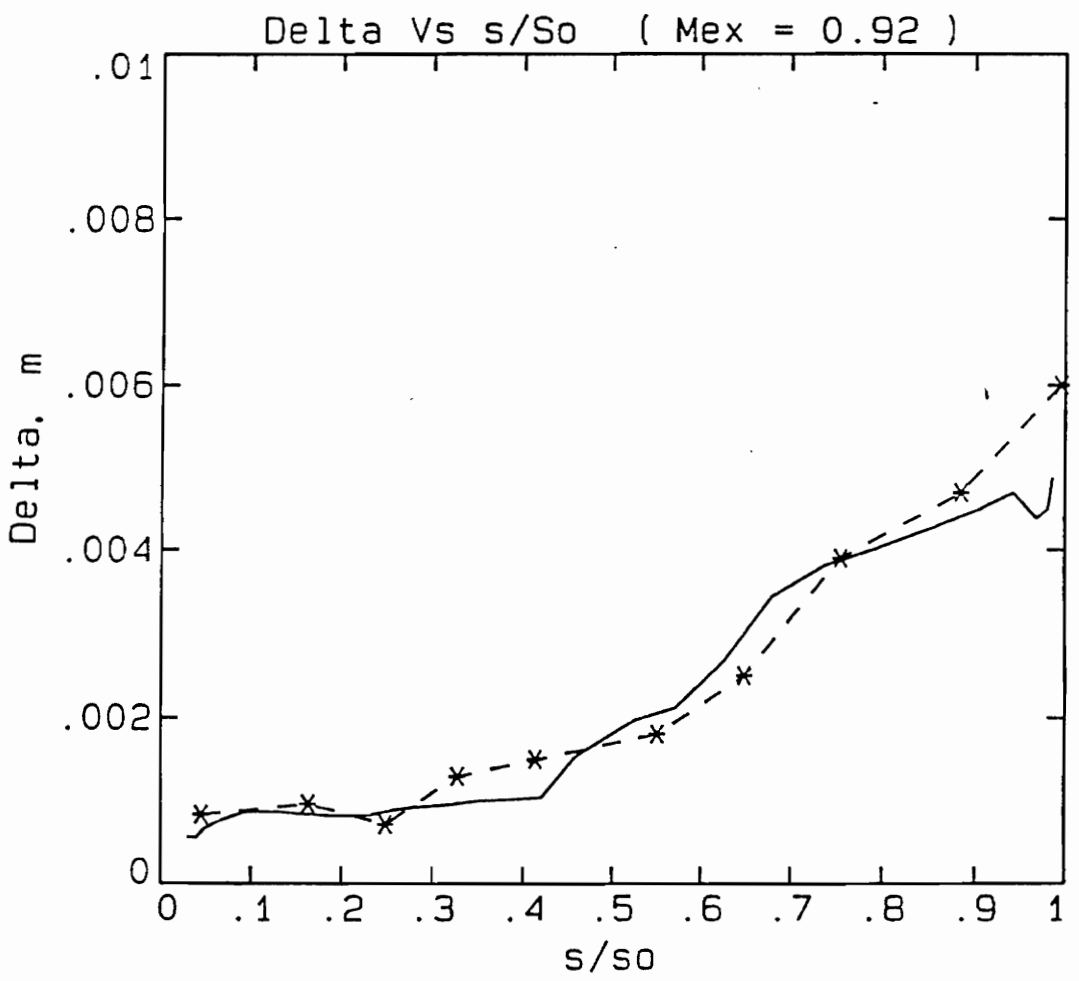

Figure 23. Comparison of Boundary Layer Thickness; data of Mee et al., 1992a

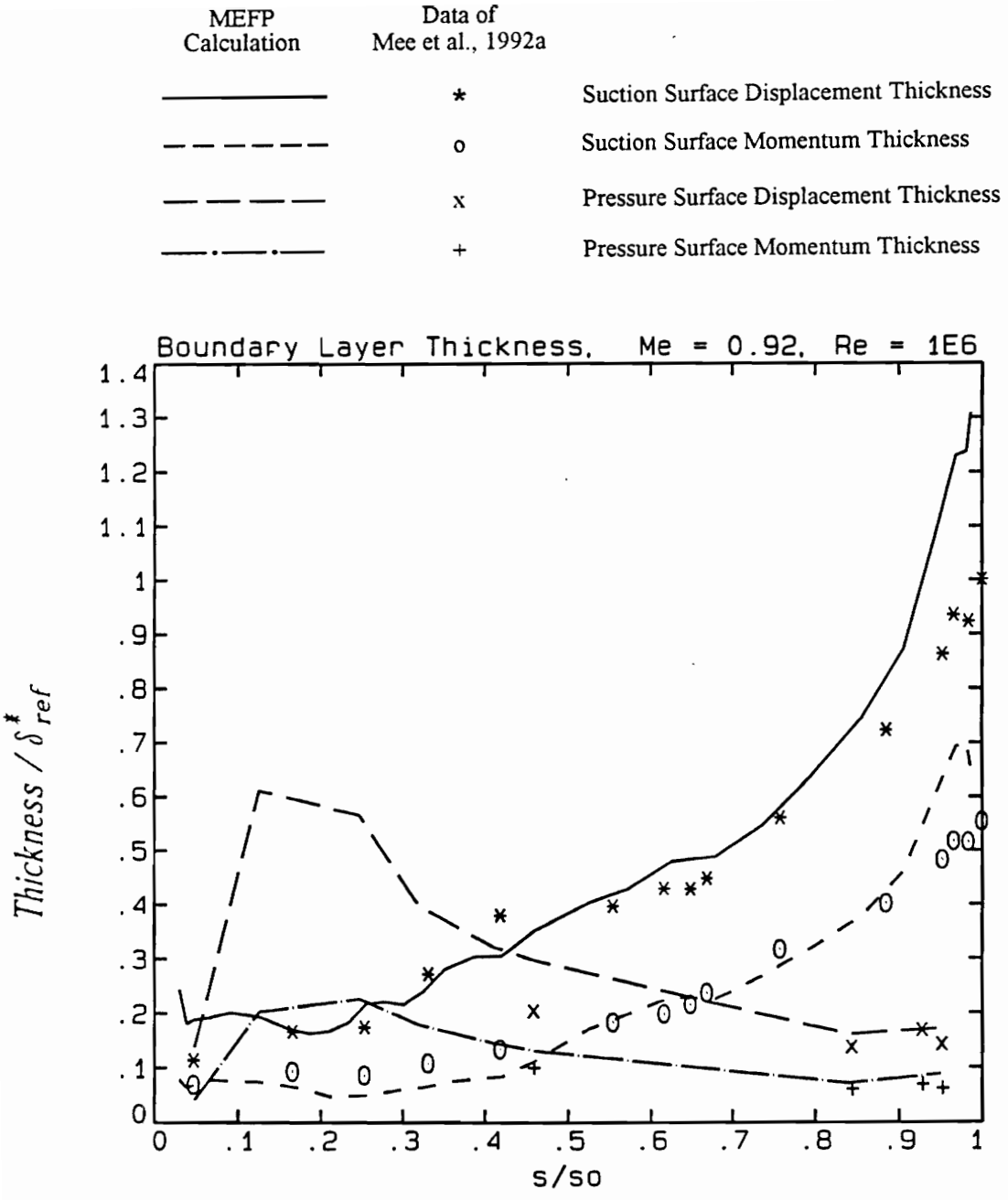

Figure 24. Comparison of Boundary Layer Parameters;data of Mee et al., 1992a

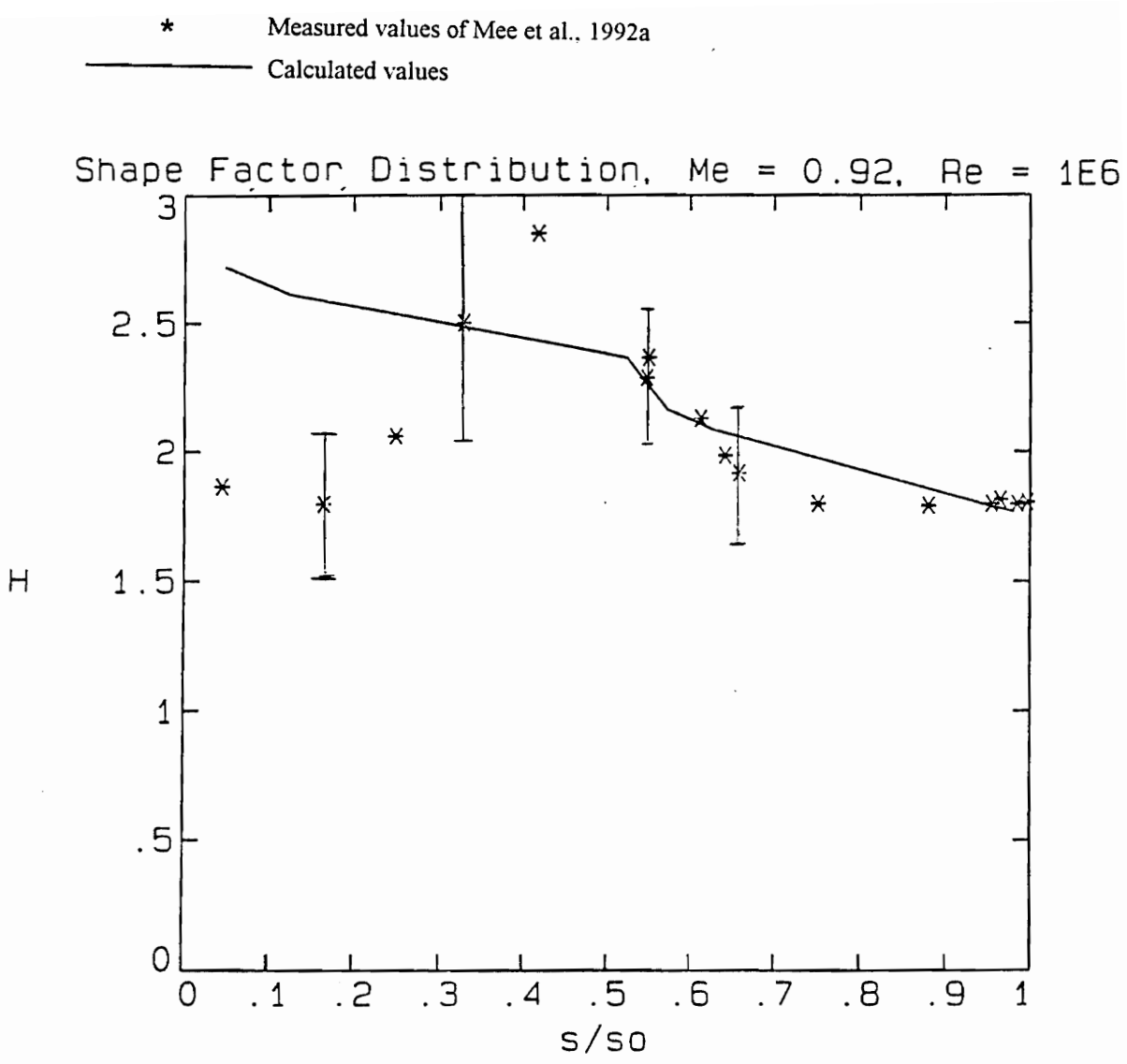

Figure 25. Comparison of Shape Factors; Data of Mee et al., 1992a

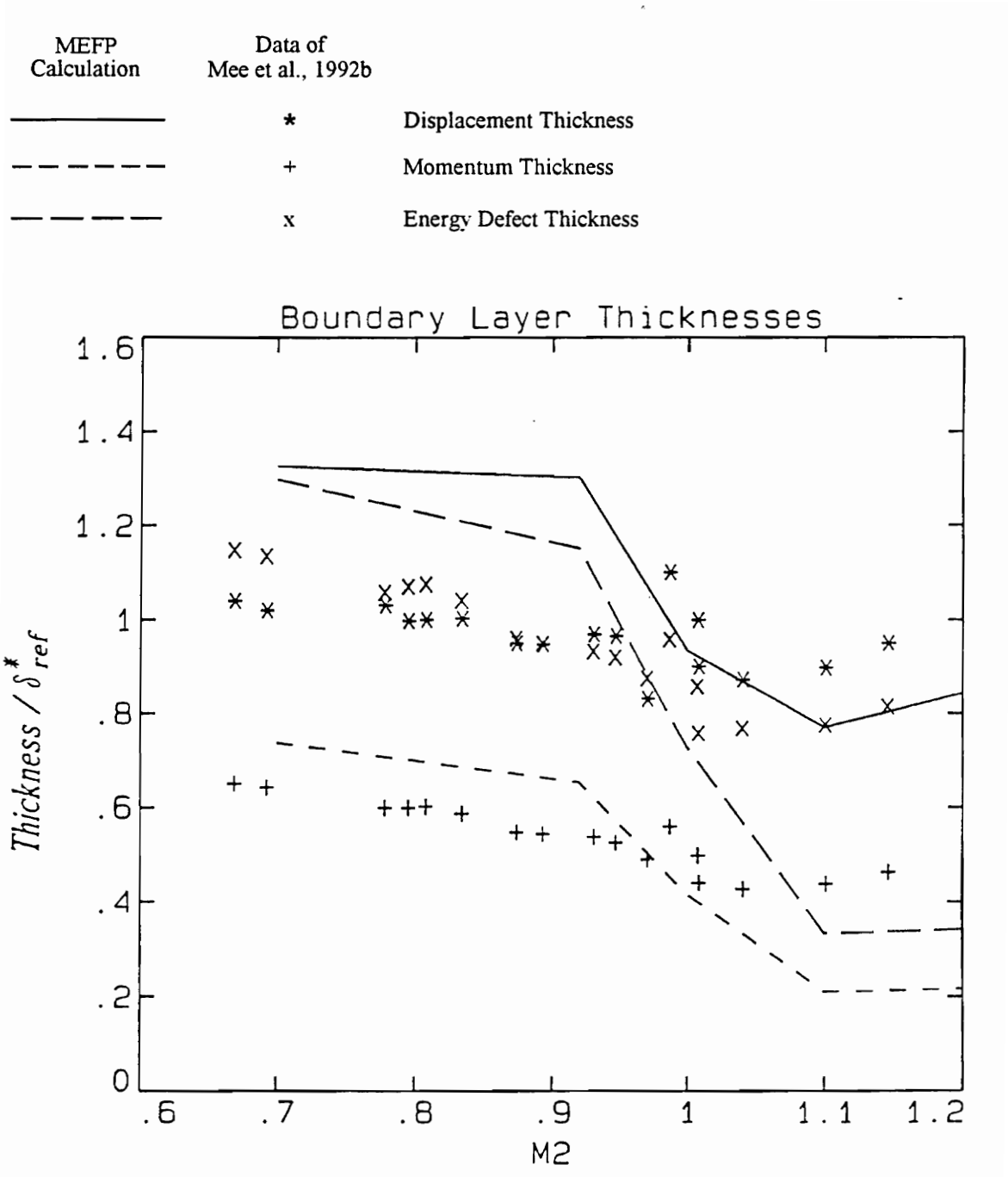

Figure 26. Variation of Boundary Layer Thicknesses with Mach Number

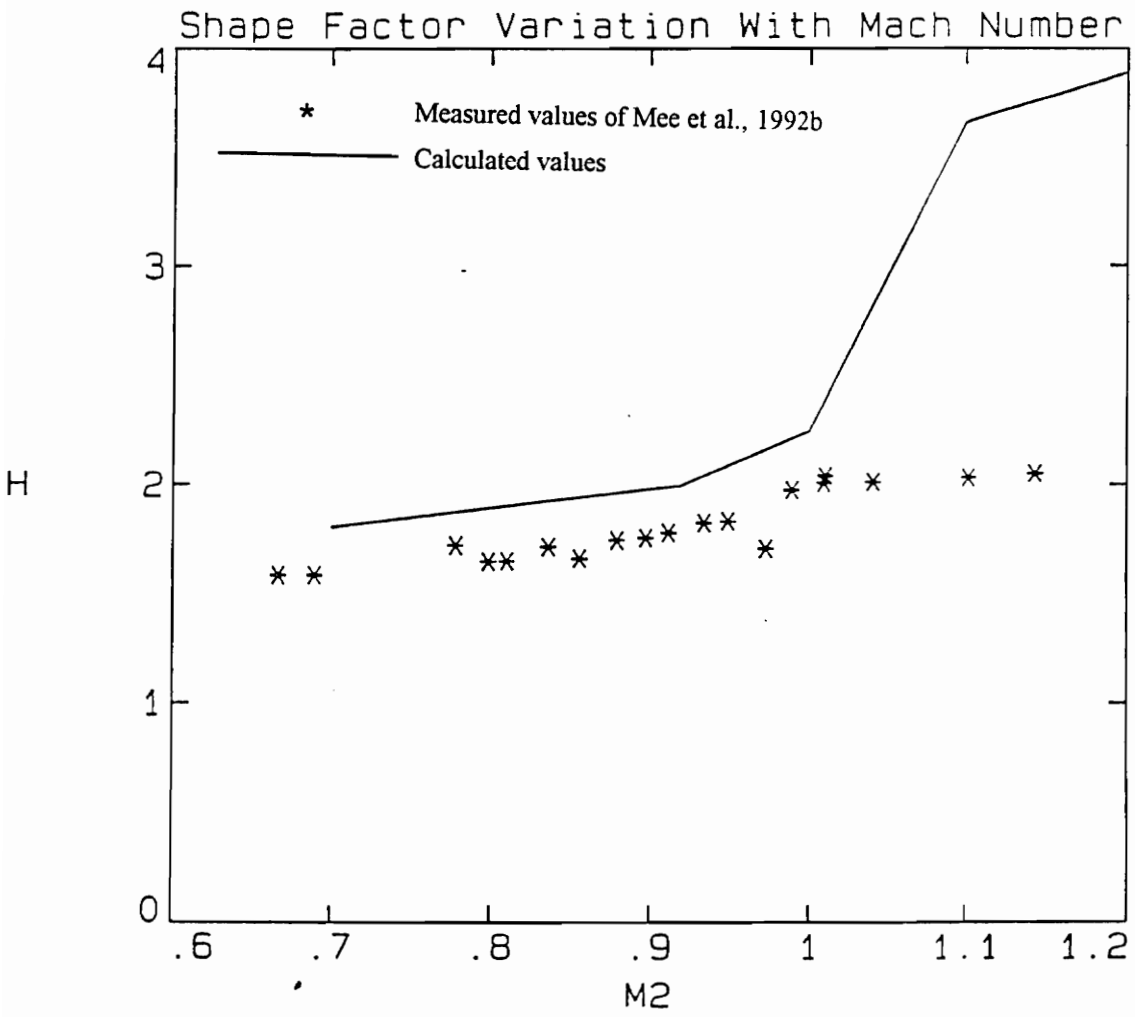

Figure 27. Variation of Shape Factor with Mach Number

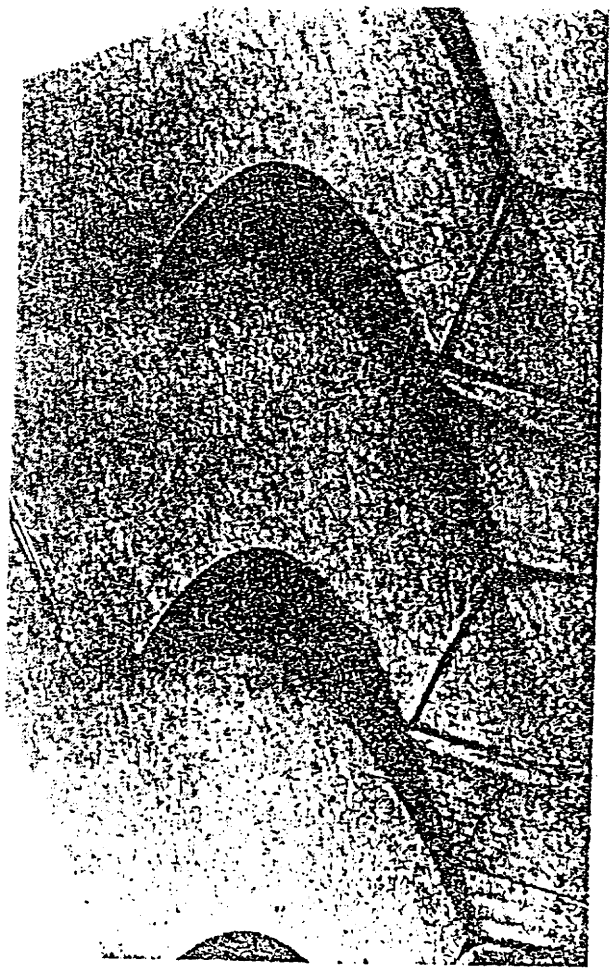

Figure 28. Schlieren Picture of the RT27 Flowfield, $M_2 = 1.1$

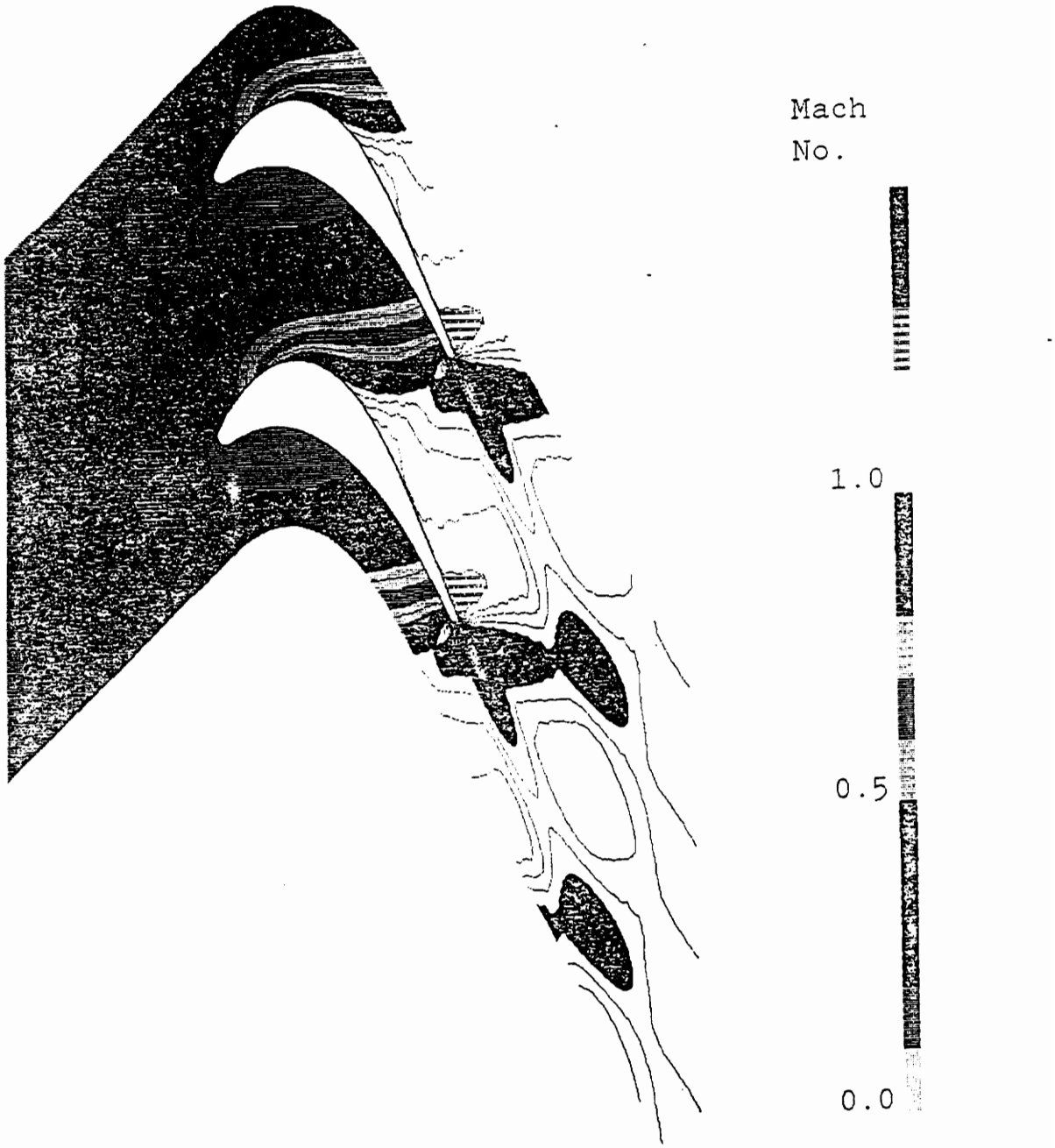

Figure 29. RT27 - Calculated Mach Number Plot, $M_2 = 1.1$

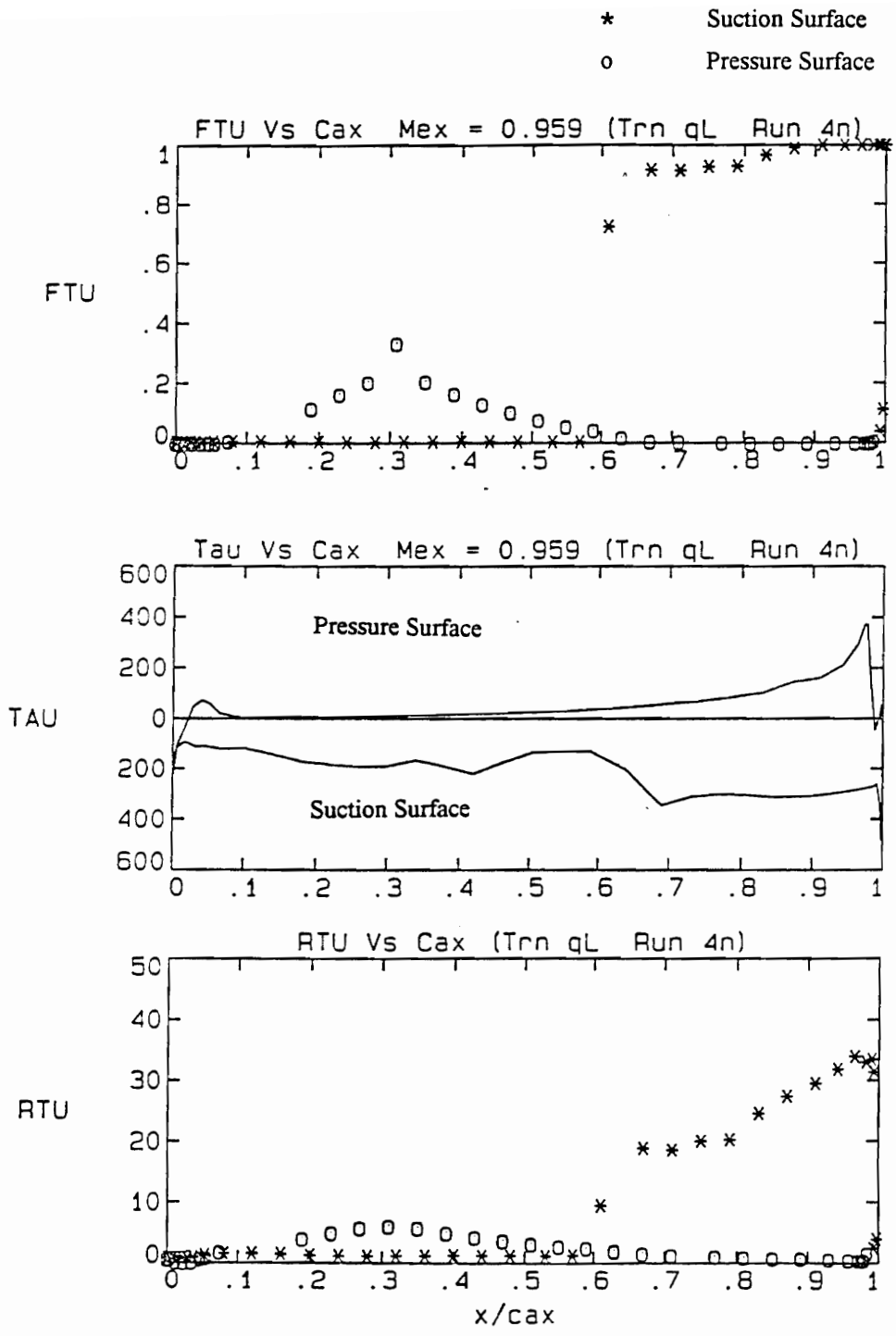

Figure 30. Transition plots for Heat Transfer Calculations; $Re = 1E6$, $M_2 = 0.959$

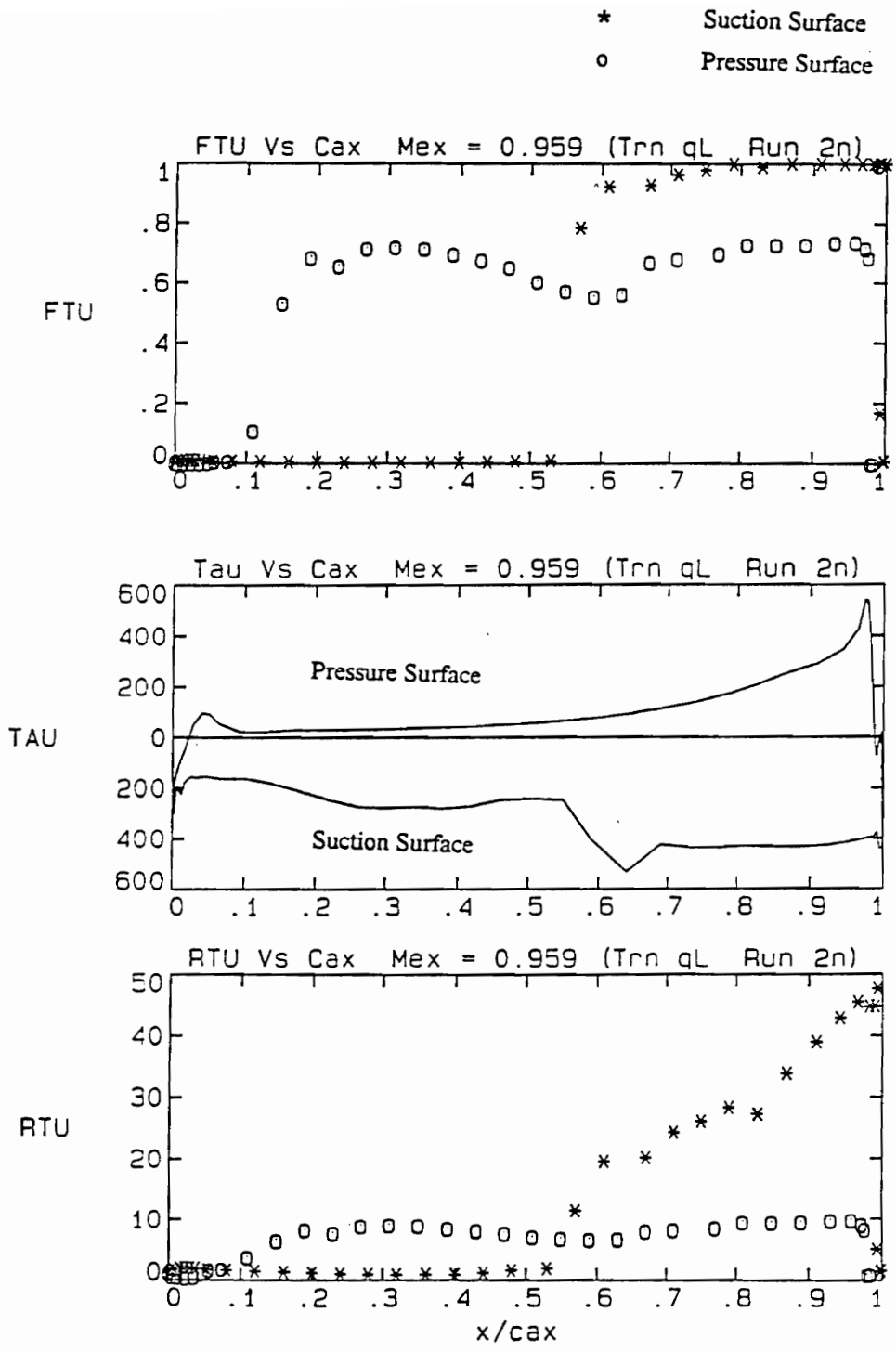

Figure 31. Transition plots for Heat Transfer Calculations; $Re = 2E6$, $M_2 = 0.959$

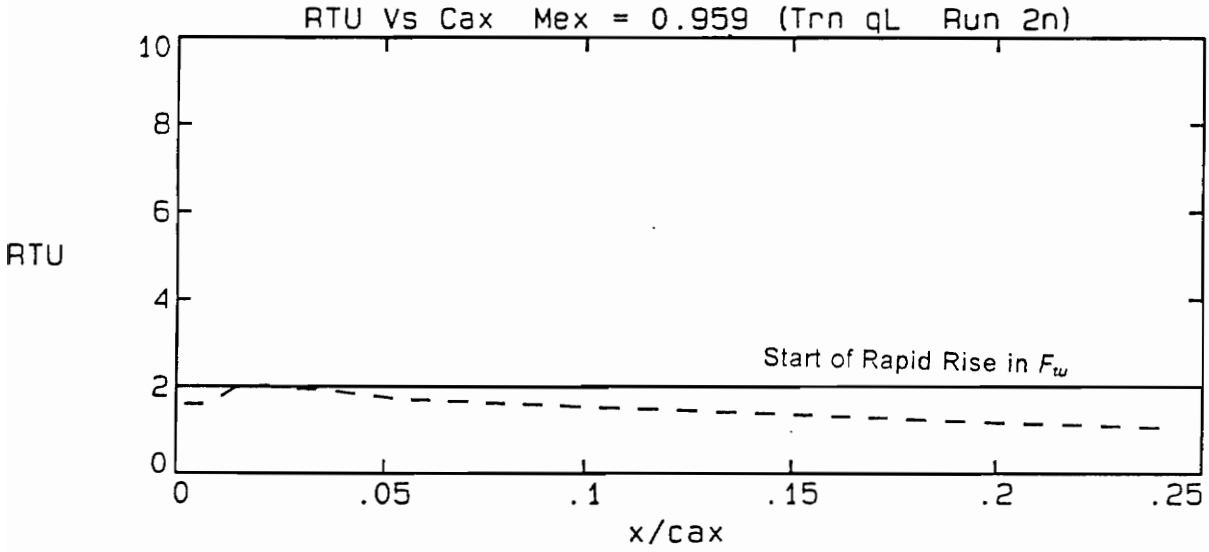

Figure 32. Reynolds Number of Turbulence - Nearness to Transition; $Re = 2E6$, $M_2 = 0.959$

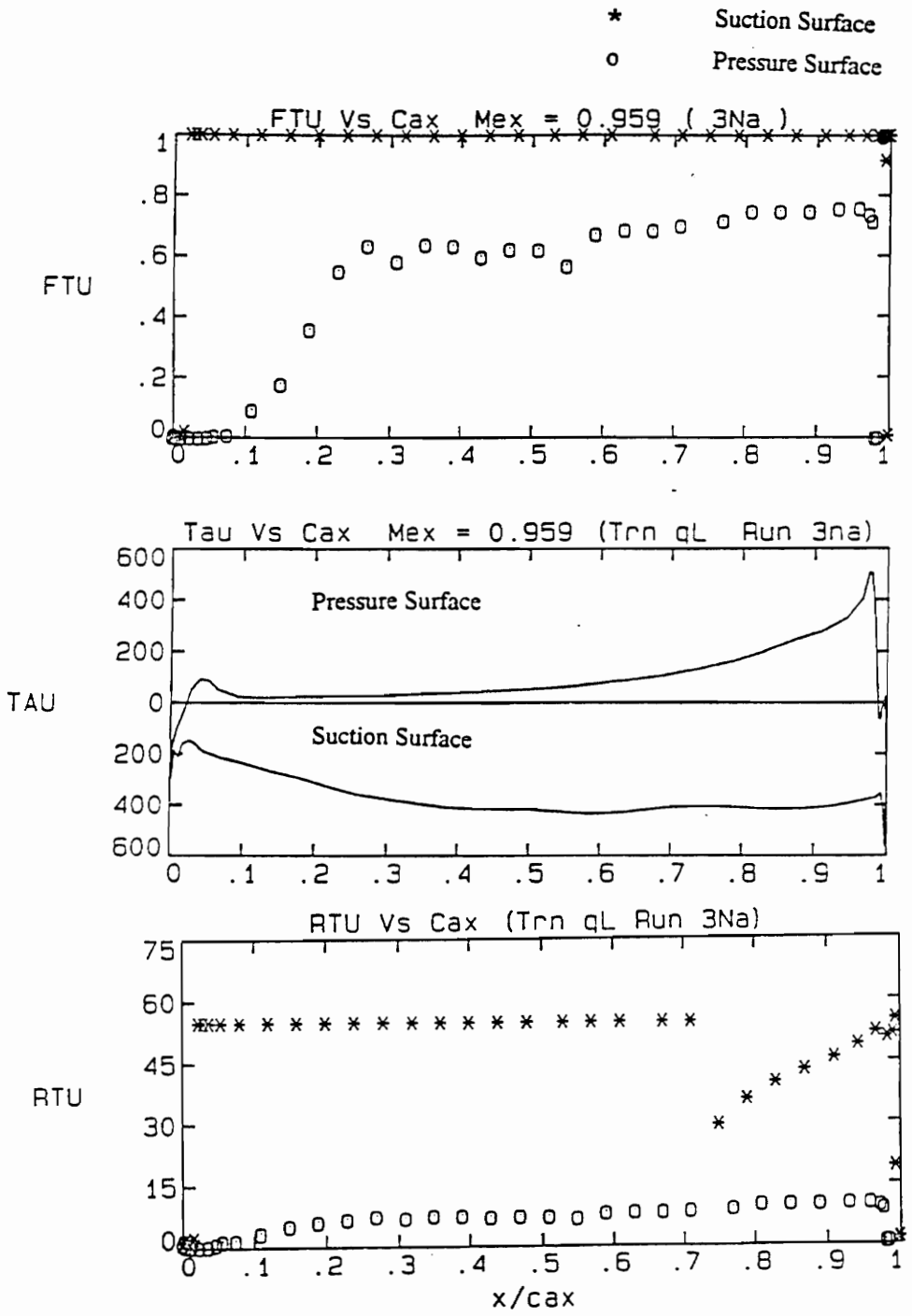

Figure 33. Transition plots for Heat Transfer Calculations; $Re = 2E6$, $M_2 = 0.959$

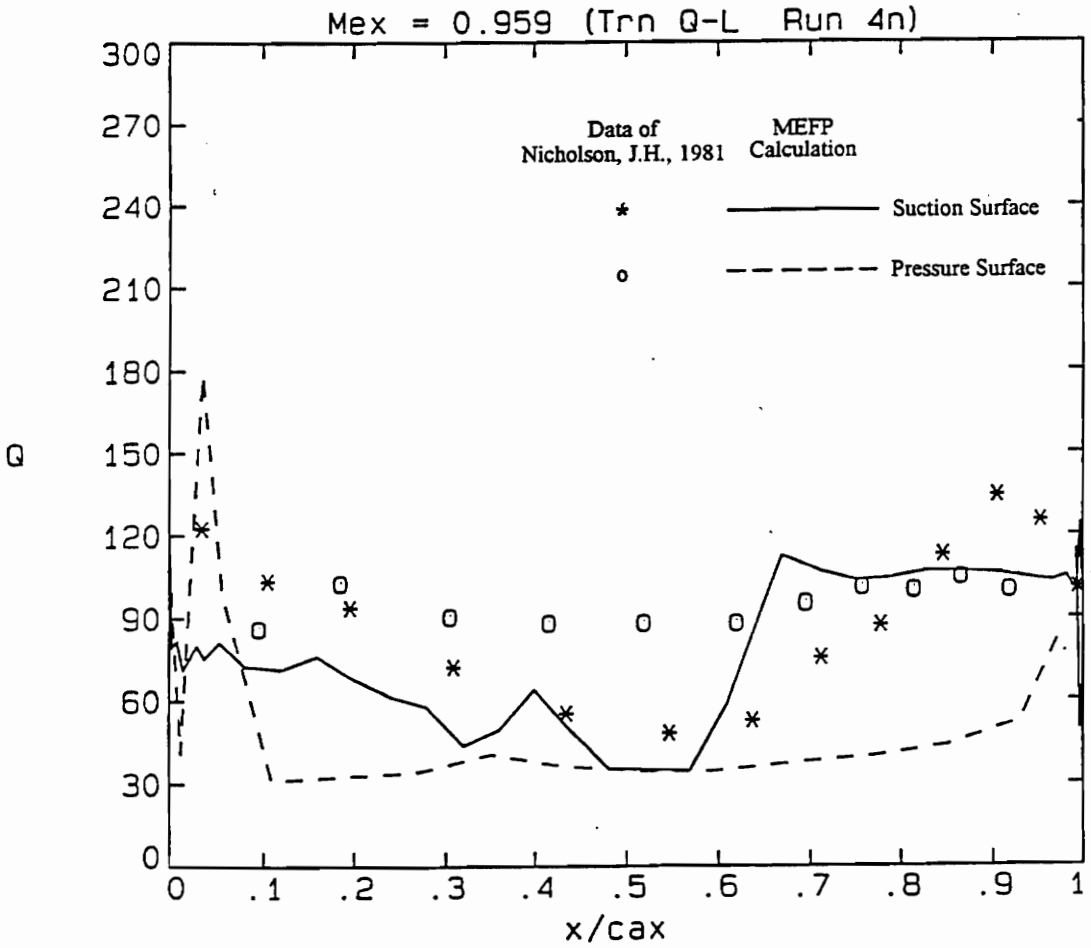

Figure 34. Heat Transfer Rate, ($\frac{kW}{m^2}$), $M_2 = 0.959$, $Re = 1E6$

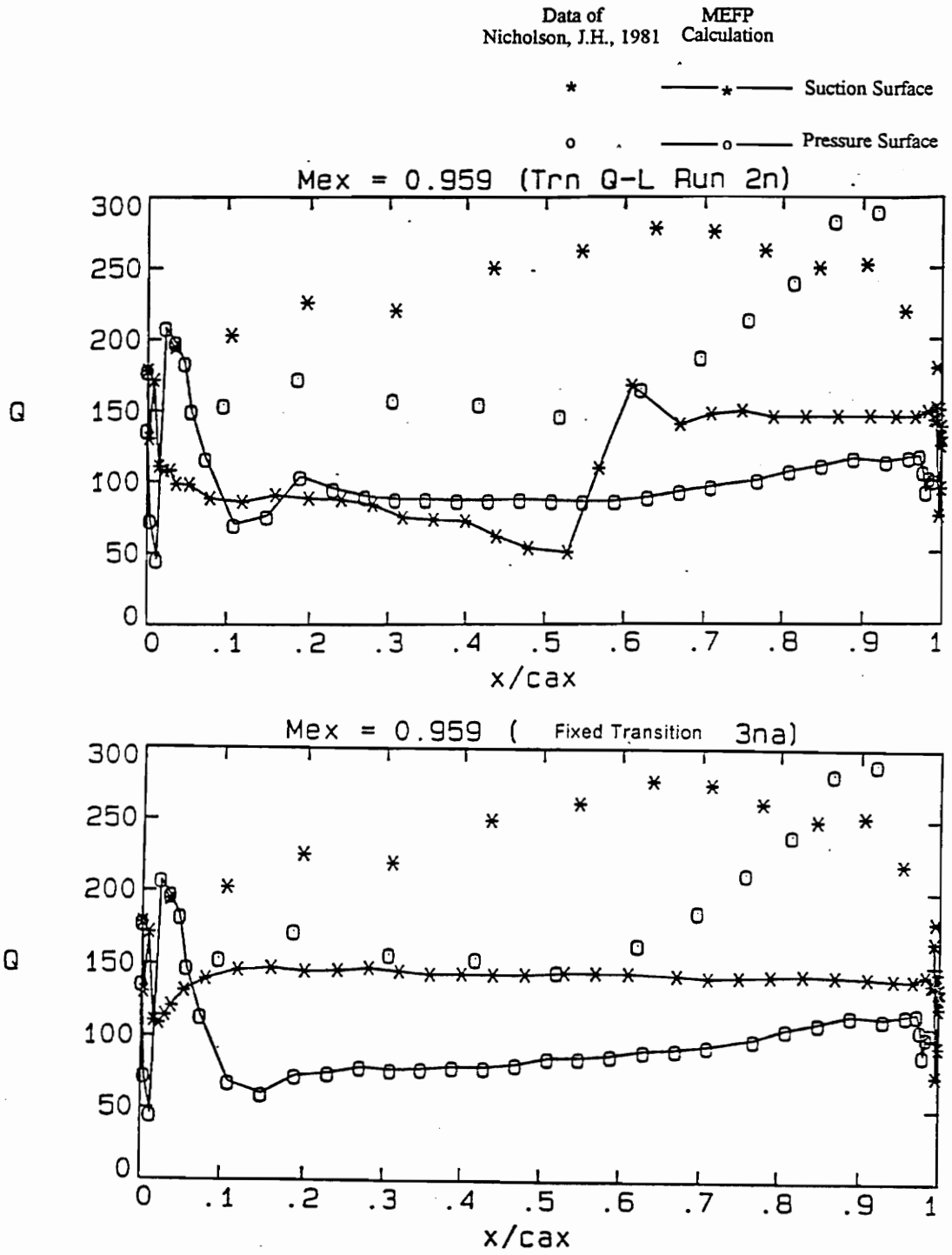

Figure 35. Heat Transfer, $(\frac{kW}{m^2})M_2 = 0.959$, $Re = 2E6$

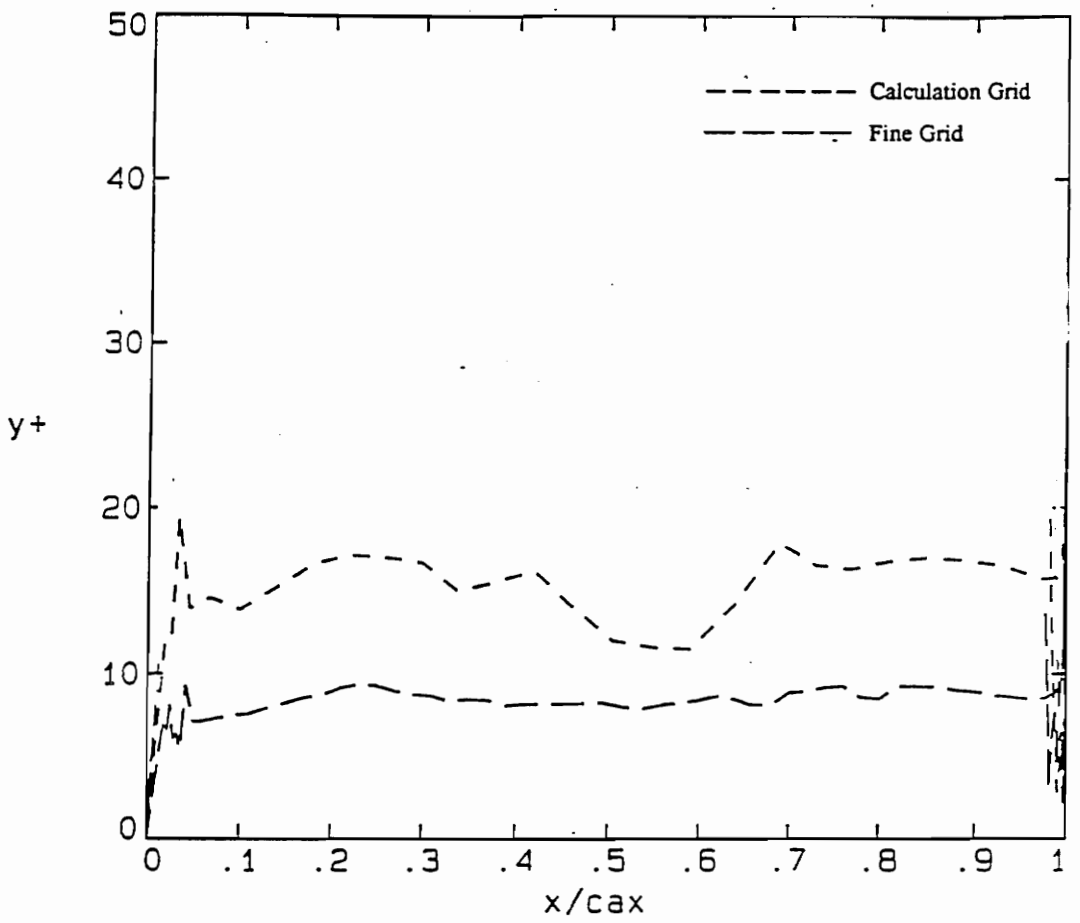

Figure 36. RT27 Computed y^+ Distributions For the Two Grids

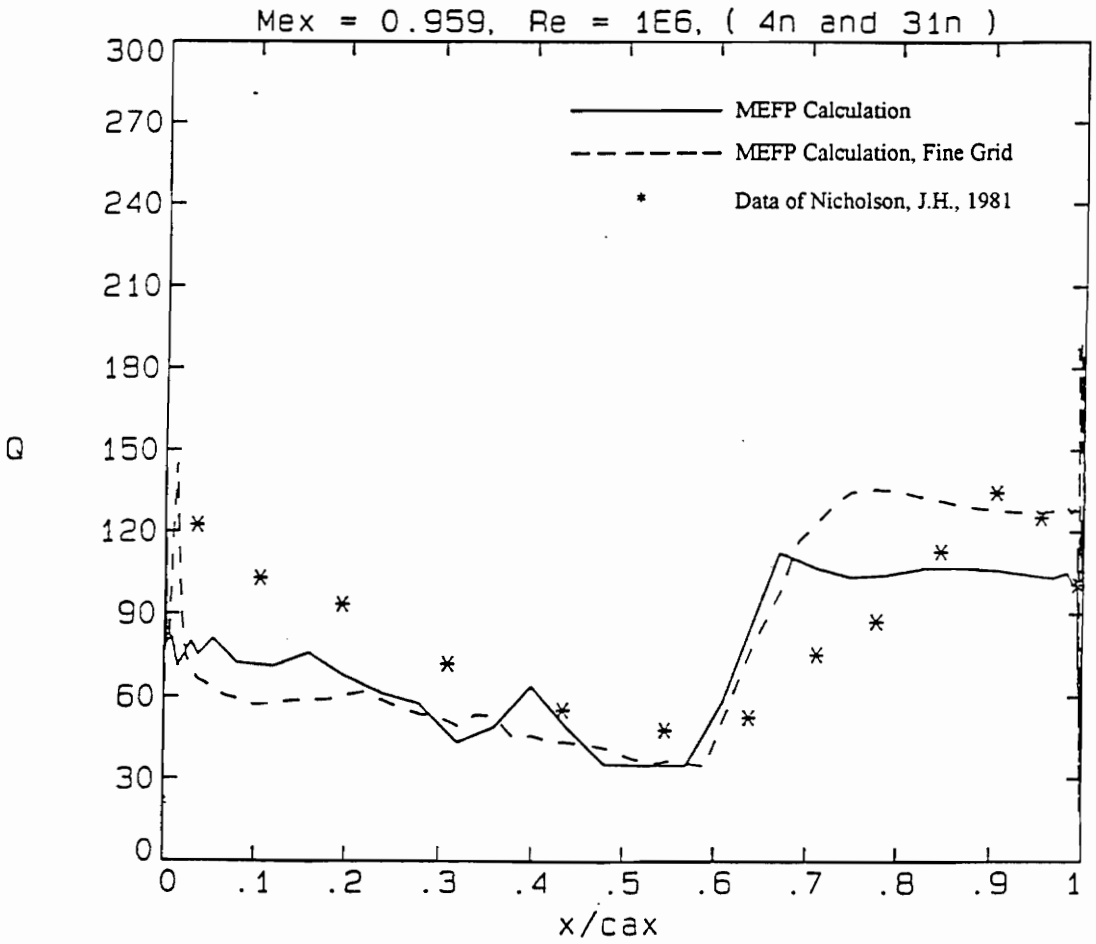

Figure 37. RT27 Variation of Computed Suction Surface Heat Transfer With Gridding ($\frac{kW}{m^2}$)

5.0 ACE Turbine Rotor Cascade

5.1 Geometry

5.1.1 Introduction

Extensive 2-D flow calculations were performed on the Rolls-Royce RD or ACE blade profile. The ACE is a high pressure gas turbine rotor section for operation at transonic speeds with a design isentropic exit Mach number of 1.15. Experimental data is available for the ACE turbine cascade from the studies of Haller, B.R.,1980. Computational work with reference to the flow field of the ACE has been reported by Dawes,W.N., et al.,1986, Camus,J-J., et al., 1983, Hah, C., and Selva., R.J., 1990, and Moore,J., and Moore, J.G., 1989. The nature and extent of the available data, pertinent to this study is summarized in Table 13.

A series of calculations was performed for exit Mach numbers in the transonic range. The flow was variously modelled as being with laminar, turbulent and transitional boundary layers.

5.1.2 The Profile

The geometry of the ACE turbine blade was made available by Rolls-Royce Limited for the purposes of the present study. It is "Plane Section Eng 8900 Turb HP ST 1 Blade Sec 50 Ver 3" from the G656 Version 2A2 Blade File utility on 30 Oct 88. The ACE turbine blade is designed for operation at transonic speeds. Like any high pressure turbine, the blade has a thick coolable trailing edge. The present calculations are for a smooth blade profile. The ACE rotor profile is shown in Figure 38, along with the key parameters of the profile.

5.1.3 Calculation Grid

The calculation grid used for the present series of calculations is shown in Figure 39. It is composed of 4602 points with 59, 39 and 2 planes each in the i, j and k directions respectively. A total of 76 points are used to envelope the blade profile.

For the flow conditions used by Haller, B.R., 1980, $\frac{\delta_1}{p} \simeq 0.00032$. For the present grid, a fixed normal distance for the near-wall point was not specified. Instead, within the blade passage, the near-wall points were placed at a fixed fraction, 0.0008 of the local blade-to-blade distance. Similar distances were used at the leading and trailing edges, giving typical normal near-wall distances / pitch of approximately 0.0006.

5.2 Summary of the Calculations

The flow was variously modelled as laminar with the onset of turbulence set at 95 % chord, fully turbulent, and transitional. The transitional and laminar flow results were solved for with 300 passes while the turbulent model was solved with 140 passes.

The parameters used to calculate the flowfield with the different flow models are tabulated in Tables 14 and 15.

5.3 Calculation Results

5.3.1 Losses in the Different Models

Figure 40 shows the mixed-out losses obtained from the transitional q-L and turbulent q-L models in comparison with the available data. Both the models predict the losses to within a percentage point. The turbulent q-L model seems to predict the losses better in the supersonic range and the transitional q-L model seems better in the subsonic range.

Figure 41 plots the mixed-out losses quantified in terms of the primary efficiency. The agreement between the predicted and measured losses is similar to that seen in Figure 40.

The different loss curves indicate that the calculations have captured the sharp rise in losses near $M_2 = 1$. Mee et al., 1992b, suggest that the rise in the overall losses is primarily due to an increase in the shock losses around an exit Mach number of one , and due to increased mixing losses at higher exit Mach numbers. The measured loss curve seems to level

off at around $M_2 = 1.2$. The calculations seem to indicate a continued trend to higher loss with higher exit Mach number.

5.3.2 Density Contours

Figure 42 shows the measured and computed density contours for $M_2 = 0.988$ and Figure 43 for $M_2 = 1.2$. The contour plots show a trailing edge shock propagating towards the suction side of the adjacent blade. There is also evidence of a weak trailing edge shock propagating downstream from the suction surface.

5.3.3 Comparison with Blade Loading Data

Figures 44-46 show the isentropic Mach number distributions plotted against axial distance. The results are for the three computational exit Mach numbers of 0.9, 0.988 and 1.2 and these correspond closely with Haller's measurements for $MA_{2k} = 0.905$, 0.987, and 1.191.

The experimental pressure distributions in Figures 44-46 were mainly obtained from Haller's tabulated data provided by M.Howard (1992). This data (the stars) was for a blade geometry with a set of film cooling holes at 60 percent of axial chord. In his thesis, Haller also shows data for a smooth blade, and in Figures 44 and 46, the points with a significant difference in measured wall static pressure are marked with a circular symbol. It appears that the cooling holes affected the flow such that the peak Mach number on the suction surface was higher than for the smooth blade. This may indicate an increase in the strength of the shock wave which could lead to an increase in the shock and boundary layer losses.

The present calculations are modelling flow over a smooth blade and are therefore not expected to show those local peaks in suction surface Mach number. The overall pressure

distributions are predicted well by the two models. In fact there is very little difference between the results with the transitional and turbulent boundary layers.

5.3.4 Trends with Variations in Exit Mach Number

Figures 47 and 48 show the calculated surface Mach number and shear stress distributions as a function of the tangent chord for the transitional q-L model. These figures allow a comparison of the calculated distributions at the various exit Mach numbers. Variations are found to occur mainly on the aft or uncovered part of the blade suction surface.

The two figures show evidence of a passage shock that grows in strength with increasing exit Mach number.

The available experimental data in Figures 44-46 indicates that the flow accelerates on the suction surface beyond the shock boundary layer interaction region at the higher exit Mach numbers while slowing down at the lower values of the exit Mach number. This trend is predicted in the calculations. At $M_2 = 1.2$, the calculated reacceleration is somewhat larger than that shown in the measurements.

The adverse pressure gradient at the lower exit Mach numbers has little effect of significance on the shear stresses in the turbulent q-L model, but is sufficient to separate the flow in the transitional q-L regime (see Figure 47). These transitional stress distributions are shown separately for easier perusal in Figure 48. At $M_2 = 0.9$, the suction side flow stays separated for a fourth of the tangent chord before reattaching while at $M_2 = 1.2$, the flow reaccelerates just as the shear stresses go to zero.

5.3.5 Blade Performance with a Laminar Boundary Layer

The flow was modelled with a laminar boundary layer with an exit Mach number of 0.8. The distributions for the laminar calculation are shown in Figure 49. An adverse pressure gradient to the flow exists over half the suction surface length. This almost separates the flow as is shown in the shear stress distribution. The shear stress goes to zero for a third of the suction surface. This could be an indication toward the design philosophy of this transonic turbine rotor.

Table 13. ACE Rotor Profile - Summary of available data

Reference	Nature of Data	Details
Haller, B.R., 1980	Experimental	Cambridge University
Camus, J-J., 1983	Experiments and Calculations	Cascade testing 3-D Potential Flow Calculations
Dawes, W.N., 1986	Computations	Time Marching Solutions Turbulent Boundary layer
Moore, J., 1989	Computations	Pressure Correction Method for the N-S Equations Laminar Boundary layer.

Table 14. Parameters for the different runs

No.	M_2	P_2/P_0	Flow Model
1	0.8	0.656	Laminar
2	0.9	0.591	Trb q-L, Trn q-L
3	0.95	0.560	Trb q-L, Trn q-L
4	0.988	0.536	Trb q-L, Trn q-L
5	1.05	0.498	Trb q-L, Trn q-L
6	1.10	0.468	Trb q-L, Trn q-L
7	1.15	0.440	Trb q-L, Trn q-L
8	1.20	0.412	Trb q-L, Trn q-L

Table 15. Calculations: Key Parameters

Calculations: Key Parameters

$$P_0 = 159519\,Pa$$

$$\mu_l = 4 \times 10^{-7} \times T^{0.68}$$

$$T_0 = 288.15\,K$$

$$q_{inlet} = 0.01\,U_{inlet} = 5.71\,m/s$$

$$L_{fre} = 0.00077\,m$$

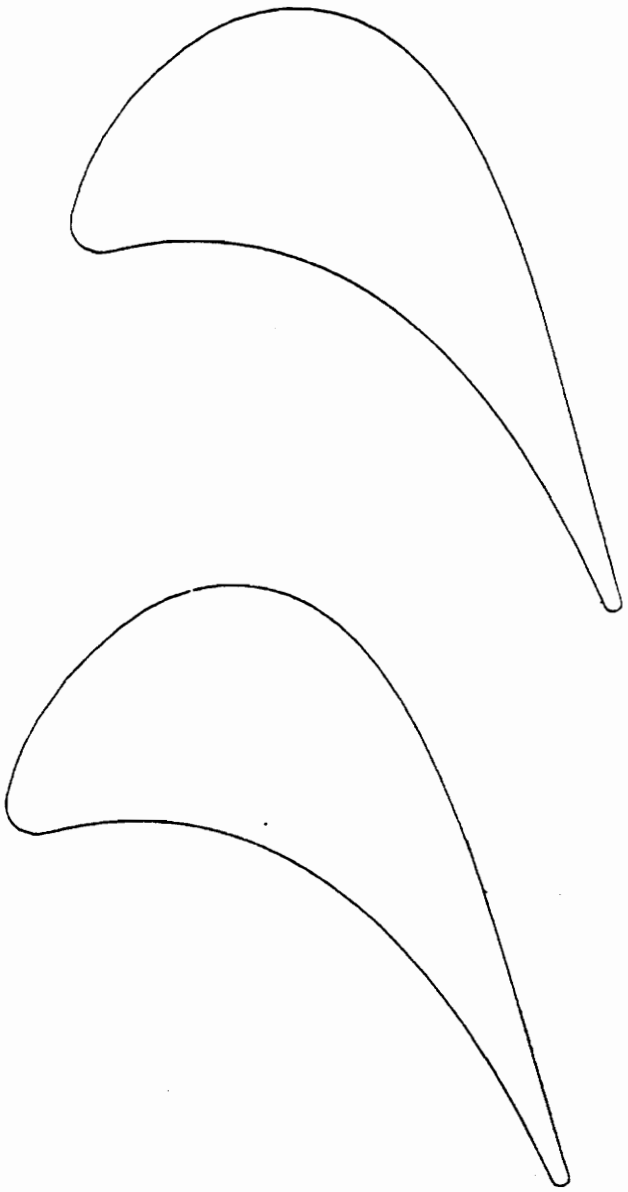

Blade Chord	=	41.7 mm
Pitch / Chord	=	0.843
Design Inlet Flow Angle	=	56.7 deg
Design Exit Flow Angle	=	66.0 deg
Design Exit Reynolds Number	=	0.92E6
Design Exit Mach Number	=	1.15
Throat / Pitch	=	0.381
TE Radius / Pitch	=	0.0014
Stagger Angle	=	29.6 deg
Nominal Exit Angle	=	62.4 deg

Figure 38. ACE Blade Profile

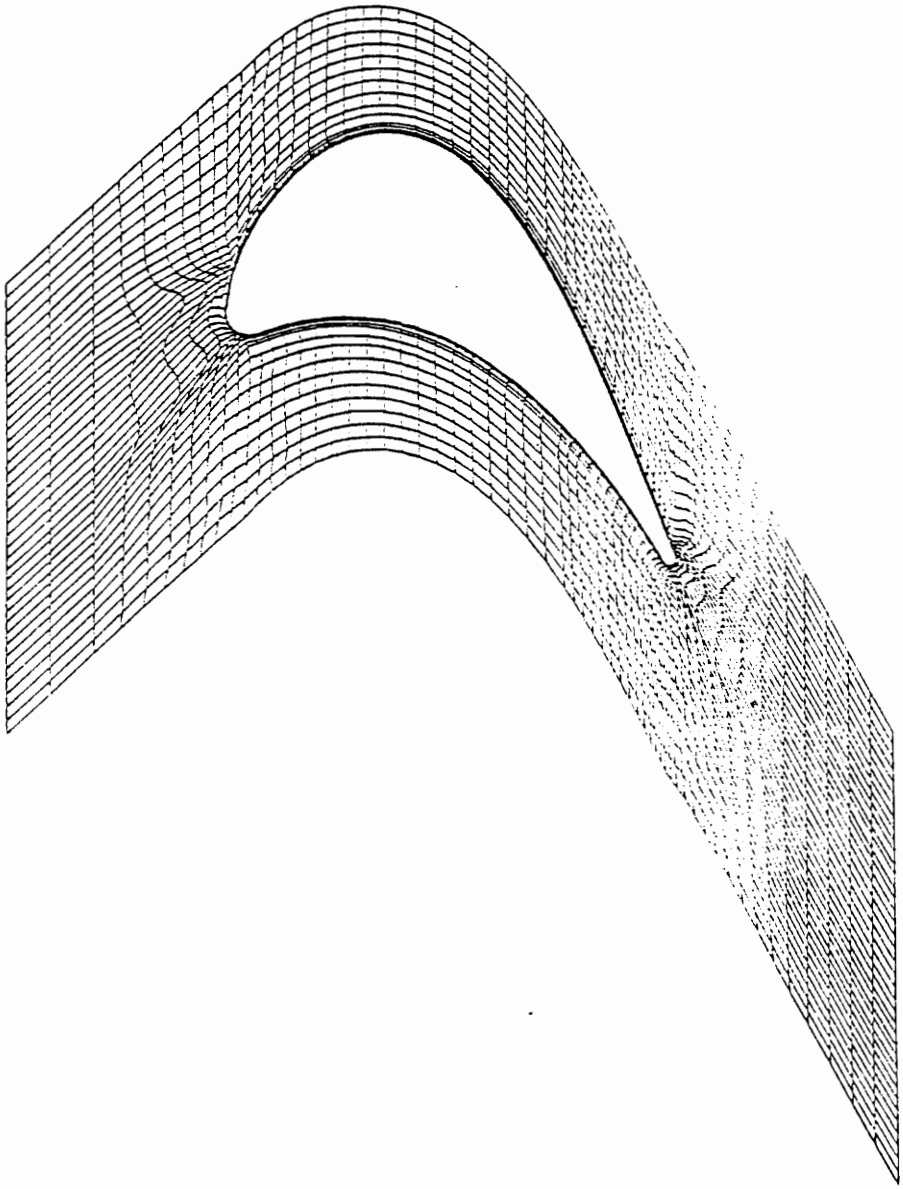

Figure 39. ACE Calculation Grid

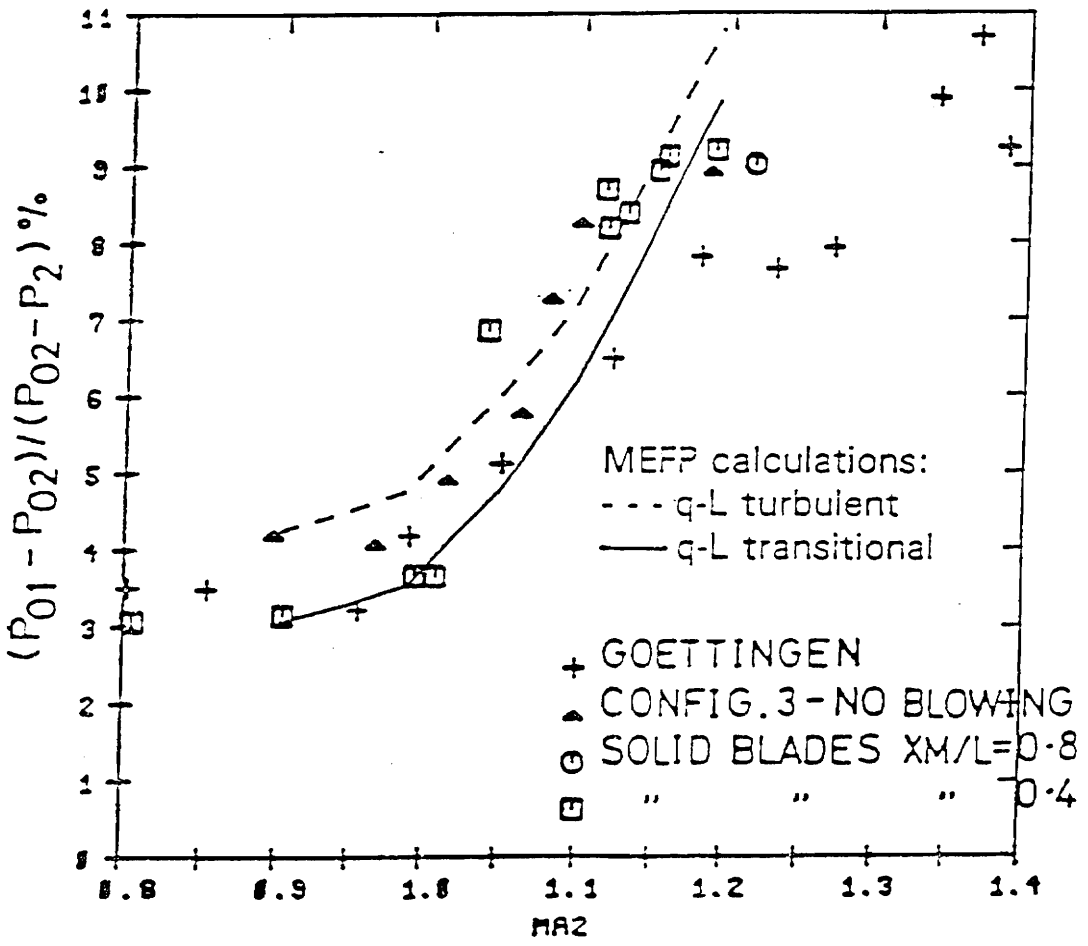

Figure 40. ACE Overall Mixed-out Loss - Comparison with Data

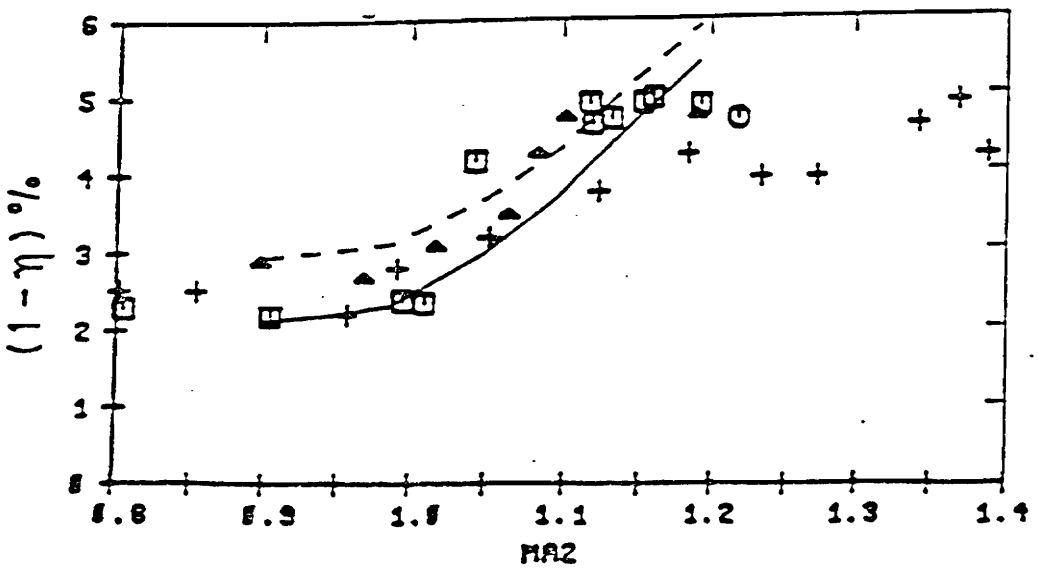

Figure 41. ACE Overall Losses in Terms of the Primary Efficiency

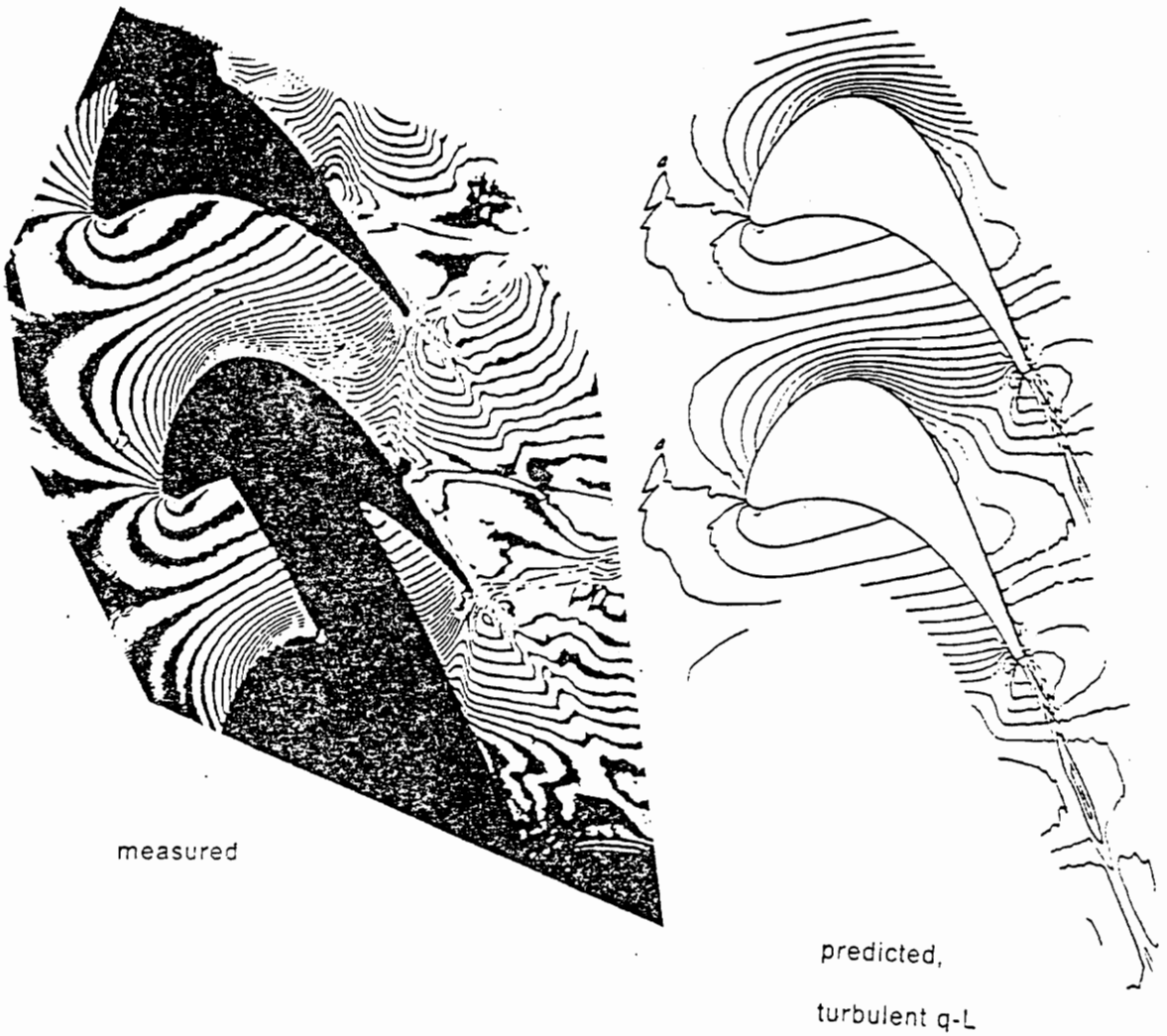

Figure 42. ACE Density Contours, $M_2 = 0.988$

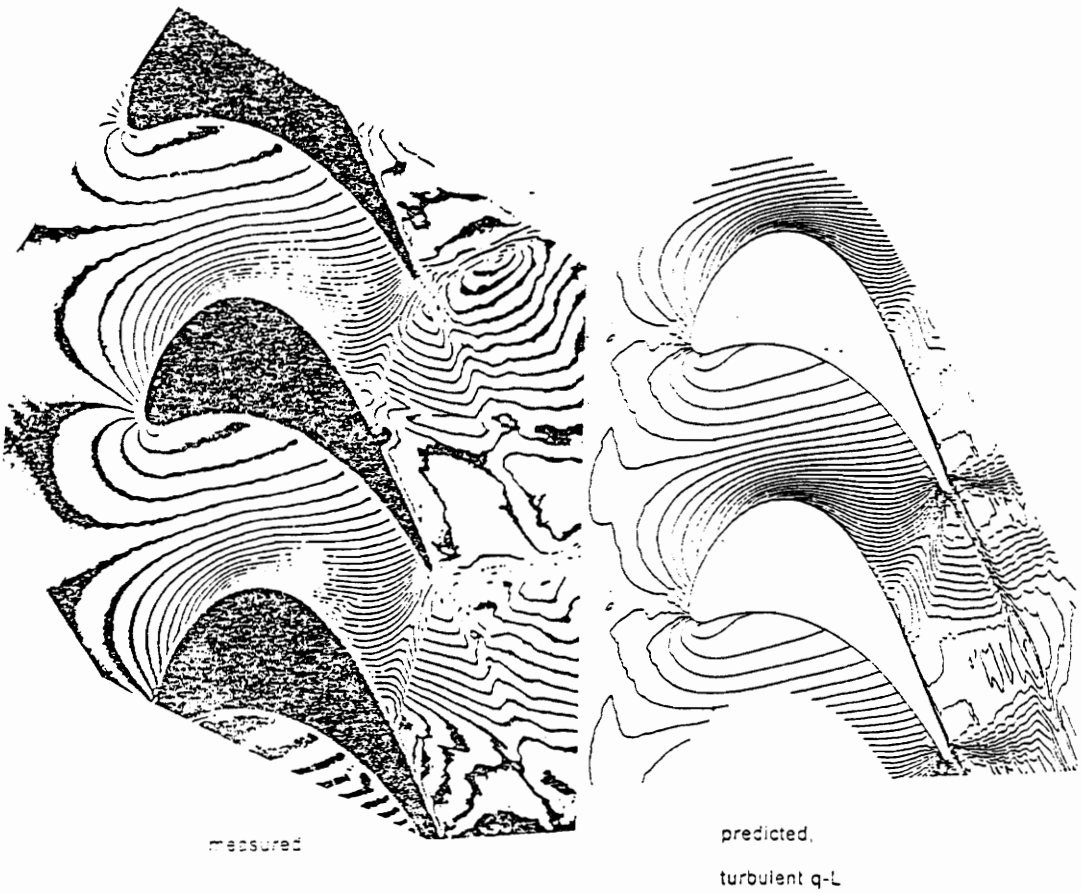

Figure 43. ACE Density Contours, $M_2 = 1.2$

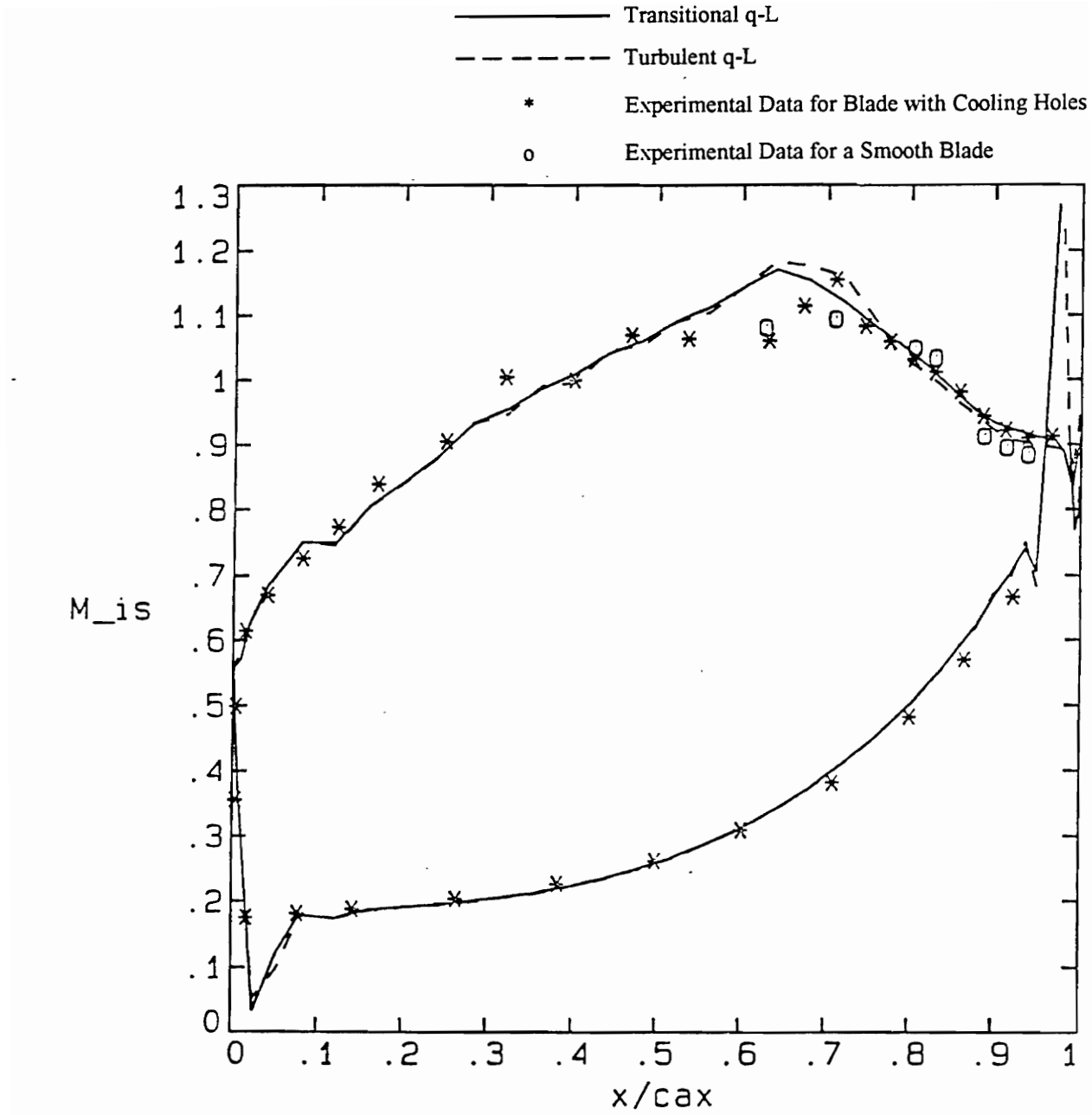

Figure 44. ACE M_{is} Vs C_{ax}, M_2 = 0.9

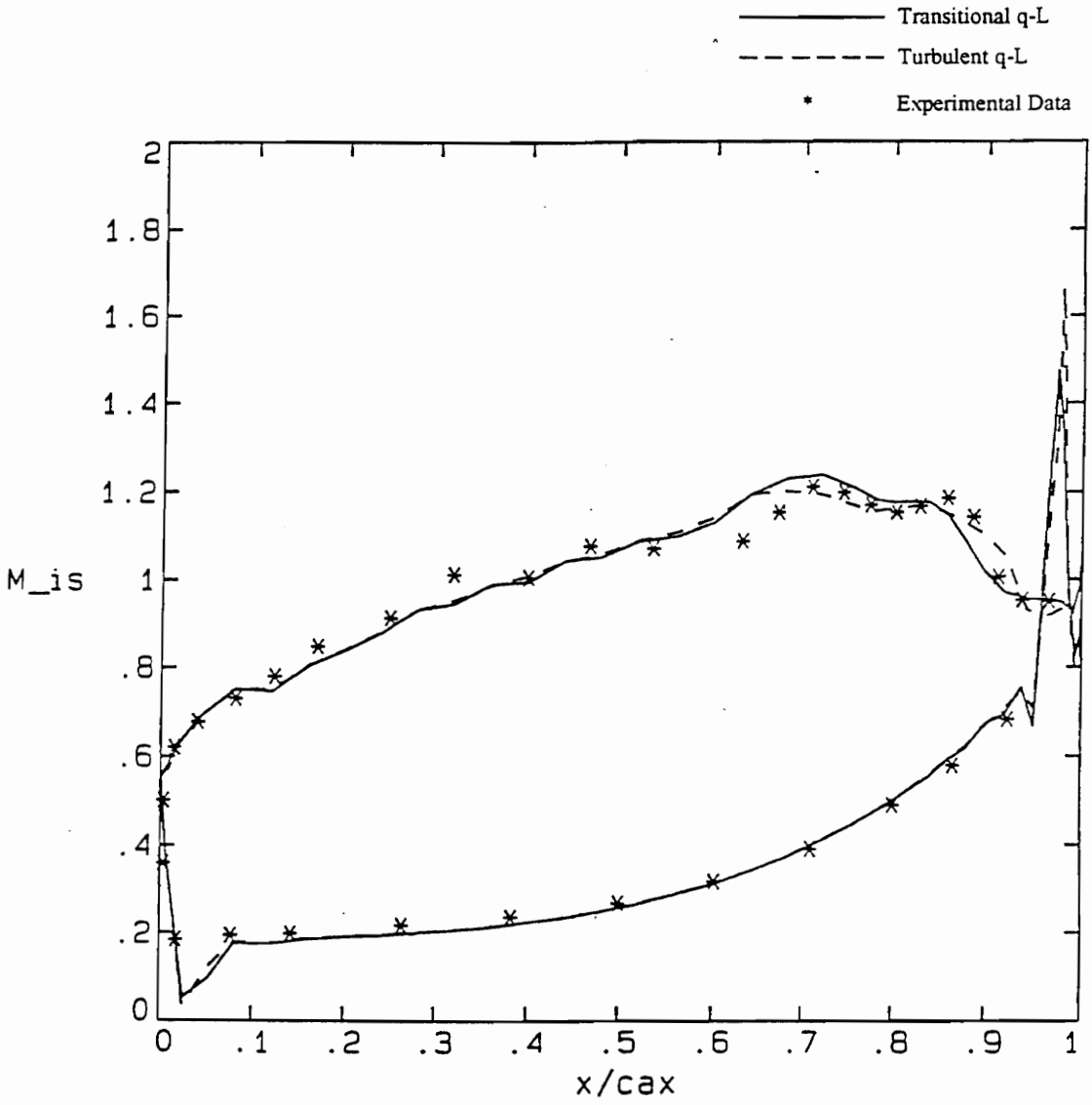

Figure 45. ACE M_{is} *Vs* C_{ax}, $M_2 = 0.988$

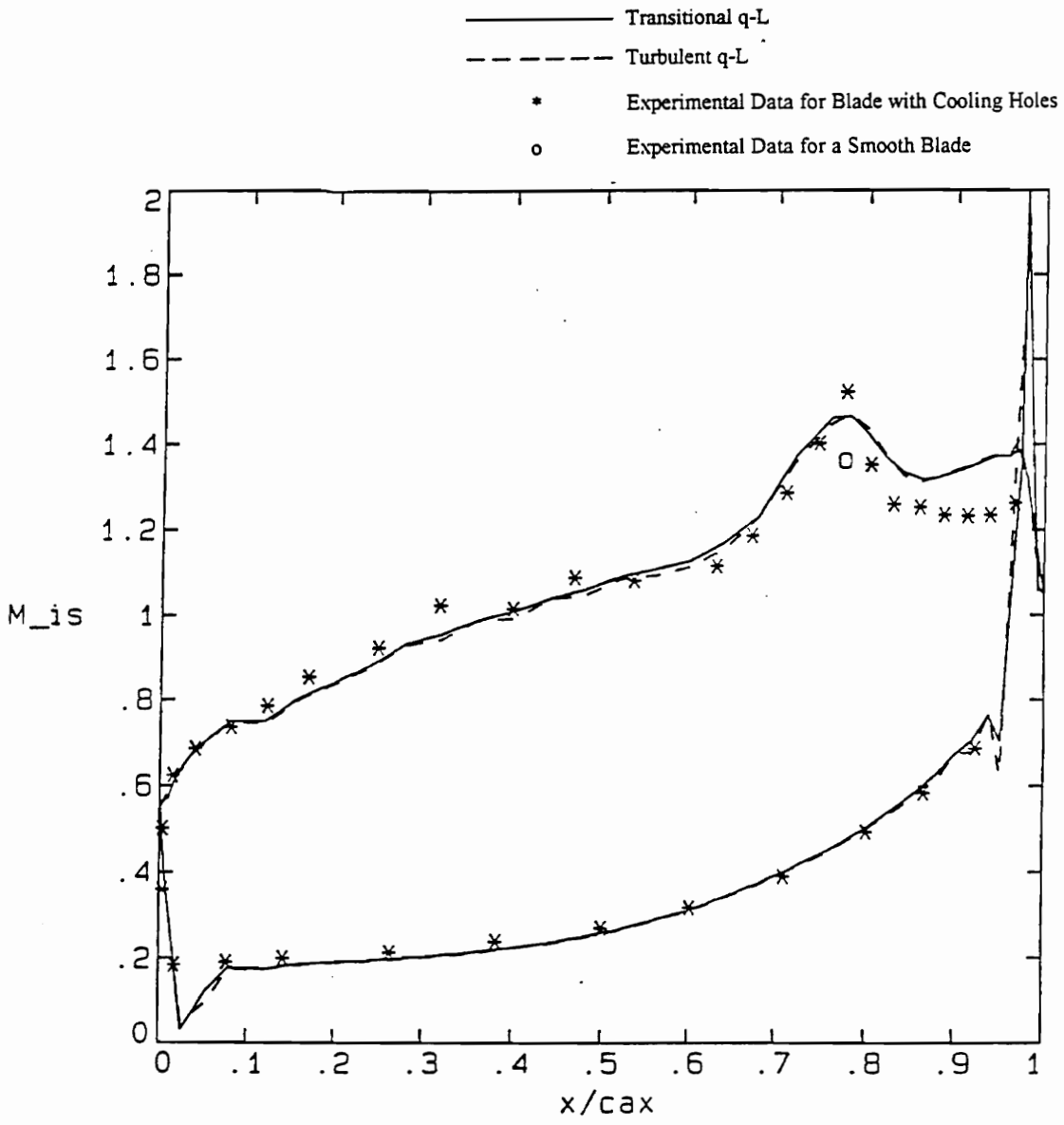

Figure 46. ACE M_{is} Vs C_{ax}, M_2 = 1.2

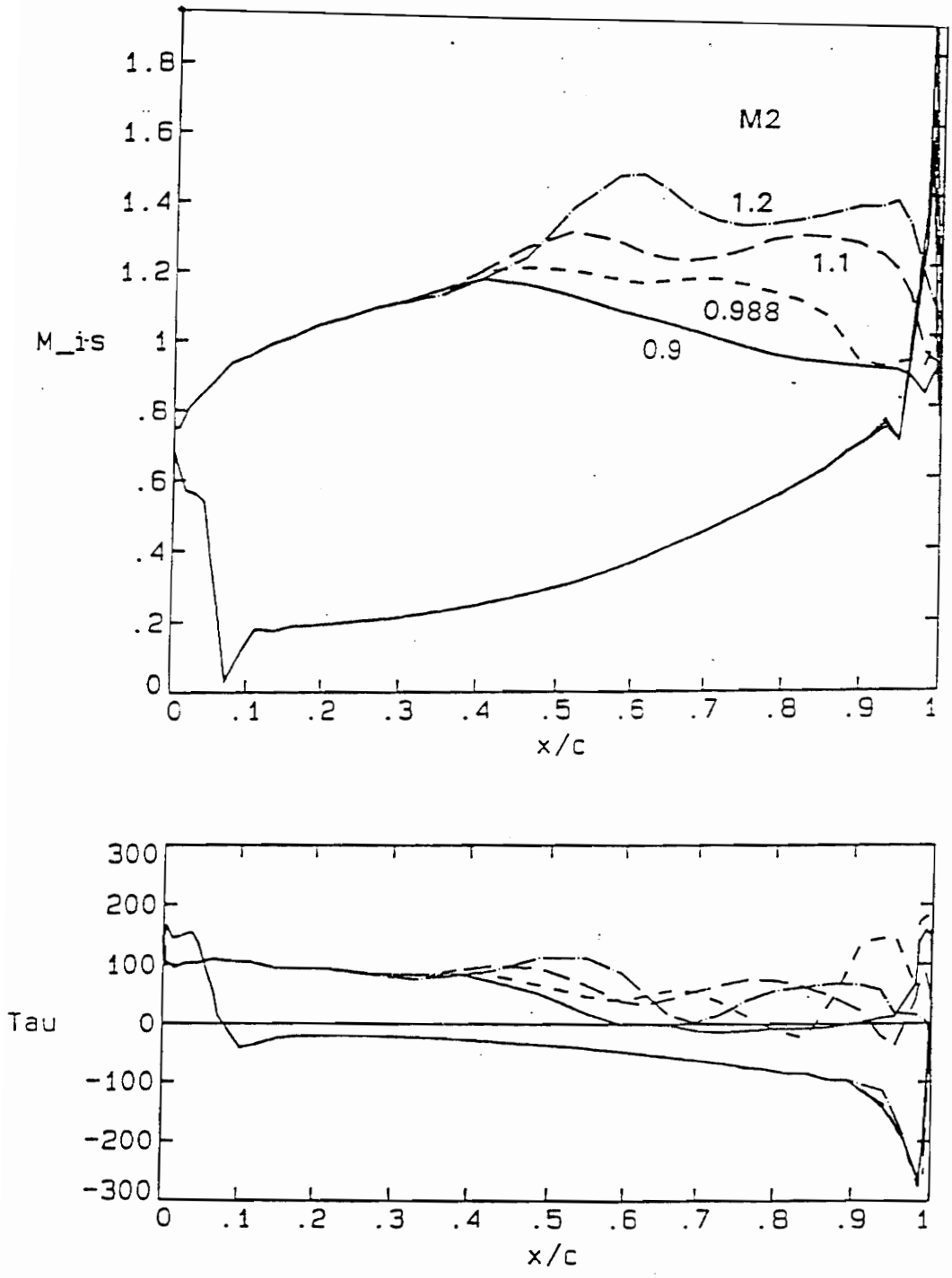

Figure 47. ACE Transitional q-L Pressure and Shear Stress Distributions

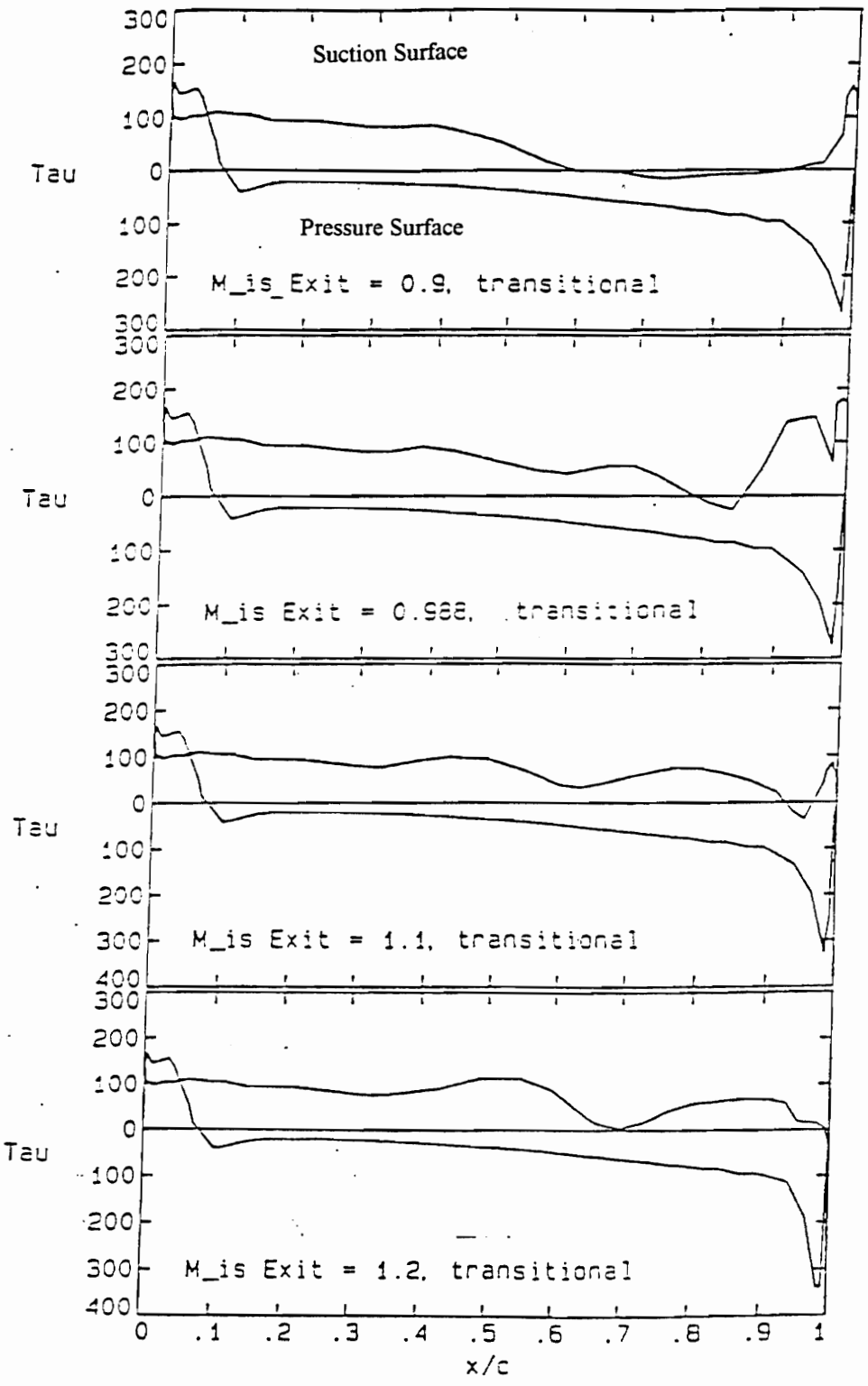

Figure 48. ACE Shear Stress Distributions Vs Tangent Chord

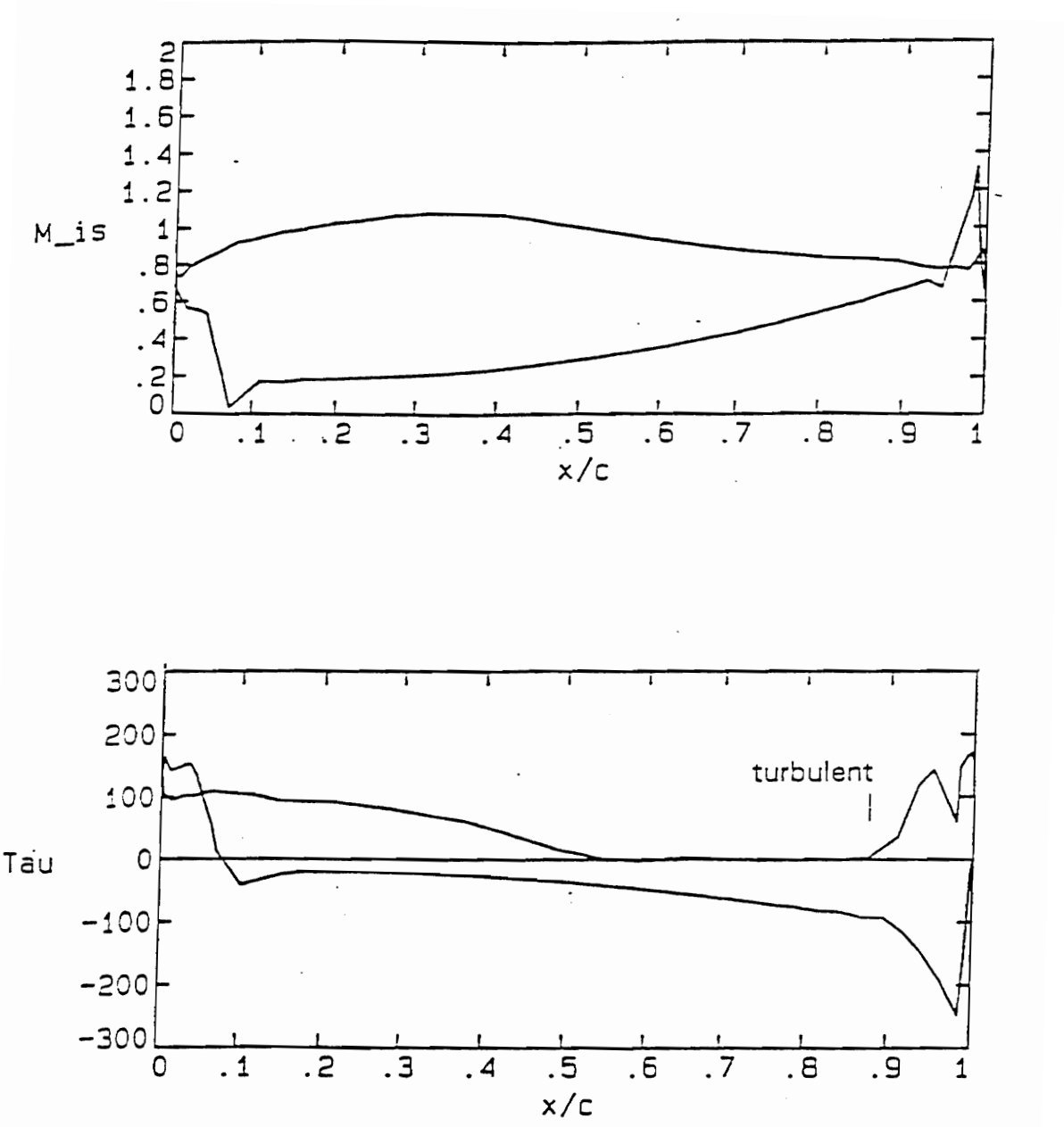

Figure 49. ACE $M_2 = 0.8$, Laminar q-L - M_{is} and τ Distributions

6.0 Conclusions

The Moore Elliptic Flow Program has been used to calculate steady two-dimensional flow and heat transfer in transonic turbine cascades. Successful calculations were performed on two different rotor profiles using a one-equation q-L transitional turbulence model. The calculations covered the range of exit Mach numbers from 0.8 to 1.2, Reynolds numbers from 0.85E6 to 2.0E6, with free stream turbulence intensities of 0.5 and 4.1 percent.

6.1 RT27

6.1.1 Transition

The location and length of the transition zone on the suction surface, as predicted by the q-L model, for the heat transfer and adiabatic calculations agrees quite well with the experimental data.

The adiabatic measurements of transition are closely matched by the predictions of the q-L model. At the design condition (M_2 = 0.92, Re = 1E6, Tu = 4.1 %), the beginning of transition is predicted at 56.8 percent of the axial chord. This agrees well with the measurements of Mee et al., 1992a (53.1 % of C_{ax}), and Mee et al., 1992b (60 % of C_{ax}). The end of transition is predicted to within 8 percent of blade axial chord for the two RT27 cascades. A higher Reynolds number promotes earlier transition on the suction surface, as indicated by the measurements of Mee et al., 1992a. This trend is well predicted by the q-L model at a Reynolds number of 2E6.

6.1.2 Boundary Layer Analysis

The distribution of the calculated boundary layer parameters around the blade at the design condition and the variation of the parameters with Mach number were compared with the experimental data.

The calculated and measured boundary layer velocity and density profiles, and the calculated and measured boundary layer thickness, δ_{99}, around the suction side of the blade show good agreement.

A comparison of the measured and calculated displacement and momentum thicknesses around the blade at the design condition shows that both the displacement and momentum thicknesses are well predicted up to 90 percent of the axial chord on both the pressure and suction surfaces.

A comparison of the calculated and measured boundary layer thickness shows that it is well predicted up to a Mach number of one. The momentum thickness at higher Mach numbers is under-predicted indicating a lower loss than is measured. The shape factor is over-predicted at the higher Mach numbers.

6.1.3 Blade Loading

The overall blade loading is well predicted. At a supersonic exit Mach number of 1.1, the gradient and the magnitude of the rise in the pressure due to over-expansion and the drop due to the shock are somewhat less in the calculations than in the measurements.

6.1.4 Heat Transfer

The peak heat transfer rate to the blade on the suction surface is predicted very closely (to within 1 %).

The computed and measured heat transfer rates were compared at a Reynolds number of 1E6 and an exit Mach number of 0.959. The rise in heat transfer rate on the suction side due to transition is well predicted, as is the onset of transition and the peak heat transfer level. This is quite important for blade life considerations. The calculated length of transition is shorter than the measured value. Both the data and the predictions suggest that the heat transfer to the pressure surface is constant over the blade at the lower Reynolds number. The calculated pressure side heat transfer rate is lower by a factor of 2 to 3.

6.1.5 Grid Refinement

A preliminary grid refinement study suggests that turbulent and stagnation heat transfer are dependent on the near-wall spacing in the range of y^+ from 8 to 20.

6.2 *ACE*

The flow in a transonic turbine blade row at a low level of freestream turbulence is modeled without numerical stability problems.

6.2.1 Losses

The overall losses as predicted by the code are in good agreement with the measurements.

A comparison of the mixed-out losses obtained from the transitional q-L and the turbulent q-L model with the available data suggests that both models predict the losses to within a percentage point. The turbulent q-L model seems to predict the losses better in the supersonic range and the transitional q-L model seems better in the subsonic range.

6.2.2 Shear Stresses

Computed wall shear stresses may indicate the motivation behind the design philosophy of this highly loaded transonic turbine blade. The flow was modelled with a laminar boundary layer with an exit Mach number of 0.8. An adverse pressure gradient exists over the second half the suction surface length. This almost separates the flow as is seen in the shear stress distribution. The shear stress goes to zero for a third of the suction surface. This could be an indication of the design philosophy of this transonic turbine rotor.

6.2.3 Shock Structure

The trailing edge shock structure predicted by the code agrees quite well with Schlieren pictures and density interferograms of the experimental cascade.

6.2.4 Blade Loading

The overall pressure distributions for the three computational exit Mach numbers of 0.9, 0.988 and 1.2 correspond closely with Haller's measurements.

7.0 Suggestions For Further Work

1. Grid Refinement

   Preliminary grid refinement studies suggest that algebraic grid refinement (presently used with the MEFP), should be supplemented with adaptive or multiple block grids to improve shock capturing and boundary layer resolution.

2. Effect of Curvature

   Computed gas-to-wall heat transfer distributions indicate that curvature effects may play a significant role in determining the state of the pressure side boundary layer. Overall heat transfer predictions should improve with the incorporation of curvature effects.

3. Shock Capturing

   The fall in pressure due to overexpansion and the rise due to the shock that follows in a supersonic flow occur over a small fraction of the blade axial chord. Mere grid refinement alone is not sufficient to capture this sharp fall and rise in the pressure. The base pressure of the flow, the freestream turbulence intensity and the shock capturing algorithm all play important roles. It would be instructive to study the effects of the base pressure and the turbulence intensity on the computed shock strengths for the profiles studied.

8.0 References

1. Adams, E.W., and Johnston, J.P., 1984, 'A Mixing-Length Model for the Prediction of Convex Curvature Effects on Turbulent Boundary Layers', Transactions of the ASME, Journal of Engineering for Gas Turbines and Power, Vol. 106, pp. 142 - 148, January 1984.

2. Camus, J-J., Denton, J.D., Soulis, J.V., Scrivener, C.T.J., 1983, "An Experimental Study of Transonic Three Dimensional Flow in a Turbine Cascade", ASME Paper No. 83-GT-12.

3. Dawes, W.N., Camus, J-J., Xu, L.P., Graham, C.G., 'Measured and Predicted Loss Generation in Transonic Turbine Blading', AGARD Conference Proceedings No. 401 on Transonic and Supersonic Phenomena in Turbomachines, Munich, Sep 1986.

4. Denton, J.D., and Xu. L.P., 1989, 'The Trailing Edge Loss of Transonic Turbine Blades', ASME Paper No. 89-GT-278.

5. Dickens, T.E., 1990, 'An Aerodynamic Investigation of a Two Dimensional Cascade of Transonic Gas Turbine Blades', M.Sc. Thesis, University of Oxford, U.K.

6. Graham, R.W., 1979, 'Fundamental Mechanisms that Influence the Estimate of Heat Transfer to Gas Turbine Blades', NASA TM 79128, 1979.

7. Hah, C., and Selva, R.J., 1990, 'Navier-Stokes Analysis of Flow and Heat Transfer Inside High-Pressure-Ratio Turbine Blade Rows', AIAA Paper No. 90-0343.

8. Haller, B.R., 1980, 'The Effects of Film Cooling on the Aerodynamic Performance of Transonic Turbine Blades', Ph.D. Dissertation, Cambridge University.

9. Horton, F.G., 1985, 'Aerodynamics and Heat Transfer of Turbine Blading', D.Phil. Thesis, University of Oxford, U.K.

10. King, P.I., 1986, 'Aerodynamics of High Performance Turbine Blading', D.Phil. Thesis, University of Oxford, U.K.

11. Mee, D.J., Baines, N.C. and Oldfield, M.L.G., 1992a, 'Detailed Boundary Layer Measurements on a Transonic Turbine Cascade', Transactions of the ASME, Journal of Turbomachinery, Volume 114, pp. 163- 172, January 1992.

12. Mee, D.J., Baines, N.C., Oldfield, M.L.G., and Dickens, T.E., 1992b, 'An Examination of the Contributions to Loss on a Transonic Turbine Blade in Cascade', Transactions of the ASME, Journal of Turbomachinery, Volume 114, pp. 155-162, January 1992.

13. Moore, J.G., 1985, 'An Elliptic Calculation Procedure for 3-D Viscous Flow', AGARD Lecture Series No. 140 on 3-D Computational Techniques Applied to Internal Flows in Propulsion Systems, June 1985.

14. Moore, J.G., and Moore, J., 1990, 'Development of a One Equation(q-L) Transition Turbulence Model', Turbomachinery Research Group, Report No. JM/90-8, Mechanical Engineering Department, Virginia Polytechnic Institute and State University, Blacksburg, VA.

15. Moore, J.G., and Moore, J.,1987, 'The Moore Elliptic Flow Program for Turbomachinery Flow Calculations 1987 Users Guide', Turbomachinery Research Group, Report No. JM-87-5, Virginia Polytechnic Institute and State University, Blacksburg, VA.

16. Moore, J.G., 1992, 'Grid Optimization - An Explicit Approach', Turbomachinery Research Group, Report No. JM/92-2, Mechanical Engineering Department, Virginia Polytechnic Institute and State University, Blacksburg, VA.

17. Nicholson, J.H., 1981, 'Experimental and Theoretical Studies of the Aerodynamic and Thermal Performance of Modern Gas Turbine Blades', D.Phil. Thesis, University of Oxford, U.K.

18. Xu, L., and Denton, J.D., 1987, 'Base Pressure Measurements on a Model of a Turbine Blade Trailing Edge', Proceedings of the International Conference on Turbomachinery, Paper No. C283/87, Institution of Mechanical Engineers, Cambridge, England.

Appendix A. Determination of the Boundary Layer Reference Thicknesses

A.1 Determination of the Boundary Layer Thickness

Figure 4(a) in Mee et al., 1992a, shows the non-dimensionalized boundary layer velocity profiles for the large chord cascade at the design conditions. The boundary layer thickness at each station is non-dimensionalized by $\delta_{99,ref}$. Figure 4(b) in Mee et al., 1992a, shows the non-dimensionalized boundary layer velocity profiles at the same conditions. In this case, the boundary layer thickness at each station is non-dimensionalized by the local boundary layer thickness. From the two figures, we obtain $\frac{\delta_{0.8}}{\delta_{99,ref}}$ and $\frac{\delta_{0.8}}{\delta_{99,local}}$ respectively, over the blade surface.

At $\frac{s}{s_0} = 0.755$, $\delta_{0.8} = 0.85$ mm. (From Figure 11 of Mee et al., 1992a). Then we can arrive at the boundary layer thickness distribution around the blade surface as

$$\delta_{99} = \left(\frac{\delta_{0.8}}{\delta_{99,ref}}\right) \times \left[\frac{1}{\left(\frac{\delta_{0.8}}{\delta_{99,local}}\right)}\right] \times \delta_{99,ref}$$

where,

$$\delta_{99,\,ref} = \frac{\delta_{0.8,\,0.755}}{\left(\frac{\delta_{0.8}}{\delta_{99,\,ref}}\right)_{0.755}} = \frac{0.85}{.142} = 5.98\ mm.$$

A.2 Determination of the Boundary Layer Displacement Thickness

From Table 5.4 of Dickens, T.E., 1990, the displacement thickness at the reference location for an exit Mach number of 1.102 is 0.2994 mm. From Figure 7 of Mee et al., 1992b, $\frac{\delta^*}{\delta^*_{ref}}$ at $M_2 = 1.102$, is 0.894. Hence, the value of δ^*_{ref} for the Mee et al., 1992b cascade ($C_{ax} = 76.9$ mm.), is 0.335 mm. This value may then be scaled to the large chord cascade using the scaling factor, $X = \frac{230.7}{76.9}$, so that $\delta^*_{ref} = 1.01$ mm.

Appendix B. Shear Stress Distribution

The shear stress is evaluated around the blade profile in terms of the velocity gradient. The X and Y components of the wall shear stress parallel to the wall are found from

$$\tau_{xn} = \mu_{eff}\frac{\partial U_x}{\partial n}$$

$$\tau_{yn} = \mu_{eff}\frac{\partial U_y}{\partial n}$$

and the total wall shear stress τ is obtained from

$$\tau = \mu_{eff}\frac{\partial U_s}{\partial n} = \frac{\tau_{xn}\Delta x + \tau_{yn}\Delta y}{\sqrt{\Delta x^2 + \Delta y^2}}$$

where Δx and Δy are the 2 dimensions of the elemental area over which the shear stress τ is associated, and s and n are the directions parallel and normal to the wall.

Appendix C. Mixed Flow Analysis

Mixed-Flow Analysis is an analytical construct often employed to study turbomachinery flows. The method consists of applying the basic conservation laws of mass, momentum and energy over a control volume with constant area. The inlet plane to the control volume is immediately downstream of the trailing edge. This is called the upstream plane of the control volume and all the flow properties at this plane are denoted with the subscript u. The exit plane of the control volume is deemed to be at a distance sufficiently long for the mixing process to be completed and the flow properties to become uniform across the control volume. (refer Figure 50) The properties at this downstream plane are denoted by the subscript d.

The conservation laws applied between the inlet and exit planes of the control volume for the mixing analysis are :-

1. Conservation of Mass

$$\int_{A_u} \rho V_x dA = \rho_d V_{xd} A$$

2. Conservation of Momentum in X direction

$$\int_{A_u} p dA + \int_{A_u} \rho V_x V_x dA = p_d A_d + \rho_d V_{xd}^2 A_d$$

3. Conservation of Momentum in Y direction

$$\int_{A_u} \rho V_y V_y dA = \rho_d V_{yd}^2 A_d$$

4. Conservation of Energy

$$T_t = T_d + \frac{V_{xd}^2 + V_{yd}^2}{2C_p}$$

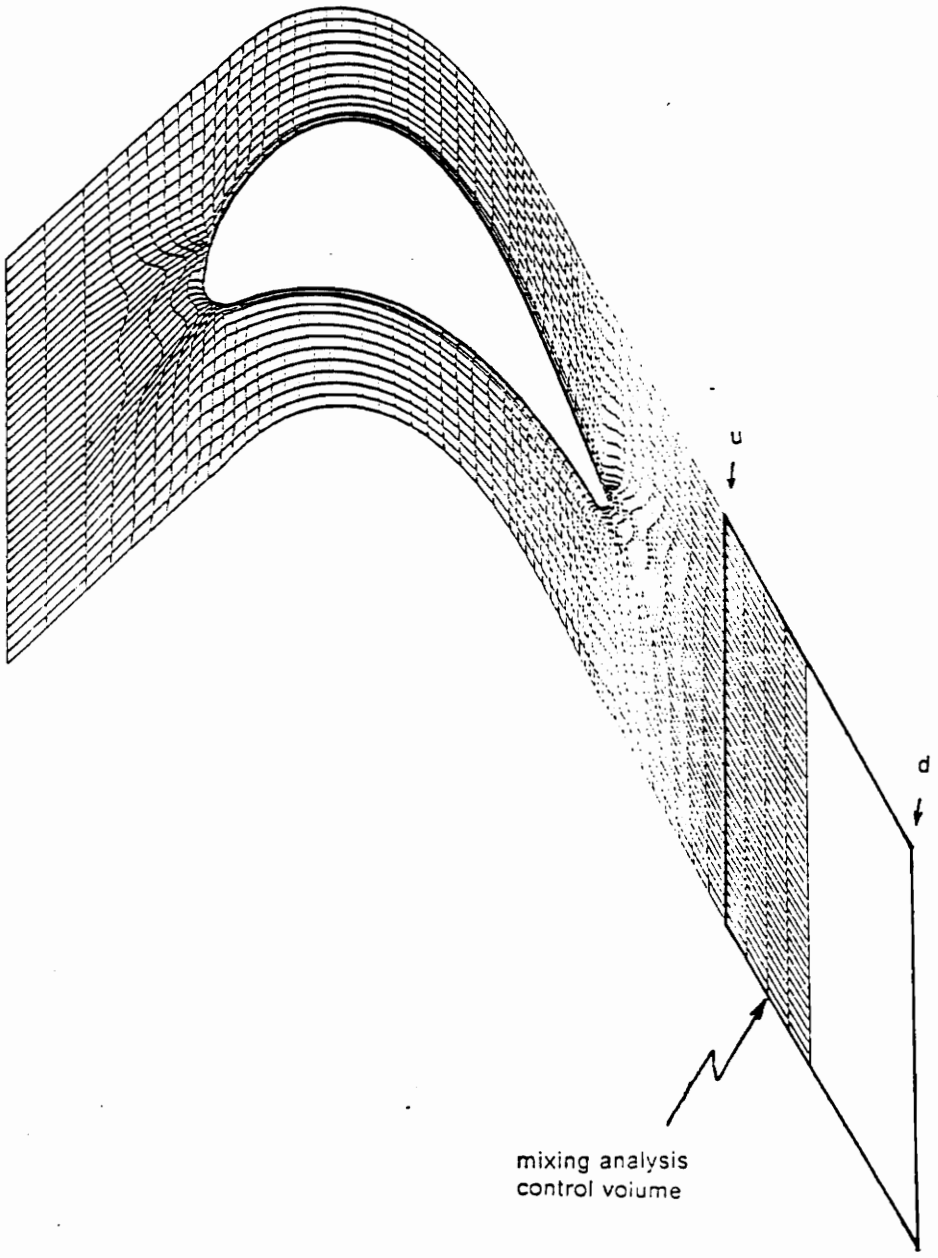

Figure 50. Upstream and Downstream Planes for Mixed Flow Analysis

Vita

S.V. Janakiraman was born in September 1969 in Madras, India. He did his schooling and undergraduate college work at Coimbatore, at Suburban HSS and PSG Tech respectively. Upon completion of his B.E., in Mechanical Engineering in 1991, he enrolled in the graduate program at VA Tech. After graduation, he plans to gain some practical experience in industry.